International Journal of Coal Geology 286 (2024) 104494

Contents lists available at ScienceDirect

International Journal of Coal Geology

journal homepage: www.elsevier.com/locate/coal

High-cellulose content of *in-situ* Miocene fossil tree stumps and trunks from Lusatia lignite mining district, Federal Republic of Germany

J. Kus [a,*,1], M. Dolezych [b], W. Schneider [†,c], J.C. Hower [d], T. Hofmann [e], E. Visiné Rajczi [e], A. Bidló [e], B. Bolodár-Varga [e], R.F. Sachsenhofer [f], A. Bechtel [f,2], K. Stojanović [g], D. Životić [h], I. Kojić [i], M. Mastalerz [j], T. Graupner [a], W.E. Lukens [k], L. Donaldson [l]

[a] Federal Institute for Geosciences and Natural Resources, Stilleweg 2, D-30655 Hannover, Federal Republic of Germany
[b] Senckenberg Natural History Collections Dresden, Königsbrücker Landstr. 159, 01109 Dresden, Federal Republic of Germany
[c] Alte Berliner Straße 13d, D-02977 Hoyerswerda, Federal Republic of Germany
[d] University of Kentucky Center for Applied Energy Research, 2540 Research Park Drive, Lexington, KY 40511, USA
[e] Institute of Environmental Protection and Natural Conservation, University of Sopron, Bajcsy-Zsilinszky u. 4, Sopron 9400, Hungary
[f] Montanuniversität Leoben, Department of Applied Geosciences and Geophysics, Peter-Tunner-Str. 5, A-8700 Leoben, Austria
[g] University of Belgrade, Faculty of Chemistry, Studentski trg 12-16, 11000 Belgrade, Serbia
[h] University of Belgrade, Faculty of Mining and Geology, Djušina 7, 11000 Belgrade, Serbia
[i] University of Belgrade, Innovation Center of the Faculty of Chemistry, Studentski trg 12-16, 11000 Belgrade, Serbia
[j] Indiana Geological and Water Survey, Indiana University, 611 North Walnut Grove Avenue, Bloomington, IN 47405-2208, USA
[k] Department of Geology and Environmental Science, James Madison University, 801 Carrier Drive, Harrisonburg, VA 22807, USA
[l] Scion, Private Bag 3020, Rotorua 3046, New Zealand

ARTICLE INFO

Keywords:
Xylite
Holocellulose
Fossil and modern wood
Second Lusatian lignite seam
Lignite
CLSM
Calcofluor-stained CLSM
micro-FTIR
Biomarkers
Carbon isotope

ABSTRACT

Second Miocene Seam Complex (2nd MFK; *germ.:* 2. Miozäner Flözkomplex) holds many *in-situ,* not permineralised fossil tree stumps and trunks with high-cellulose contents. The state of preservation of a set of *in-situ* fossil trees (*Taxodioxylon cryptomerioides*, *Sciadopityoxylon wettsteinii*, and *Quasisequoioxylon piskowitzense*) collected from three open-cast mines (Welzow-Süd, Meuro, and Piskowitz) in Lusatia lignite mining district, Federal Republic of Germany was investigated using a multi-method research schema.

Examination of preservation state of thermally immature fossil woods revealed: (1) well-preserved (non-deformed, non-degraded, and non-flattened) textinite, (2) a retained structural integrity represented by multi-layered (multi-zoned) cells with primary, secondary cell wall, and middle lamella, (3) microfracturing restricted to secondary walls only, (4) preservation of polyphenolic parenchyma cells (PP cells), (5) excellent preservation of pits in ray tracheids, (6) presence of amorphous silica (opal-A) coating, and (7) crystalline silica (opal-CT) fillings of small-bladed crystals.

Thermogravimetric analysis results showed dissimilar gelification status of fossil samples, supporting chlorite holocellulose assay results. The latter indicated anomalously high-cellulose values (15.6–37.6% holocellulose). The micro-FTIR data obtained revealed an excellent preservation of both hemicellulose (bands at 1740 and 1245 cm^{-1}) and cellulose (bands at 1110 and 1040 cm^{-1}). Micro-FTIR spectrometry indicated lack of preferential hydrolytic removal of polysaccharides in examined samples.

* Corresponding author.
E-mail addresses: J.Kus@bgr.de (J. Kus), Martina.Dolezych@senckenberg.de (M. Dolezych), james.hower@uky.edu (J.C. Hower), hofmann.tamas@uni-sopron.hu (T. Hofmann), visine.rajczi.eszter@uni-sopron.hu (E. Visiné Rajczi), bidlo.andras@uni-sopron.hu (A. Bidló), varga.bernadett@uni-sopron.hu (B. Bolodár-Varga), reinhard.sachsenhofer@unileoben.ac.at (R.F. Sachsenhofer), ksenija@chem.bg.ac.rs (K. Stojanović), dragana.zivotic@rgf.bg.ac.rs (D. Životić), ivankojic@chem.bg.ac.rs (I. Kojić), mmastale@indiana.edu (M. Mastalerz), Torsten.Graupner@bgr.de (T. Graupner), lukenswe@jmu.edu (W.E. Lukens), lloyd.donaldson@scionresearch.com (L. Donaldson).

[1] With greatest respect, the authors devote this paper in honor and in memory of Dr. Wilfrid Schneider, former Section Head of Coal Petrography at lignite mining company LAUBAG, Federal Republic of Germany and coryphe (eminent authority) in the field of coal petrography and palaeobotany of lignite in open-cast mines of eastern Federal Republic of Germany.

[2] Present address.Wismarer Str. 5, D-56075 Koblenz, Federal Republic of Germany (A. Bechtel).

[†] Deceased Author.

https://doi.org/10.1016/j.coal.2024.104494
Received 24 November 2023; Received in revised form 12 March 2024; Accepted 17 March 2024
Available online 21 March 2024
0166-5162/© 2024 Federal Institute for Geosciences and Natural Resources, Germany. Published by Elsevier B.V. This is an open access article under the CC BY license (http://creativecommons.org/licenses/by/4.0/).

Biomarker patterns in lignite revealed forested and prevailing reed-mire vegetation. The results indicated lower contribution of Cupressaceae and emergent macrophyta to precursor organic matter of Welzow-Süd in comparison to Piskowitz lignite. Piskowitz lignite formed in permanent mire with stable water table under reducing, mesotrophic conditions. In contrast, more pronounced water level fluctuations (reducing to slightly oxic settings) and/or post-depositional events are postulated for Welzow-Süd samples.

Biomarker assemblages obtained from fossil wood show a distinct dominance of diterpenoids and $\delta^{13}C$ values (−24.6 ‰ to −20.3 ‰) that clearly confirm gymnosperm sources. Distributions of diteprenoids and sesquiterpenoids, as well as fatty acids indicate the higher amount of saturated diterpenoids (pimarane, abietane) in fossil than in modern wood. This indicates reducing conditions promoting hydrogenation reactions. In addition to low Eh, preservation of cellulose in fossil wood was also favored by acidic conditions, very low degrees of aerobic fungal degradation, and protection of wood by Cupressaceae-derived resins.

While $\delta^{13}C$ values of fossil wood are generally consistent with stratigraphic trends and chemotaxonomical classification, slightly elevated $\delta^{13}C$ values recorded in *T. cryptomerioides* and *S. wettsteinii* in Welzow-Süd and Meuro open-cast mines, respectively, compared to published $\delta^{13}C$ data of fossil gymnosperm wood are also indicative for good cellulose preservation.

Both preservation of *in-situ* Miocene fossil stumps and trunks and retention of high-cellulose contents are suggested to be related to high-amplitude temporal fluctuations associated with repeated eustatically-controlled wet-dry cycling inducing: (1) weathering of tuff- and rhyolite-dominated acidic volcanics and Lausitz granodiorite, (2) associated erosion of saprolites, and (3) peat-sourced circulation of humic acid- and fulvic acid-rich waters. The latter led to the formation of Middle Miocene kaolinite deposits, as well as to the release of silicic acid and its subsequent precipitation in form of opal-A. The latter influenced preservation of high-cellulose contents in fossil wood.

1. Introduction

Preferential decomposition of cellulose over lignin is often postulated to occur during the coalification process of humification and gelification, although the specific chemical changes during peat decomposition are not clearly defined or determined (Bracewell et al., 1980; Benner et al., 1984; Spackman et al., 1988; van der Heijden and Boon, 1994). The corresponding variations in biodegradation-based macromolecular products are mainly attributed to peat decomposition itself, and to a lesser extent, to the degree of changes in vegetation. Following accelerated biochemical alteration during shallow burial, biochemical constituents of deposited and accumulated plants undergo, among other processes, water loss, cross-linking dehydroxylation, and decarboxylation. The resulting cell wall polymers can constitute cellulose, "hemicellulose" (a mixture of at least three polymers), and lignin (Spackman et al., 1976).

According to Klavins et al. (2008), it is assumed that labile compounds, including polysaccharides (i.e., cellulose), are, in general, preferentially decomposed. The remaining refractory aromatic and aliphatic compounds are then residually enriched during peat mineralization (mode of fossilization). This remains largely in agreement with Biester et al. (2014), who argue that changes in the molecular composition indicate that peat decomposition in the bog is mainly characterised by preferential decomposition of phenols and polysaccharides, and relative enrichment of aliphatics during drier periods. Further, using ^{13}C NMR, Hatcher and Clifford (1997) showed that coalification to lignite can be accompanied by: (1) loss of residual cellulose, (2) loss of methoxyl functional groups on lignin, and (3) the formation of catechol-like structures from lignin. The continuous removal of cellulose with an increasing level of gelification is accompanied by the progressive loss of methoxyl groups during the process of gelification (Russell and Barron, 1984).

In addition to cellulose, also lignin undergoes molecular changes. According to Fengel (1991), alterations of molecular lignin are reflected by reactions of oxidation, demethylation, loss of hydroxyl groups, and, consequently, condensation. These changes also can occur at an early stage of diagenesis and lead to gradual biotransformation of the lignin macromolecule, giving rise to an aromatic hydrocarbon network as suggested by Venkatesan et al. (1993). It is also suggested that cellulose decomposition and transformation of lignin can take place simultaneously at the peatification stage, although at a dissimilar rate (Hatcher, 1988; Mastalerz and Bustin, 1994; Drobniak and Mastalerz, 2006). In addition, the preferential degradation of polysaccharides and relative enrichment of aliphatics may be, in some cases, caused predominantly by vegetation changes and additionally modified by peat decomposition processes. Biester et al. (2014) indicated that wet conditions were attributed to higher abundance of *Sphagnum* in relation to lignin-containing graminoids and less intense decomposition of polysaccharides.

Yet, the remarkable preservation of xylite, which points toward resistance of the fossil wood and toward removal of hemicellulose, and/or its exhaustive biodegradation, enclosing, among others, depolymerisation reactions, emphasises another mechanism of conservation. This is in line with the impedance of biochemical depolymerisation as suggested by Bates and Hatcher (1989), Bates et al. (1991), Fengel (1991), Moers et al. (1994), Yang et al. (2005), and Lechien et al. (2006). The existence of well-preserved, non-petrified Miocene fossil wood or xylite has been reported from: (1) the Entre-Sambre-et-Meuse (ESEM) area in Belgium (Fairon-Demaret, 1992; De Putter et al., 1996; Lechien et al., 2006), (2) the Bükkábrány open-cast coal mine (*Taxodiaceae* tree trunks) in Hungary (Erdei et al., 2009; Hámor-Vidó et al., 2010; Bardet and Pournou, 2015), (3) Bílina open-cast coal mine (*Ulmus pyramidalis* - fossil wood with fossil leaves and fruits) in Czech Republic (Sakala, 2002), (4) Achlada lignite mine (upright stems and trunks of possible autochthonous character) in Greece (Oikonomopoulos et al., 2015), (5) Kolubara and the Kostolac basins (lignite) in Serbia (Đoković et al., 2018), (6) Jóźwin IIB, Drzewce, and the Jaroszów open-cast mines (xylite) in Poland (Bechtel et al., 2007b; Fabbri et al., 2009; Marynowski et al., 2018, 2019), (7) Bełchatów lignite deposit (xylite) in Poland (Drobniak and Mastalerz, 2006), (8) Borków gypsum quarry (xylite) in Poland (Marynowski et al., 2023), (9) Bees Nest Pit (xylite) in Derbyshire, central England, UK (O'Keefe et al., 2020), and (10) Lusatia lignite mining district (xylite), Federal Republic of Germany (Potonié, 1895; Gothan, 1906; Dolezych, 2005).

The extraordinary preservation of European Miocene fossil wood trucks and stumps, often-encountered *in-situ*, as well as their non-petrified woody tissue, is astonishing. As such, the existence of remarkable preservation of non-petrified fossil wood in Entre-Sambre-et-Meuse (ESEM) area in Belgium reveals a well-preserved cellulose structure contained in fossil wood collected from the corresponding Florennes peat deposit (Lechien et al., 2006). In general, solid state ^{13}C NMR and analytical pyrolysis of fossil non-petrified wood indicate that preservation of cellulose and its bioavailability is largely influenced by progress of lignin modification. In addition, and although not proceeded

further, Lechien et al. (2006) suggested that yet another possibility for a good preservation of the cellulose structure may exist. This possibility is related to presence of polyphenolic compounds, such as tannins, which may inhibit an extensive bacterial degradation, as discussed by Given (1984). Correspondingly, Hámor-Vidó et al. (2010) suggested that the sudden burial of non-petrified, cellulose-rich *Taxodium* trunks in the Bükkábrány open-cast coal mine, Hungary has led to: (1) decay of lignin under suboxic, anoxic conditions and to (2) precipitation of ligninphenol saturated fluxes. The latter is thought to reduce microbial activity and to preserve the *in-situ Taxodiaceae* tree trunks. Although not determined, Oikonomopoulos et al. (2015) implied high-cellulose content in the majority of the examined lignite beds (not specifically xylite), pointing to well-preserved tissues. Accordingly, the well-preserved tissues reflected low bacterial activity resulting in humification of cellulose-rich plant remnants in the Achlada lignite deposit in Greece. As for the high holocellulose content of Miocene xylite collected from Jóźwin IIB open-cast mine in Poland, Marynowski et al. (2018) reported the presence of a complex monosaccharides composition without disaccharides. The corresponding preservation of α- and β-arabinose, α- and β-arabinofuranose, α- and β-xylose, and α- and β-mannose, supports their origin from biopolymer degradation and not from microbial degradation. The obtained results indicate possible degradation products of hemicellulose. In contrast, Miocene xylite in the Jaroszów open-cast mine was characterised by dominance of disaccharides (trehalose) and saccharols (mannitol and arabitol), with trehalose and mannitol identified as products of fungal metabolism. Marynowski et al. (2018) suggested that Miocene xylite in Jaroszów open-cast mine was to some extent degraded by white-rot fungi, which preferentially utilised lignin as opposed to cellulose. Further, yet another possible mechanism for preservation of Miocene conifer wood from Bełchatów coal deposit in Poland was proposed. Drobniak and Mastalerz (2006) indicated respectively that the remarkably good preservation of the examined fossil wood reflects the protection of wood by conifer resins, as well as by early anaerobic conditions.

According to Eissmann (2002), prior to the middle Eocene and before the onset of lignite formation, the pre-Paleocene land surface was subjected to intense kaolinization, which continued into the Pliocene. Sedimentation prevailed across the area during basin subsidence, leading to the formation of shallow depressions, in which lignite seams developed. In Lusatia, lignite-bearing strata can be observed to directly overlap kaolin deposits (Standke and Strauss, 1991).

Although in general, the reported studies applied various techniques to investigate lignite and non-petrified fossil wood, e.g.: (1) coal and organic petrology, and (2) organic geochemistry or cellulose content determination and others, the final synthesis of molecular, morphological, and palaeoclimatic data is missing and the overall refinements of respective hypotheses toward high-cellulose preservation remain challenging. Yet, European relics of Miocene lignite deposits characterised by *in-situ* occurrence of well-preserved fossil tree stumps and trunks provide a unique opportunity to study and address palaeoclimate control on the exceptional fossil preservation as well as on the development of economically viable kaolinite deposits.

The proposed approach integrating numerous different optical, physical, and geochemical methods allows for implementation of numerous investigative methods with the overall aim to in-depth examination of the *in-situ* Miocene fossil tree trunks and stumps present in Piskowitz (Pis), Meuro (M), and Welzow-Süd (WS) open-cast mines located in Lusatia lignite mining district, eastern Federal Republic of Germany. Such an approach enabled the implementation methodology of a complex study such as that of the cellulose-high content of fossil wood in the Lusatia lignite mining district. Consequently, it also ensured its multifaceted manner to address numerous influences and constraints of the *in-situ* preservation of cellulose-rich fossil tree stumps and trunks like these examined from Lusatia. As such, it provides rare insights into terrestrial palaeoclimate and environmental evolution during Miocene in the Lusatia, delivering information on preservation state of non-mineralised fossil woods and the retention of high-cellulose contents. Apart from evolution of palaeoclimate, palaeoenvironment and vegetation, it also points toward the concurrent formation of fossil soil related to weathering of Lusatia granodiorite and the genesis of kaolinite deposits on the northern flank of the Lusatia Mountain. The latter strengthen the important role of kaolin deposits in the present industrial development of Saxony and their important economic factor in this region (Schellenberg and Kleeberg, 1997).

In the present study, a detailed and thorough examination of *in-situ* fossil wood and modern analogues was performed by means of various optical methods and other techniques with the aim to provide a hypothesis for the high content of cellulose in examined xylite and its extraordinary *in-situ* preservation. Contrary to the biodegradation processes of polysaccharides in xylite during peat decomposition, a mechanism that explains the non-biomineralised occurrences of well-preserved xylite is proposed and discussed.

The objective of this study is to collate and synthesise scientific results obtained and related to non-biomineralised occurrences of well-preserved fossil wood and lignite from the Middle Miocene Second Miocene Seam Complex (2nd MFK; *germ.:* 2. Miozäner Flözkomplex) of the M, WS, and Pis open-cast mines of the Lusatia lignite mining district, Federal Republic of Germany. The investigations are aimed at:

(1) the performance of a detailed and thorough examination of *in-situ* fossil wood and modern analogues by means of various optical methods to detect cellulose in the examined xylite,
(2) the determination of cellulose contents to compare the obtained results with data derived from former cellulose content investigations of Miocene xylite,
(3) the establishment of the sources and depositional environment of organic matter (OM), and comparison of the results with conclusions derived from previous palaeobotanical and petrographic investigations,
(4) the examination of the potential of biomarker assemblages and micro-FTIR data to provide additional explanation for preservation of cellulose in fossil wood, and.
(5) the investigation of stable carbon isotope ($\delta^{13}C$) to enable comparison of Miocene whole wood samples.

2. Geology and taxonomic composition of palaeoflora of the Second Lusatian lignite seam

The Lusatia (Lusatia Anticlinorium), part of the Cadomian continental crust of Gondwana, is composed of a folded, not and low-grade metamorphosed Neoproterozoic turbiditic greywacke intruded by numerous bodies of Cadomian plutons and covered by lower to middle Cambrian and lower Ordovician to Mississippian onlap sequences (Kröner et al., 1994; Kasiński et al., 2004; Escher et al., 2020). During the Variscan orogeny, the Lusatia collided with the Mid-German Crystalline High along the SE edge of the Rheno-Hercynian Zone (East Avalonia terrane). In the Early Carboniferous time (Mississippian), the Lusatia was elevated (due to advancing nappes from the SE) and subjected to erosion. During the Late Variscan stage (340–295 Ma) in the Saxo-Thuringian Zone, extension-related magmatism started at ca. 330 Ma, while the collisional magmatism ceased at ca. 320 Ma (Kroner and Romer, 2010). Tectonic relaxation and decompression of the orogenic structure resulted in the Pennsylvanian and Cisuralian extension, deep erosion, and generation of intramontane, molasse basins, locally with substantial input of plant material (resulting in present-day coal seams), and significant volcanic activity. The end of Variscan orogeny was associated with an emplacement of the post-kinematic Variscan plutons (Klomínský et al., 2010; Escher et al., 2020).

Degradation of the orogen was so advanced that in the Lopingian (Zechstein) and Triassic, the area was again covered with shallow sea sediments. After the sea regression in the Early and Middle Jurassic, a new marine invasion took place in the Late Jurassic. Due to a long period

of deep erosion in the Early Cretaceous, these sediments were almost completely removed, and only a few limited patches of the Jurassic strata are now present in the Elbe Zone along the Lusatia Thrust. In the Late Cretaceous, the whole territory was again deeply lowered and subjected to marine transgression. The Cenozoic sedimentary sequence in the Lusatia lignite mining district is the result of several transgressive pulses with intercalated regressive phases occurring at the southern edge of the Northwest European Cenozoic Basin (Fig. 1). Transgressions from the north or northwest induced flooding events, while in regressive phases, extensive alluvial fans from the southern mainland brought in terrestrial sediment loads. The sea retreated at the beginning of the Paleogene, when the entire Bohemian Massif was influenced by tectonic, compressional stresses related to the formation of the Alpine-Carpathian fold belt in the south (Ziegler et al., 1995). The rise of sea level in the late Early Miocene (Hemmoorian transgression) followed in the investigation area. After a regression phase with major peat formation events around the Lower-Middle Miocene boundary, a renewed sea-level rise resulted in the widest extension of marine-brackish beds over the pre-Cenozoic basement in the south of the region (higher Reinbekian transgression, Middle Miocene; Standke et al., 1993). Development of widespread coastal mires occurred along the southern coastal periphery, giving rise to peat formation and accumulation (Rascher et al., 2005, 2006; Standke, 2006; Escher et al., 2020). The alternation of marine-brackish deposits of sand, silt, and clay together with terrigenous clay, sand, and coal seams (1st to 4th MFK; *germ.*: 1. bis 4. Miozäner Flözkomplex) directly reflect the influence of sea level rise and fall (Standke et al., 1993; Standke, 2010). During the Oligocene and to an extent during the Miocene, the Oligocene Guttau Volcano Group in eastern Saxony, Federal Republic of Germany influenced the evolution of an associated maar lake (Lorenz et al., 2003; Suhr et al., 2006; Pfeiffer and Suhr, 2008). The Guttau Volcano Group is a volcanic unit at the northwestern margin of the Lusatia Volcanic Field, forming part of the Cenozoic Central European Volcanic Province (Tietz et al., 2013; Büchner et al., 2014). Typical volcanic structures include scoria cones (e.g., Stolpen Volcano) as well as related lava lakes, lava flows, vents, maars, and lava (crypto) domes. The Guttau Volcano Group combines three maars (Kleinsaubernitz maar, Barth maar, Buchwalde maar) and at least four cinder cones (the volcanoes Schafberg und Eisenberg are former scoria cones with lava lakes; Büchner et al., 2015a, 2017). Twenty-three $^{40}Ar/^{39}Ar$ age determinations range almost exclusively between 35 and 27 Ma with a climax age between 32 and 29 Ma (Büchner et al., 2015b). Above volcanic breccias, lapilli tuffs were deposited. According to Büchner et al. (2015a), the subsequent stage of uplift and denudation of the granodioritic rocks as well as exposition of the lava body exerted a dominant influence on the Eocene-Miocene landscape.

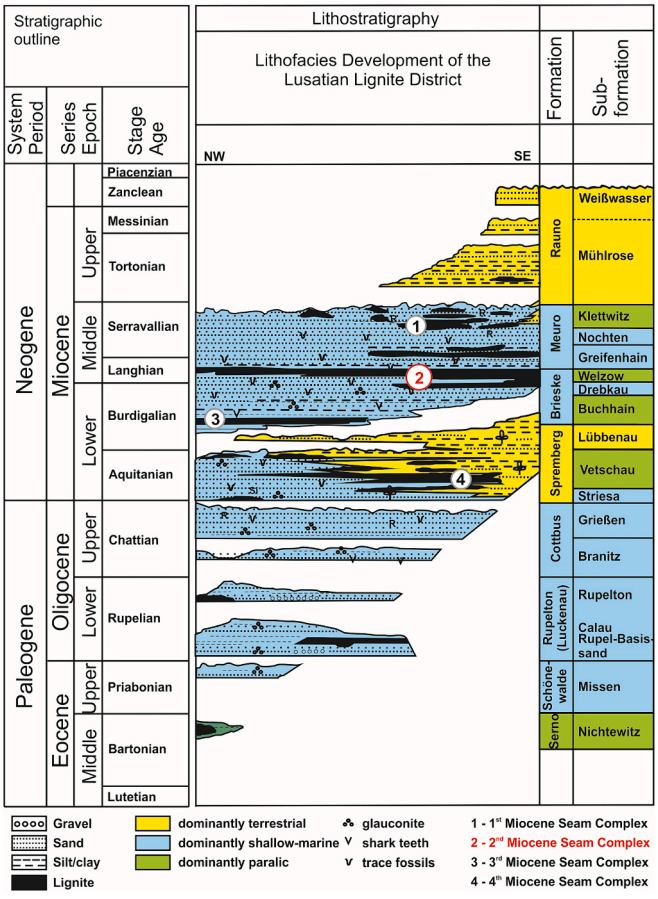


Fig. 1. Generalised stratigraphy of the Lusatia Lignite District, Federal Republic of Germany with major lithostratigraphic units. Compiled data adopted and modified from Escher et al. (2020). The formations and subformation displayed after Standke (2008) and modified after Stratigraphic Chart v. 2023/09 and STD (2016).

As a corollary of extensive exploitation, the Second Lusatian lignite seam (2nd MFH; *germ.:* 2. Miozäner Flözhorizont) of Middle Miocene age, has yielded a wealth of palaeobotanical information (Schneider, 2009, 2010). Taxonomic and taphonomic interpretation of pollen records (e.g., Thiergart, 1937; Krutzsch, 1970), seeds (Mai, 2000, 2001), leaf cuticles and leaves (e.g., Jähnichen, 1965; Bönisch, 1990; Schneider, 1967–2009), and woods (e.g., Dolezych, 2005, 2011; Dolezych and Schneider, 2007; Kunzmann et al., 2009) has been used successfully in facies and palaeoenvironmental analysis of the 2nd MFK. Its flora appears to be characterised by angiosperms and conifers, mostly representing members of the Cupressaceae sensu lato (Cupressaceae sensu stricto + Taxodiaceae), as well as Sciadopityaceae, Geinitziaceae, and Pinaceae.

The individual seam layers of the 2nd MFH show a distinctive succession of mire facies (swamp and bog facies respectively sensu Schneider (1992, 2004), Dolezych (2005), and references therein), which can be distinguished on the basis of combined coal-petrographic and palaeobotanical characteristics. The taphocoenoses are related to the facies types, which are largely determined by nutrient availability and the groundwater table. The following types, named after the characterizing floral elements, are recognised: (1) F-facies (Riparian-forest facies). Taphocoenosis is characterised by *Tetraclinis*, *Salix*, *Alnus*, *Acer*, *Liquidambar,* and ferns. Root remains are present. The facies represents a bottomland forest. (2) K-facies (*Glyptostrobus* mire (swamp) facies). Taphocoenosis is dominated by conifer remains, often with big *Glyptostrobus* woods in characteristic superposition. The facies represents a eutrophic peatland (forest swamp facies). (3) S-facies (*Sequoia* open canopy-woodland facies). Taphocoenosis is dominated by conifer remains, often *Sequoia* on topographic highs; other big conifers *Taiwania* and *Cunninghamia* can germinate and grow. Around these conifers, *Magnolia*, *Kalmiophyllum*, *Quercus*, and *Ocotea* have habitats. (4) A-facies (Angiospermous bush mire facies (bush-swamp facies). Taphocoenosis is dominated by angiosperms such as *Magnolia*, *Quercus*, and Ericaceae, with subordinate remains of conifers such as *Taiwania* and *Cunninghamia*. The tree islands occupy increasing areas and connect together into a large unit of mire. (5) G-facies (Glumiflorae reed facies). Taphocoenosis yields no wood but mainly fragments of *Graminophyllum*, *Glumophyllum*, *Brasenia*, *Myrica*, and palms. The G-stratum is embedded in *Pinus*-Strata. (6) O-facies (*Sphagnum* bog facies). Strata including up to 30% *Sphagnumsporites* and charred *Sphagnum* tissues were found in all layers of the 2nd MFH. The *Sphagnum* strata are embedded in G-facies. (7) P-facies (*Pinus* woodland facies). Taphocoenosis dominated by remains of conifer woodland with mainly Pinaceae, furthermore, palms and angiosperms of the families Cyrillaceae and Ericaceae. (8) MCy-facies (cf. *Cryptomeria-conferta* bog facies). Apart from dominant *Marcoduria*-roots, taphocoenosis probably contains the conifer *Cryptomeria*. The facies represents a deposit of material from an extremely nutrient-

poor and acidic environment. (9) MSc-facies (*Sciadopitys* bog facies). Apart from dominant *Marcoduria*-roots, taphocoenosis includes the conifers *Sciadopitys* and *Cathaya*; furthermore, angiosperms such as *Myrica, Cyrilla*, *Kalmiophyllum, Phyllites*, and *Illipophyllum* (cf. Sapotaceae) are present. The facies represents a deposit of material from an extremely nutrient-poor and acidic environment. (10) X-facies (*Cupressospermum* forested mire facies). Taphocoenosis is dominated by the conifer *Cupressospermum saxonicum*. The facies represents a eutrophic mire deposit. (11) MQu-facies (*Quasisequoia* mire (bog) facies sensu Schneider, 2009). Taphocoenosis presents a deposit of remains of *Quasisequoioxylon piskowitzense*, *Enormicutis coronata*, *Inaperturopollenites dubius* (a pollen assigned to Taxodiaceae), and *Marcoduria*-roots.

3. Samples

Lignite and fossil wood samples were collected in the open-cast mines Welzow-Süd (WS), Meuro (M), and Piskowitz (Pis), located in the Lusatia lignite mining district in Saxony, Federal Republic of Germany (Fig. 2B). The Pis lignite collected from the upper embankment are most likely age-equivalent to the Middle Miocene 2nd MFH. The lignite samples from the WS open-cast mine were collected by Jolanta Kus, from the M open-cast mine by Wilfrid Schneider, and from the Pis open-cast mine by Jochen Rascher from the GEOmontan, Freiberg, Federal Republic of Germany. Fossil wood samples were collected by Martina Dolezych and were as follows: *Taxodioxylon cryptomerioides* (LIMS-Nr.: 1708242, from the WS open-cast mine, Germany, 1. Flözbank, coal seam Nr. 2, M-facies); *Sciadopityoxylon wettsteinii* (LIMS-Nr.: 1708243, from M open-cast mine, Federal Republic of Germany, 2. Flözbank, coal seam Nr. 2, M-facies) and *Quasisequoioxylon piskowitzense* (LIMS-Nr.: 1708244, Pis open-cast mine, Saxony, Federal Republic of Germany) (Table 1). The Lims-Nr. indicates the sample number within the Federal Institute for Geosciences and Natural Resources (BGR) sample database. Identification and determinatnion of xylotomical taxa of the three fossil wood samples were conducted at the Senckenberg Natural History Collections Dresden, Dresden, Federal Republic of Germany and were first published in Kus et al. (2020). The species were also identified from other open-cast mines in the Lusatia lignite mining district (Dolezych, 2005, 2011). Fossil wood samples (30–40 g) were ground and 0.2–0.63 mm particle fraction was used for preparation of thin sections for xylotomic investigation (Dolezych, 2005; Kus et al., 2020). The referenced material (specimens) is housed at private collection of German paleobotanist and geologist Martina Dolezych and maintained to support research at the Senckenberg Natural History Collections Dresden, Dresden, Federal Republic of Germany. For the sake of comparison, intact heartwood tissues of the respective present-day analogues were also investigated: *Sequoiadendron giganteum* and *Cryptomeria japonica* were sampled by Ulrich Pietzarka from the Botanical Garden at Tharandt at the Technical University Dresden, Federal Republic of Germany, whereas *Sciadopitys verticillata* was collected from the garden of Wilfrid Schneider at Hoyerswerda, Saxony, Federal Republic of Germany

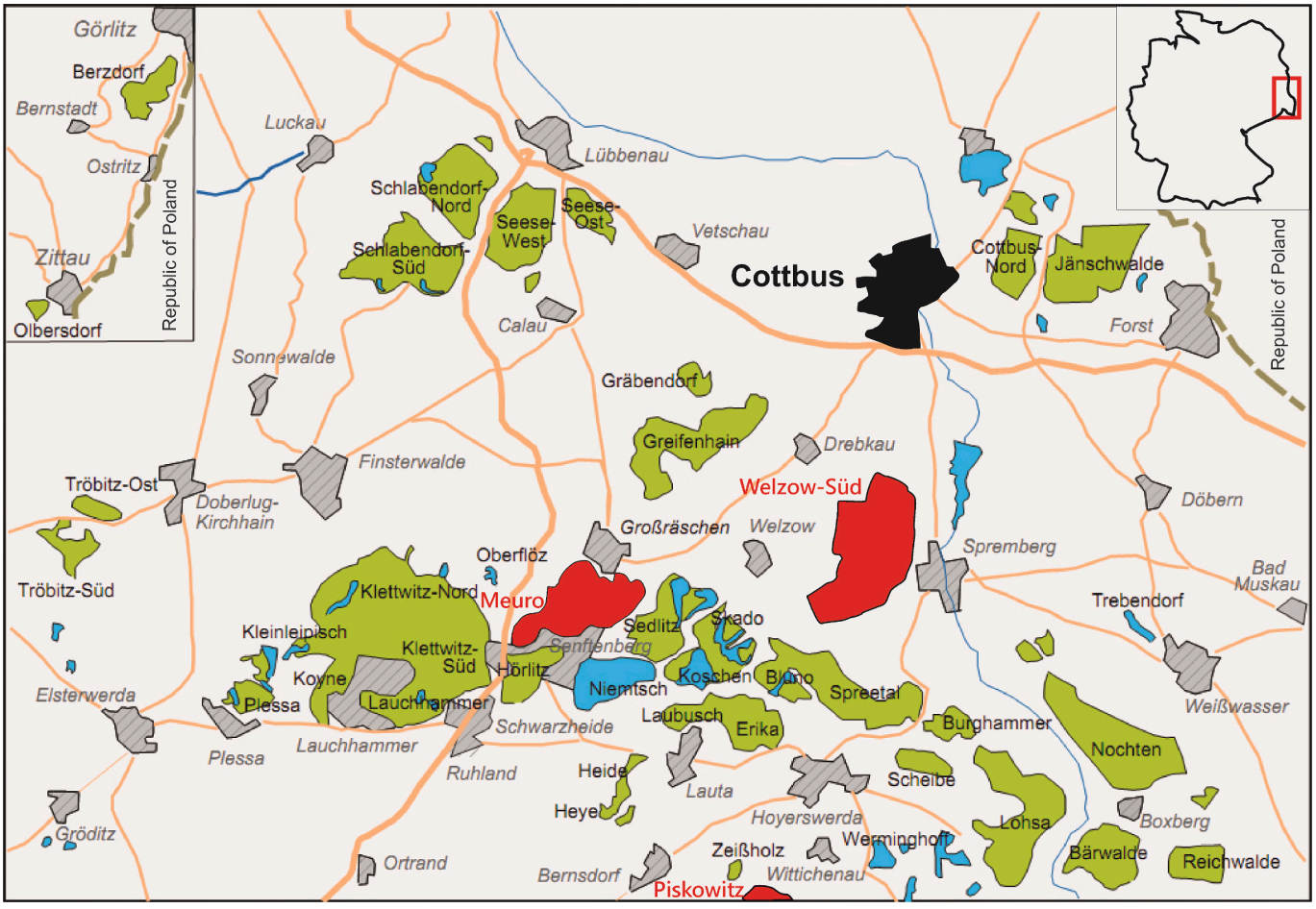


Fig. 2. Overview map of the Lusatia Lignite District, indicating lignite deposits in closed and active open-cast mines. In red: study area of an active open-cast mine of Welzow-Süd (WS), and closed open-mines of Meuro (M), and Piskowitz (Pis). In green: other closed and active open-cast mines; in blue: lakes (flooded, disused open-cast mines); in grey: townships. The source of Federal Republic of Germany location map is Wikimedia Commons contributors, "File:Germany location map.svg", Wikimedia Commons, the free media repository (accessed, December 14th, 2021). (For interpretation of the references to colour in this figure legend, the reader is referred to the web version of this article.)

Table 1
The studied fossil wood, recent wood, and lignite samples.

Sample ID	Sample type	Species	Source	Stratigraphy	Facies	References
LIMS-Nr.: 1708242	Fossil wood	*Taxodioxylon cryptomerioides* Schönfeld	Welzow-Süd (WS) open-cast mine, Germany	1. Flözbank, Second Lusatian lignite seam (2nd MFH)	M-facies	Dolezych and Schneider (2006); Dolezych (2011); Kus et al. (2020)
LIMS-Nr.: 1708243	Fossil wood	*Sciadopityoxylon wettsteinii* Jurasky	Meuro (M) open-cast mine, Germany	Second Lusatian lignite seam (2nd MFH)	M-facies	Dolezych and Schneider (2007); Mann et al. (2017); Kus et al. (2020)
LIMS-Nr.: 1708244	Fossil wood	*Quasisequoioxylon piskowitzense* Dolezych et Burgh	Piskowitz (Pis) open-cast mine, Germany	Lignite seam Piskowitz*	NA	Dolezych (2005, 2011); Kus et al. (2020)
LIMS-Nr.: NA	Modern wood	*Sequoiadendron giganteum* (Lindl.) J.Buchholz	Botanical Garden of Tharandt at the Technical University Dresden, Germany	Recent	NA	NA
LIMS-Nr.: NA	Modern wood	*Cryptomeria japonica* D. Don	Botanical Garden of Tharandt at the Technical University Dresden, Germany	Recent	NA	NA
LIMS-Nr.: NA	Modern wood	*Sciadopitys verticillata* Siebold & Zucc.	Garden of Dr. Wilfrid Schneider at Hoyerswerda, Saxony, Germany	Recent	NA	NA
LIMS-Nr.: 1900123 1900124	Lignite WS 1 WS 2	NA	Welzow-Süd (WS) open-cast mine, Germany	Second Lusatian lignite seam (2nd MFH)	NA	Feiler and Sschneider (1987); Escher et al. (2020)
K-Nr.: 21004	Lignite	NA	Meuro (M) open-cast mine, Germany	Second Lusatian lignite seam (2nd MFH)	NA	Mai (2001); Schellenberger (2011); Escher et al. (2020)
LIMS-Nr.: 1827171 1827172 1827173	Lignite Pis 1 Pis 2 Pis 3	NA	Piskowitz (Pis) open-cast mine, Germany	Lignite seam Piskowitz*	NA	Heinicke (1905); Süß (1959); Schneider (2009, 2010)

Legend: LIMS-Nr.: – sample ID of lignite from Kus et al. (2020); NA – non-available information; * – most likely age-equivalent to Second Lusatian lignite seam (2nd MFH) of Middle Miocene age; M-facies – *Marcoduria*-Facies.

(Table 1).

4. Methods

4.1. Incident light microscopy and CLSM

The preparation of polished blocks of fossil wood was conducted in LAOP (Laboratories for Applied Organic Petrology), Tübingen, following the German Standard Methods DIN 22020–2: 1998–08 and the guidelines published in Taylor et al. (1998). Thin sections of fossil wood samples were prepared in BGR (Federal Institute for Geosciences and Natural Resources, Hannover, Federal Republic of Germany).

Optical microscopy examinations of polished blocks and thin sections were carried out at the Federal Institute for Geosciences and Natural Resources (BGR, Hannover) under non-polarised and polarised light, at magnification of 500× and 1000× using a Leica DMRX incident-light microscope equipped with an MP*V* Compact 2 microphotometer photomultiplier tube (PMT), halogen lamp (12 V, 100 W), HBO® Lamp (103 W/2, 12 V), and Leica Oil P 50×/0.85 oil-immersion objective. Leica Type F immersion oil ne = 1.518 (23 °C) was used for microscopic examinations. Filters used for analysis in fluorescence mode were Leica excitation filter BP 355–425, dichroic mirror RKP 455, and barrier filter LP 460. Photomicrographs were captured under incident white light and blue-light excitation using a Leica digital fluorescence camera DC 300 F at 1.300 × 1030 pixels and were stored using Image Access Premium 09 software. The maceral nomenclature applied in this paper follows ICCP System 1994 adopted by the International Committee for Coal and Organic Petrology (Sýkorová et al., 2005; Pickel et al., 2017).

The prepared thin sections were analyzed by the Leica Confocal Scanning System (CLSM), TCS SP5 II at the Federal Institute for Geosciences and Natural Resources (BGR, Hannover). The confocal system is equipped with an inverted microscope DMI 6000 CS Bino fitted with visual (VIS) Ar-laser with laser lines at 458 nm, 476 nm, 488 nm, 496 nm, and 514 nm; the DPSS-laser at 561 nm; and the HeNe-laser at 633 nm. The confocal images were acquired in fluorescence mode using a HCX PLAPO oil immersion objective (total magnification 630×, NA 1.4) with an Acousto-Optical-Beam-Splitter (AOBS®). The confocal scanning system is composed of free programmable scanners with frequencies ranging from 1 to 1400 Hz. Three photomultiplier tubes represent the filter-free spectral detectors. The emitted autofluorescence displayed in the CLSM images, projections, and 3-D reconstructions was generated by a selection of distinct laser lines of the Ar, DPSS, and HeNe lasers and detected at specific emission wavelengths by the spectral imaging detector SP. The CLSM images display intensity values measured by the chosen spectral detectors and represent 256 greyscale images. The greyscale images are converted to false colour images by assigning different primary colours to each of the detector channels. The primary colour assignment assures that the false colour image corresponds to a very similar colour range in a real colour photomicrograph from incident light microscopy. The false colour image is displayed using an RGB colour model. Confocal images and 3-D reconstructions were produced using Leica Application Suite Advanced Fluorescence (LAS AF SP5 3D Visualisation) software version 2.4.1. During image acquisition in XY, XZ, YZ, and XYZ modes, each line was scanned bidirectional eight times and images were captured as 2-D images in up to 1024 × 1024 pixels, in *.jpg format. The consecutive confocal images obtained at increments of up to 0.25 µm were stacked as optical sections in the Z direction using the maximum projection method to create a composite 3-D projection.

4.2. Calcofluor-stained CLSM

Polished sections of the samples were stained with Calcofluor White (0.01% aq.) for 10 min at room temperature before being examined under a Leica SP5 confocal microscope using 355 nm excitation and 430–550 nm emission (Kitin et al., 2020). The calcofluor-stained CLSM mentod was applied at Scion, Rotorua, New Zealand.

4.3. SEM Investigations

Scanning electron microscopy and energy-dispersive X-ray

spectroscopy (SEM/EDS) analyses were carried out using an MLA 650F (Quanta 650 FEG system, FEI Company) equipped with two EDX detectors (XFlash Detector 5030, Silicon Drift Detector; Bruker Nano) for semi-quantitative element analysis without standardization. The SEM was operated at 15 kV in high-vacuum mode, with a 5.5 nm beam spot size. To improve the quality of the analyses, the polished sections were coated with carbon to ensure surface conductivity. Back-scattered electron (BSE; concentric back-scattered [CBS] detector); and secondary electron (SE) detectors were used. The SEM investigations were carried out at the Federal Institute for Geosciences and Natural Resources (BGR, Hannover, Federal Republic of Germany).

4.4. Cellulose examination

For the holocellulose content determination, the fossil and modern wood samples (30 to 40 g) were ground using a hammer mill. The samples were sieved and the 0.2 to 0.63 mm particle fraction was used for further analyses. The determination of the holocellulose content was accomplished using the method of Rowell et al. (2012). About 0.1 g of a sample was placed into a glass tube and 2.5 ml of hot distilled water, 20 µl acetic acid (96%), and 40 mg sodium chlorite were added. The tube was covered with a glass stopper and the mixture was heated in a water bath at 70 °C for 1 h. After each succeeding hour, portions of 20 µl acetic acid and 40 mg sodium chlorite were added. This process was repeated seven times. After the last cycle, samples were left in the water bath overnight. At the end of a 24 h reaction, samples were cooled and filtered on a G2 glass funnel filter, and the holocellulose was washed with 10 ml acetone and water until the yellow colour was removed. The prepared holocellulose was dried at 105 °C and then weighed. As fossil wood samples can contain significant amounts of inorganic components which remain in the prepared holocellulose, the ash yield was determined and the results were corrected accordingly. The ash yield determination of the holocellulose was done as follows: 25 mg of the prepared holocellulose was weighed into an alumina crucible and heated in a furnace to a final temperature of 600 ± 10 °C over a period of 60 min. Final temperature was maintained for 120 min. After cooling to ambient temperature, the remaining solids were weighed.

The cellulose content determination was carried out using the method of Kürschner and Hoffer (1929) as follows: 1 g of ground and sieved sample was refluxed with 25 ml nitric acid (30%):ethanol (96%), 1:4 (*v*/v) extraction solution for one hour, representing one digestion cycle. The solution was decanted and the digestion cycle was repeated using 25 ml of the same solvent. For modern wood samples 3 cycles were applied, whereas for fossil samples 6 cycles were applied. The produced cellulose was filtered using a G2 glass filter funnel, washed with 96% ethanol (10 ml) and hot water (500 ml). Cellulose was dried at 105 °C and weighed. Content of cellulose was given in % on dry wood basis. Three parallel measurements were run for each sample. The described method of Kürschner and Hoffer (1929) involves digestion of samples using nitric acid and ethanol in various cycles depending on sample complexity. Digestion dissolves lignin and hemicelluloses yielding yellowish-white cellulose as a residue. One of the drawbacks of the method is if there are interfering compounds present (resin acids) or if the structure of lignin is altered in such way that it becomes insoluble in the digestion medium. It was observed that the usual two digestion steps were not enough for the studied samples (colour was still light brown); thus, digestion was repeated with a total of six consecutive steps for the fossil samples. However, the colour after that was still brown. The holocellulose content determination was carried out at the University of Sopron, Sopron, Hungary.

4.5. Thermogravimetric analysis

Thermogravimetric analysis (TGA) of the fossil and modern wood samples (30 mg) was performed by a Mettler Toledo TGA/DSC 1 type thermogravimeter (Mettler Toledo, Columbus, Ohio, USA), using alumina crucibles, a constant heating rate of 10 °C/min and air atmosphere between 25 and 650 °C. Ash yield of the samples was estimated from the final mass loss at 600 °C. The TGA investigations were performed at University of Sopron, Sopron, Hungary.

4.6. Elemental analysis, ash yields and Rock-Eval pyrolysis

Elemental analysis (*V*ario EL III, CHNS/O Elemental Analyzer, Vario MAX CNS Elementar Analyzer, Elementar Analysensysteme GmbH) was performed to determine the contents of total carbon, total nitrogen, and total sulphur. About 80–100 mg of the samples were weighed into ceramic crucibles and tungsten oxide catalyst was added. Combustion was carried out at 1140 °C.

For the determination of the Fe, content the samples were first digested using nitric acid:hydrogen peroxide 5:2 *v*/v mixture in a VELP Scientifica DK20 digester (VELP Scientific Srl, Usmate, Italy) at 180 °C for 60 min, then measurement was carried out using an ICE 3500 type Atomic Absorption Spectrometer (Thermo Fisher Scientific, Waltham, USA).

The TOC contents were determined on a LECO CS-230 (Leco Instrumente, Federal Republic of Germany) on carbonate-free sample aliquots. About 20 mg of each sample was burned in a high-frequency induction furnace in an oxygen atmosphere by use of the absorption signal at the infrared (IR) detector. The instrument was calibrated using commercially available standards (LECO). Reproducibility of the measurements was ±0.02%.

Ash yield determination in lignite, fossil and recent wood samples followed ISO 1171 (1997).

Rock-Eval pyrolysis of lignite, fossil and modern wood samples was performed on a TOC/Rock-Eval-6 apparatus following a standard procedure described in Espitalié et al. (1985) and Lafargue et al. (1998). The IFP 160000 standard has been used for calibration. The programmed heating rate of both the pyrolysis and the oxidation ovens was 25 °C /min. Pyrolysis was done in the temperature range from 300 to 650 °C, while oxidation was performed up to 850 °C. The entire process was managed using the software "RockSix".

Elemental analysis (Vario MAX CNS Elementar Analyzer, Elementar Analysensysteme GmbH) was carried out at the at University of Sopron, Sopron, Hungary. Elemental analysis (Vario EL III, CHNS/O Elemental Analyzer), ash yields, and Rock-Eval pyrolysis were performed at the University of Belgrade, Belgrade, Serbia.

4.7. Micro-Fourier transform infrared (micro-FTIR) spectroscopy

The micro-FTIR analysis was performed on polished sections of fossil wood samples on a Nicolet 6700 spectrometer connected to a Nicolet Continuum microscope operated in reflectance mode. The resolution was 4 cm^{-1} over the range 700–4000 cm^{-1} wavenumber, and a golden plate was used to generate a background spectrum. Reflectance micro-FTIR spectra were subjected to Kramers-Kronig transformation to correct for transflectance and band shifts. IR-peak assignments to functional groups followed published sources, for example Chen et al. (2012), Rochdi and Landais (1991), and Wang and Griffiths (1985). Cellulose and lignin bands assignment followed that in Drobniak and Mastalerz (2006), with the dominance of cellulose bands occurring in the 1000–1100 cm^{-1} region and the majority of lignin bands located in the 1100–1300 cm^{-1} region. Ten spectra were generated on each sample along the transect of the wood, and then the OMNIC program was used for obtaining the average spectrum that was used to determine peak integration areas. The micro-FTIR analysis was performed at the Indiana University, Bloomington, USA.

4.8. Stable carbon isotope ($\delta^{13}C$) analysis

For bulk carbon isotope analysis of TOC, powdered fossil wood samples were treated with HCl to remove inorganic carbon. Carbonate-

free samples were placed into tin foil boats and combusted using an elemental analyser (Flash EA 1112) at 1020 °C in an excess of oxygen. The resulting CO_2, separated by column chromatography, was analyzed online by a Delta-V isotope ratio mass spectrometer (ThermoFisher Scientific). Stable isotope ratios are reported in delta notation ($\delta^{13}C$) relative to the Vienna-Pee Dee Belemnite (V-PDB) standard. The reproducibility of the total analytical procedure was in the range of 0.1–0.2 ‰. The stable carbon isotope ($^{\delta 13}C$) analysis was carried out at the James Madison University, Harrisonburg, USA.

4.9. Biomarker analysis

Extractable organic matter (EOM, bitumen) was extracted from the pulverised lignite using Soxhlet extraction with dichloromethane (DCM)/methanol (MeOH) azeotrope (88:12, v:v) over 48 h. Copper was added to remove elemental sulphur during the extraction process. The asphaltenes were precipitated from bitumen with *n*-hexane-DCM solution (80:1) and the remainder (maltenes) was separated into aliphatic, aromatic and NSO (polar fraction, which contains nitrogen, sulphur, and oxygen compounds) fractions using micro-column chromatography. Silica gel 60, previously activated at 180 °C for 8 h, was used as adsorbent (0.6 g SiO_2 per 20 mg of sample). The aliphatic fraction was eluted with *n*-hexane, the aromatic fraction with mixture of *n*-hexane and DCM (7:3, v:v), and the polar fraction with chloroform/MeOH mixture (1:1, v:v).

Aliphatic and aromatic fractions (dissolved in *n*-hexane) were analyzed by gas chromatography–mass spectrometry (GC–MS). A gas chromatograph Agilent 7890 A GC (HP-5MS column, 30 m × 0.25 mm, 0.25 μm film thickness, helium carrier gas with constant flow of 1.5 cm^3/min) coupled to an Agilent 5975C mass selective detector (70 eV) was used. Details of GC–MS analysis are given in a previous publication (Kojić et al., 2021). The individual peaks were identified based on the mass spectra and retention times. Data were processed with a ChemStation Enhanced Data Analysis Software. Absolute concentrations of individual compounds were calculated using peak areas from Total Ion Chromatograms (TICs) of aliphatic and aromatic fractions in relation to those of internal standards (deuterated *n*-tetracosane for aliphatic hydrocarbons and deuterated naphthalene for aromatic compounds). The concentrations were normalised against TOC contents. Additionally, for the calculation of certain biomarker parameters, *n*-alkanes, sterenes and hopanoids were integrated from their specific mass chromatograms (aliphatic fractions) *m/z* 71, *m/z* 215, and *m/z* 191, respectively.

Aliquots (5 g) of dry fossil and modern wood fragments were extracted for approximately 1 h using a mixture of DCM and MeOH in a Dionex ASE 200 accelerated solvent extractor. Zymark Turbo Vap 500 device was used to separate the extracts from the solvent. Extracts were dissolved in a mixture of *n*-hexane:DCM (80:1, v:v) and asphaltenes were subsequently separated by centrifugation. The *n*-hexane-soluble organic compounds (maltenes) were subdivided into aliphatic and aromatic hydrocarbons and polar NSO components using a Köhnen-Willsch MPLC (medium pressure liquid chromatography) instrument (Radke et al., 1980).

Aliphatic and aromatic fractions were analyzed using a gas chromatograph equipped with a 60 m DB-5MS fused silica column (i.d. = 0.25 mm; 0.25 mm film thickness) and coupled to a ThermoFisher ISQ quadrupole mass spectrometer (GC–MS system). GC–MS conditions were the same, as described by Bechtel et al. (2019). Data were processed using an Xcalibur data system. Individual compounds were identified based on retention times in TICs and by comparison of the mass spectra with published data. Relative percentages and absolute concentrations of various compound groups were calculated using peak areas in TICs in relation to those of internal standards added in known concentrations (squalane for the aliphatic fraction and 11′-binaphthyl for the aromatic fraction). The concentrations were normalised to the TOC contents.

Fatty acids were separated from the polar fraction by saponification with 6% KOH solution in MeOH at 80 °C for 3 h. The neutral polar lipids (mostly alcohols) were recovered by extracting with *n*-hexane (3 times). After separation of neutral polar lipids, the KOH/MeOH solution was acidified with 50% HCl and then fatty acids (FAs) were extracted by *n*-hexane (3 times). The obtained *n*-hexane extract, containing FAs, was dried using anhydrous Na_2SO_4. Fatty acids fraction was further derivatised with BSTFA (*N*,*O*-bis(tri methylsilyl)trifluoroacetamide) for 1 h at 80 °C to form trimethylsilyl esters and analyzed by GC–MS, using the same procedure as for the aromatic fraction of wood samples.

The biomarker analyses were carried out at the Montanuniversität Leoben, Leoben, Austria and the University of Belgrade, Belgrade, Serbia.

5. Results

5.1. Incident light microscopy-image analysis

The polished lignite blocks from fossil wood samples (Table 1), investigated by means of non-polarised incident white light and UV, are displayed in Fig. 3.

The anatomical features observed in non-polarised mode in the transverse section include, among others, an abrupt transition from early to late wood occurring in secondary xylem (Fig. 3A–C). The abrupt transitions might be modified by environmental factors of drought, repeated defoliation, etc., and triggers such as severe cold, substrate, soil pH, soil moisture availability, etc. These triggers, acting like stressors, can increase the vulnerability of the fossil tree to bacteria and wood detrition. Contrary to the latewood cells, the early cells occasionally appear to be compressed. However, the overall degree of tissue compression prior to or during the early phases of peatification is minor and is inferred to fossil wood compression during sedimentation.

The existence of structural integrity associated with the multilayered cell walls is well-presented. The often-zonated cell wall is visible in Fig. 3D and can be differentiated into three distinct layers on the μm scale. The cell walls of the late wood are occasionally associated with microcracks penetrating the inner layer only (Figs. 3E–F). The cell walls of the earlywood are generally lacking similar microcracks.

No traumatic resin ducts were observed, leading to the assumption that resin structures related to biotic and abiotic stressors, such as insect attack, pathogen infection, frost damage, or physical wounding, were largely lacking. Instead, polyphenolic parenchyma cells (PP cells) are present (Figs. 3G–H), being sites for synthesis and storage of phenolic compounds. These are of defensive character. According to Krokene et al. (2008), the PP cells in recent conifer species are specialised for synthesis and storage of phenolic compounds, being abundant in the xylem of all conifers. The PP cells are also involved in a range of inducible defense responses, including activation of existing PP cells, production of new PP cells, and formation of wound periderm. Radially orientated rays (Fig. 3I) consist of thin-walled parenchyma cells and are supposed to transport water, minerals, and nutrients. The rays are occasionally resinous and abnormally enlarged. The cell walls of rays are smooth.

Thin sections of xylitic tissue from fossil wood samples, investigated by means of non-polarised and polarised transmitted light microscopy, are shown in Fig. 4. The cell walls of fossil woody tissue display optically anisotropic entities (Figs. 4C, F). They exhibit maxima and minima of light intensity under crossed polars. The xylite show an undulating extinction, which in some cases exhibits a helical nature. In contrast with modern cellulose material, this is distinctive for fossil cellulose fibers. Tissue birefringence results from the anisotropy of the fibrous structure, which forms the cellular matrix. The cell wall optical anisotropy is due to preserved cellulose fibers, which are important agents in soft tissue depolarization and birefringence. Sen (1956) and Barghoorn (1952) pointed out the heterogeneity of cellulose in different parts of primary and secondary cell walls of fossilised woody tissues.

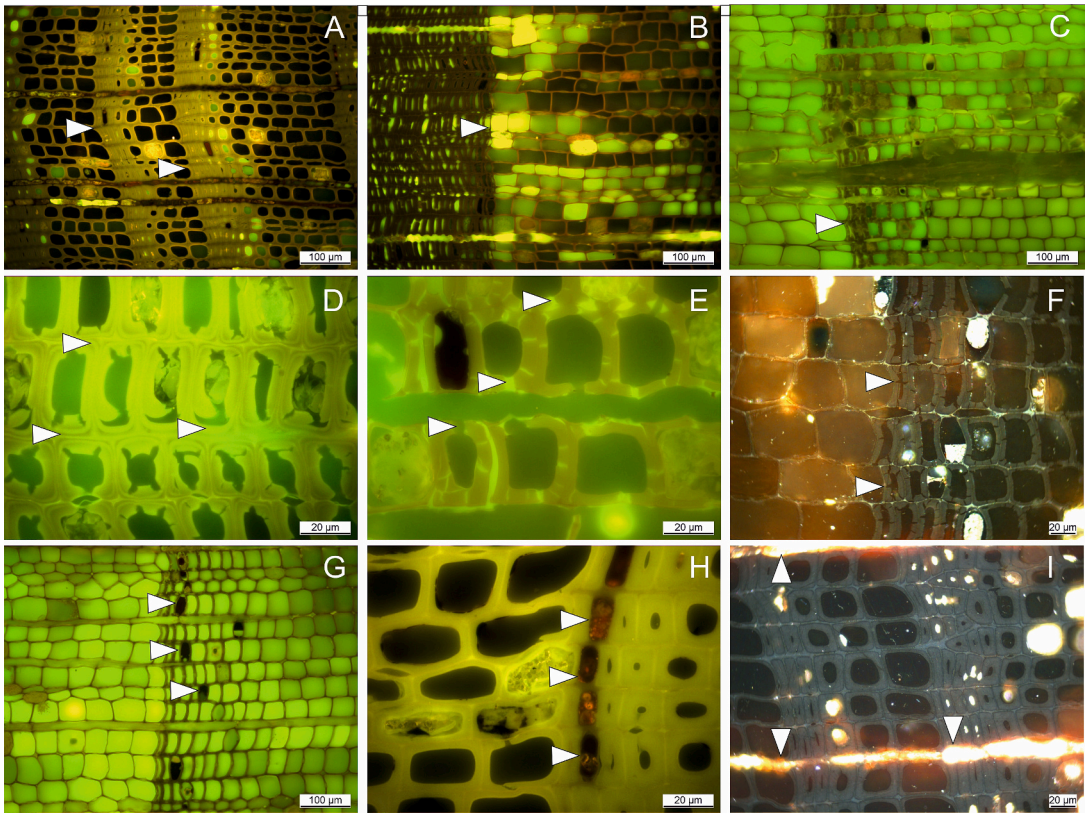


Fig. 3. Photomicrographs of xylitic tissue of fossil wood samples in polished blocks. A, B, C – Abrupt transitions from early to late wood. D – Multilayered cell walls. E–F – Extensive microcracking. G–H–I – Polyphenolic parenchyma cells (PP cells). I – Radially orientated rays. Photomicrographs are taken under non-polarised white light and UV-light with oil-immersion objective 50 × .

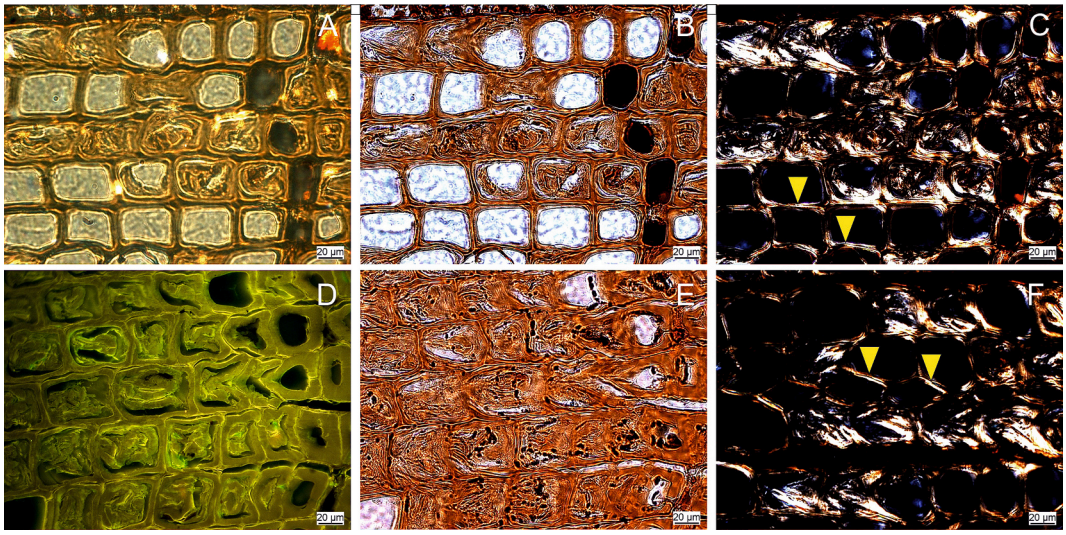


Fig. 4. Photomicrographs of xylitic tissue of fossil wood samples in thin sections. A – Xylite with polyphenolic parenchyma cells (PP cells) under transmitted light, bright field, and oriented at 90°. B – Xylite with polyphenolic parenchyma cells (PP cells) under transmitted light, bright field, and oriented at 90°. C, F – Optically anisotropic layer as observed and indicated under transmitted light, bright field, crossed polars. D, E – Xylite with polyphenolic parenchyma cells (PP cells) under UV fluorescence and under transmitted light, bright field, oriented at 90°, respectively. Photomicrographs are taken with oil-immersion objective 50 × .

5.2. CLSM-image analysis

Lignitic matter examined in thin sections under CLSM is represented by intact fossilised wood with well-preserved cellular tissue (Fig. 5).

In the microscopic transversal section, the xylem is composed of early- and latewood cells with a remarkable degree of preservation. The tissue, largely not humified and scarcely gelified, displays a discrete outline of the so-called annual rings (Fig. 5A). The non-deformed, non-degraded and non-flattened xylem tissues contain lignified cells characterised by well-preserved, non-porous walls. The respective cell walls display a characteristic zonated type of microstructure, characterised by varying fluorescence intensities (Figs. 5B). The primary cell walls are

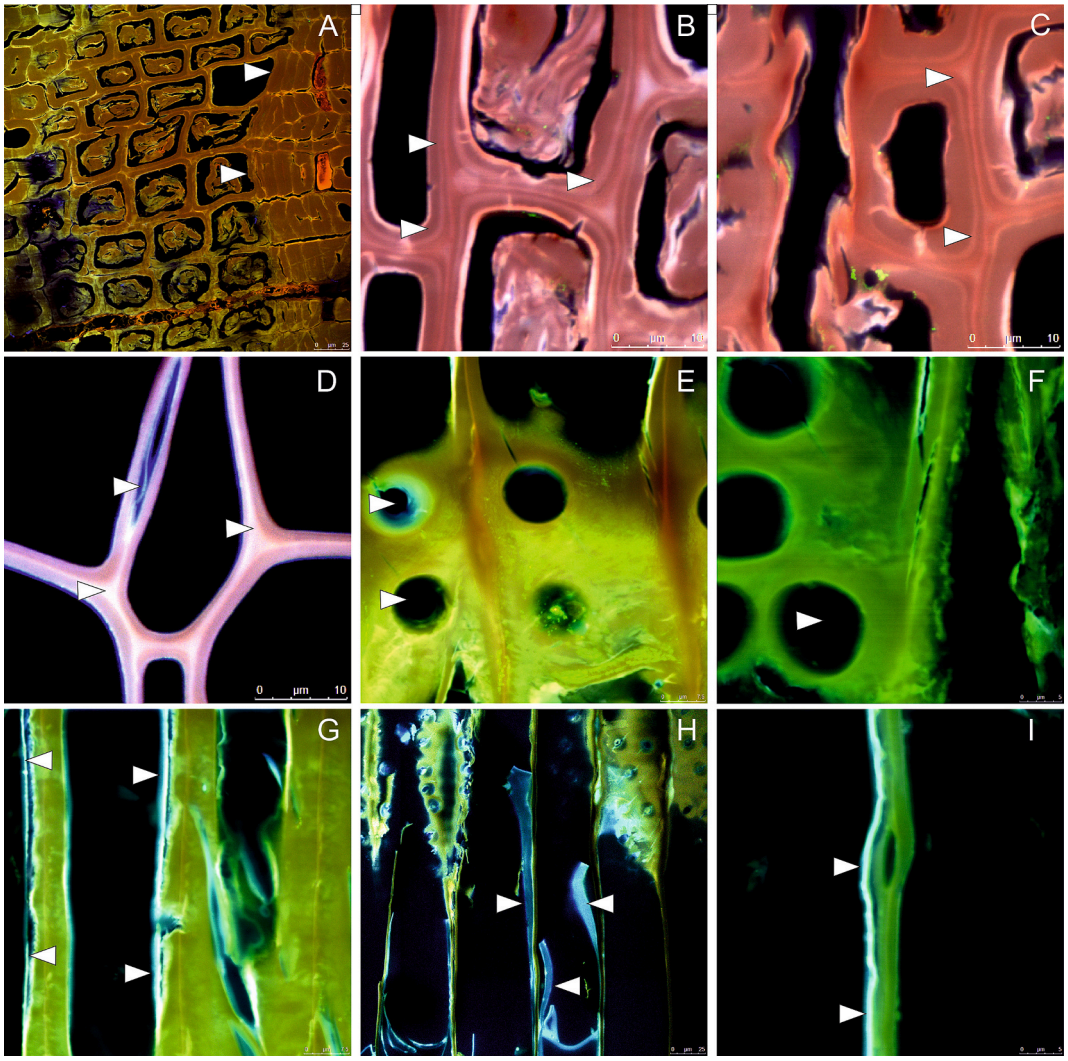


Fig. 5. Confocal laser-scanning microscope (CLSM) images of huminite examined in thin sections of lignite samples from the Piskowitz open-cast mines; CLSM images captured with oil objective 63 × and 1.4 NA by application of Argon, HeNe-lasers excitations with 458 nm, 488 nm, 594 nm laser lines, scan format 1024 × 1024. Excitation at 405 nm, 496 nm, 633 nm and emission at 410–800 nm. A – Transition from early- to latewood cells. Note, the remarkable degree of preservation. B to C – Triple zonation in earlywood cells of variable lateral extent and thickness. D – Middle lamella. E to F – Pits in transverse sections. G to H – Internal and external coating of high intensity, well-visible and well-differentiated structure as indicated by arrows.

associated often with middle lamella. The secondary cell walls display a triple zonation of variable lateral extent and thickness. The cell walls are associated with microfractures of crosscutting character. The diameter of microfractures ranges generally between 0.5 µm and 8.0 µm wide and stretches across the secondary wall and, to a minor extent, the primary cell wall; however, it does not lead to a wall disintegration. The primary and secondary cell walls are optically well-differentiated. The submicroscopic fillings of the observed cell lumens are partially present with relatively few exemptions, of most, probably phlobaphinite (Figs. 5A–B). This indicates that biochemical gelification of the woody tissue was not widespread and that impregnation of cell tissues by humic acid or fluid humus colloids was syngenetically or epigenetically not pertinent or hampered. Decreased biochemical gelification presumably can be related to relatively dry conditions (Sýkorová et al., 2005). In the transverse sections, intercellular canals or radial resin canals are present together with rays. The transverse section displays pits (Figs. 5E–F). Tracheids show open-bordered pit membranes with torus, as demonstrated and observed in coal pellets under incident-light microscope by Kus et al. (2020). The displayed cross sections showed, among others, tracheids, axial parenchyma, and a transition from early- to latewood stages. Figs. 5G–I show internal and external coating of high intensity displaying a relatively dense and fractured appearance. The coating resembles amorphous silica (opal-A) being precipitated and overlaying the cell walls of the parenchyma. The morphology of elongated, thin-walled stripes mirrors the lateral extent of the adjacent cell walls. Given that amorphous and crystalline silica as detected by SEM (refer to section 5.6 for further information) do not generally exhibit strong fluorescence, the intensity of the observed coating points to a reflected laser-related signal, confirming the silica-related morphology.

At present, there are two key theories which describe and hypothesise on the origin of huminite/vitrinite primary fluorescence: the first is the bitumen/cellulose theory (Ottenjann et al., 1982; Teichmüller and Durand, 1983; Russell and Barron, 1984) and the second is the lignin theory (Stout and Bensley, 1987). In the bitumen/cellulose theory, the decreased entrapment of bitumen or elimination of cellulose is suggested to account for the continuing loss of primary fluorescence. In the other theory, the presence of lignin is hypothesised to account for primary fluorescence of huminite/vitrinite macerals, with the lignin-rich middle lamella region displaying a higher level of fluorescence than the cellulose-rich secondary wall.

5.3. CLSM-emission intensity

Fluorescence spectroscopy of fossil woody tissues, i.e., xylite observed in thin sections under CLSM, was conducted on well-preserved cellular tissue, i.e., on early- and latewood cells. The intensity of signal emissions at diverse locations within the sample is related to the fluorescence emission colour of the examined wood cell walls and middle lamella as well as cell walls in the fossil woody tissue examined in Fig. 6 and Fig. 7, respectively. As displayed, the selected regions of interests (ROIs) are in areas of relatively higher and lower intensity fluorescence emissions (Fig. 6A–C). It was noted that the respective locations of higher and lower intensity fluorescence emissions correspond to the paler and darker colours of the studied wood cell walls and the middle lamella, respectively (Fig. 6D). The findings in fossil woody tissues contained in Miocene lignite deposits confirm the previously observed dependence between the fluorescence emission colour and emission intensity for *Tasmanites* enclosed in Devonian source rocks as studied by Hackley and Kus (2015) and Hackley et al. (2020). The emission spectra for middle lamellas and cell walls in the examined range from 400 to 800 nm show two peaks with different location of maximum relative intensity at several excitation wavelengths. It is also associated with a decaying tail. Fig. 6D shows that there are two peaks of about 485 and 550 nm. It has been demonstrated in previous studies that epoxy resin and recent wood samples emit these two bands, respectively (Gallot-Lavallée et al., 2005; Li et al., 2017; Mishra et al., 2018). The fluorescent intensity varies greatly, independently of the simultaneously applied excitation wavelengths of 405 nm, 489 nm, and 633 nm. These results indicate that autofluorescence signals do not depend on the excitation wavelength itself.

5.4. CLSM-spectral fluorescence parameters of xylite

The spectral emission signals of fossil woody tissues (cell walls of secondary xylem) were derived from randomly selected and representative ROI as displayed in Fig. 7. The emission data sets were generated with three laser excitation wavelengths (405 nm, 489 nm, and 633 nm) and were averaged from up to 10 ROIs. In Figs. 7D–F, emission spectra of fossilised xylite are displayed. These spectra show clearly again that two peak positions of individual fluorescent spectra resemble similar peaks displayed in Fig. 6D. The primary fluorescent peaks are at λ_{max} of about 485 nm, whereas the secondary shoulder peak appears at about 550 nm emission wavelengths (Figs. 7D–F). The second individual peaks vary marginally from sample to sample (Table 2; Fig. 7G). Results displayed in Fig. 7G show three averaged fluorescence emission spectra obtained for the three examined samples. The derived spectral fluorescence parameters are displayed in Table 2. The analyzed spectra between 500 nm and 800 nm are characterised by a similar shape, reflecting a primary peak and secondary shoulder peak. The primary lambda max ($\lambda 1_{max}$, nm) parameter is stable and ranges between 486 nm and 487 nm, whereas the secondary shoulder ($\lambda 2_{max}$, nm) varies to a larger extent between 542 nm and 546 nm. The highest $\lambda 2_{max}$ values and the red/green quotient (R650/G500) value were recorded for *Taxodioxylon cryptomerioides* in the WS open-cast mine. The same applies to the I_{max}/I500 spectral parameter (quotient of spectral intensity at maximum and

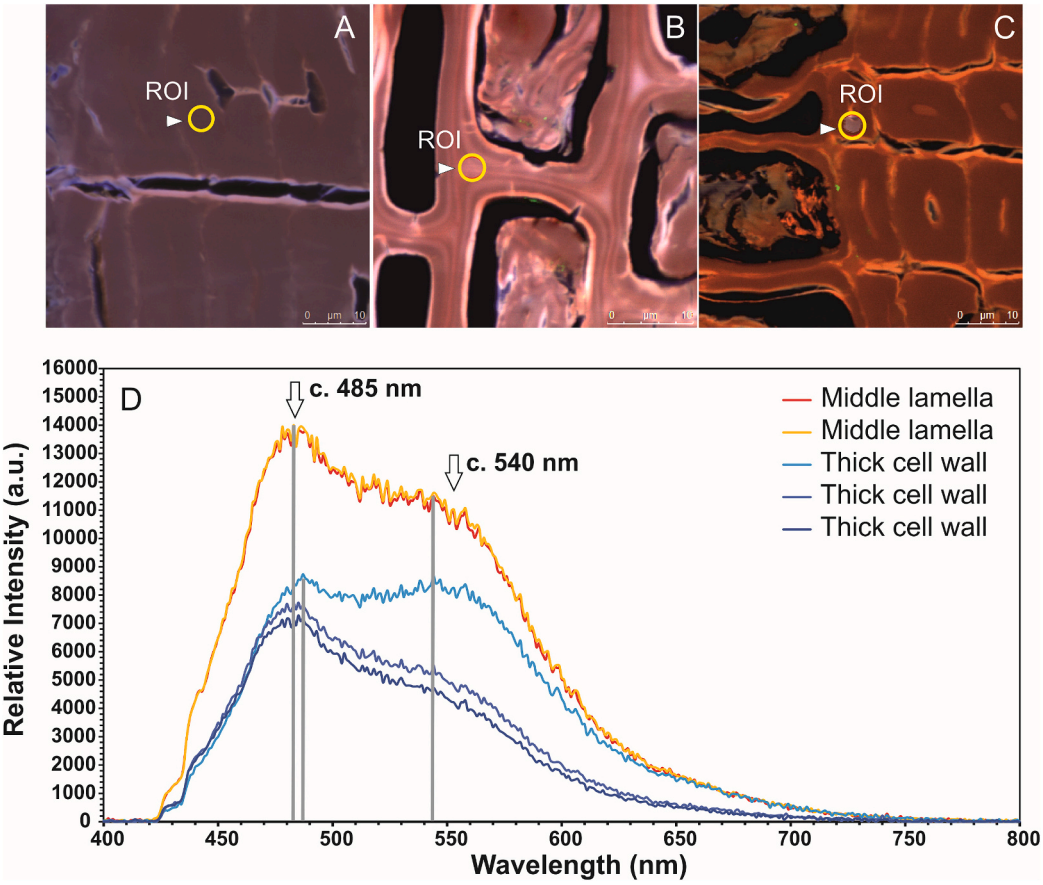


Fig. 6. Confocal laser scanning microscopy (CLSM) images and plots of emission spectra of xylite in cell walls. CLSM images captured with oil objective 63 × and 1.4 NA by application of Argon, HeNe-lasers excitations with 458 nm, 488 nm, 594 nm laser lines, and scan format 1024 × 1024. A to C – CLSM images of typical locations of ROI measurements in latewood cells. D – CLSM plots of emission spectra as a function of location within xylitic woody tissue in thin section.

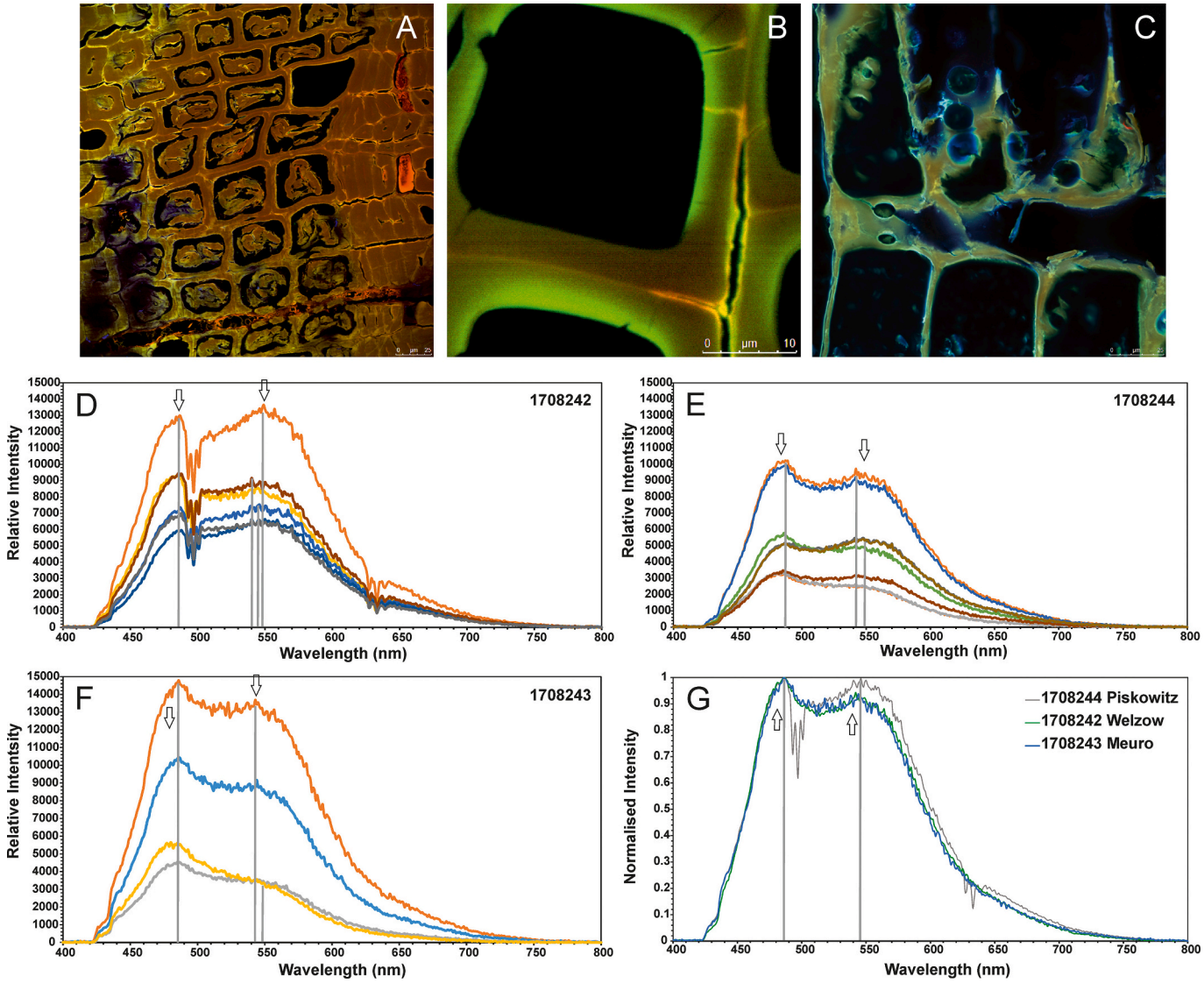


Fig. 7. Confocal laser scanning microscopy (CLSM) images and plots of emission spectra of xylite in cell walls. CLSM images captured with oil objective 63× and 1.4 NA by application of Argon, HeNe-lasers excitations with 458 nm, 488 nm, 594 nm laser lines, and scan format 1024 × 1024. A – Largely not humified cellular tissue (huminite) in transversal section in Welzow-Süd open-cast mine (*Taxodioxylon cryptomerioides*). B – Middle lamella and thick cell walls. Note, different fluorescence intensities in Meuro open-cast mine (*Sciadopityoxylon wettsteinii*). C – Earlywood cells in Piskowitz open-cast mine (*Quasisequoioxylon piskowitzense*). D – Individual emission spectra from cell walls from ROIs in WS. E – Individual emission spectra from cell walls from ROIs in M. F – Individual emission spectra from cell walls from ROIs in Pis. G – Averaged Emission spectra from cell walls from ROIs in WS, M, and Pis.

spectral intensity at 500 nm) with value of 1.26. The derived results for fossil wood samples of *Taxodioxylon cryptomerioides* differ largely from the remaining two samples. Although the number of data points is insufficient and a much higher data set would be required to provide statistical significance of the results, it can be stated that λ_{max} and R650/G500 parameter of the fossil wood tissues shows very poor correlation with the reflectance of early- and latewood cells and lignite rank data after Kus et al. (2020). Similar correlations between spectral parameters

Table 2
The CLSM-derived spectral parameters of the fossil wood samples.

Sample type	Sample ID	Species	$\lambda 1_{max}$ (nm)	SD	$\lambda 2_{max}$ (nm)	SD	R650/G500	Imax	Imax/I500	Source
Fossil wood	LIMS-Nr.: 1708242	*Taxodioxylon cryptomerioides* Schönfeld	487	0.003	546	0.010	0.24	8629	1.26	Welzow-Süd (WS) open-cast mine, Germany
	LIMS-Nr.: 1708243	*Sciadopityoxylon wettsteinii* Jurasky	487	0.002	544	0.001	0.15	8814	1.13	Meuro (M) open-cast mine, Germany
	LIMS-Nr.: 1708244	*Quasisequoioxylon piskowitzense* Dolezych et Burgh	486	0.001	542	0.013	0.19	5958	1.12	Piskowitz (Pis) open-cast mine, Germany

Legend: N – number of individual measurements; λ_{max} – Spectral maximum; SD – standard deviation; R650/G500 – red/green quotient; Imax – Intensity of the spectral maximum; Imax/I500 – quotient of spectral intensity at maximum and spectral intensity at 500 nm.

related to liptinite macerals (sporinite, alginite) and rank, performed with aid of a 150-W xenon lamp as an excitation source, were established for the Panandhro lignite (Misra, 1992). In thermally altered liptinite, Ting (1977) observed a corresponding shift of λ_{max} toward longer wavelengths, which is similar to the trend observed by Misra (1992).

5.5. Calcofluor-stained CLSM

The calcofluor staining reveals blue fluorescence from cellulosic parts of the walls and green or red fluorescence from lignified walls (Figs. 8A–C). The calcofluor signal is stronger in the latewood than in earlywood. Calcofluor staining indicates traces of residual cellulose associated with thick-walled latewood tracheids in all three samples but notably less staining in *Sciadopityoxylon wettsteinii* (Fig. 8B). *Taxodioxylon cryptomerioides* and *Sciadopityoxylon wettsteinii* are shown in transverse view, while *Quasisequoioxylon piskowitzense* is a radial longitudinal view. Multiseriated, oppositely arranged bordered pits are visible in *Quasisequoioxylon piskowitzense* as soft-rot cavities (Fig. 8C). It is not clear to what extent calcofluor staining allows detecting residual cellulose, as some fluorescence is originating from the resin used to prepare the polished sections, but staining associated with cell walls is most likely to represent residual cellulose. Fine-dispersed resins in cell walls (textinite A) was not observed in the examined samples.

5.6. SEM investigations

Amorphous (opal-A) and crystalline silica (opal-CT) have been detected in cells of secondary xylem tissues of the fossil wood samples (Figs. 9A–F). Opal-A is a non-crystalline form of hydrous silica ($SiO_2{\cdot}nH_2O$). It can often consist of submicrometre-sized spheres. Crystalline silica, the opal-CT ($SiO_2{\cdot}nH_2O$), typically consists of small bladed crystals that form aggregates of spherical lepispheres 5 to 20 μm in diameter (Figs. 9B–E). The opal-CT blades of the spheres reveal typical irregularly ragged edges. The spherical lepispheres are composed of blade-shape cristobalite and tridymite (Henchiri, 2007; Flörke et al., 1976). These two polymorphs of silica form these microcrystalline blades. The microcrystalline blades are also described as rosettes of authigenic silica formed during low-temperature diagenesis. Opal-A, as a morphologic expression of the incipient mineral phase of unstable amorphous silica, can be converted to opal-CT (Jones and Segnit, 1971). The origin of opal-CT precipitation from silica-rich solutions is well observed, as these rosettes of authigenic silica have grown in the residual pore space of the cell lumen.

Amorphous silica occurs partially as laminar coatings and cell infillings in early- and latewood tissues as well as in radially orientated rays (Figs. 9F–I). Although it is generally not associated with other minerals, an exemption is the co-occurrence of amorphous silica with a titanium mineral. Coatings dominantly display a multilayered character with a general thickness of < 5 μm. The multilayered lining is dissected in part by numerous microfractures, displaying a crosscutting character (Fig. 9F). This corrosion (microfracture) effect does not affect the cell wall itself. Opal-A does not display corrosion pitting. Lateral continuity of these multilayered coatings in the cell lumen is variable and ranges from laterally intact to dominantly fragmented (Figs. 9F, H).

5.7. Kürschner-Hoffer cellulose content

First, the cellulose content of wood samples (Table 3) was determined using a standard method for woody samples (Kürschner and Hoffer, 1929), which has been applied earlier successfully for fossil wood samples (Hámor-Vidó et al., 2010). The results of the Kürschner-Hoffer cellulose for modern wood samples (47.56 to 53.97%; Table 3) varied within the usual ranges of cellulose content (45 to 55%) (Fengel and Wegener, 1989). However, the corresponding values obtained for the fossil samples were unexpectedly high (53.04 to 54.31%). According to published data, cellulose levels of Miocene wood can vary between 1.4 and 43.1% (Schleser et al., 1999; Bechtel et al., 2002, 2007b). The published cellulose contents were determined using the sodium hydroxide/sodium chlorite method (Sohn and Reiff, 1942), as well as the acidified sodium chlorite oxidation of Wiesberg (1974). In general, the cellulose levels of fossil wood depend on age, environment, and other factors. In some Eocene samples, its content can reach up to 48% (Hatcher and Breger, 1982), providing the cellulose content is determined by applying sodium chlorite oxidation according to method of Passer (1957). As these obtained results indicate elevated cellulose values, a further explanation is required. Therefore, the cellulose content of the investigated samples was also evaluated using other more modern methods.

5.8. Chlorite holocellulose assay

The advantage of the chlorite holocellulose assay (Table 3) is that it is carried out in six to seven cycles using *in-situ* evolved chlorine gas as an oxidizing agent, which dissolves aromatic substances (lignin) and extractives out of the wood and leaves structural carbohydrates unaffected. The holocellulose content of the modern wood samples corresponds to the values (65.36 to 68.95%) usually determined for softwoods (Pettersen, 1984). The values of the fossil samples were lower (15.56 to 37.59%) compared to the respective modern samples (Table 3) and were found in the range usually determined for Miocene (5 to 23 Ma) fossil wood samples (1.4 to 43.1%) (Schleser et al., 1999; Bechtel et al., 2002, 2007b; Hámor-Vidó et al., 2010).

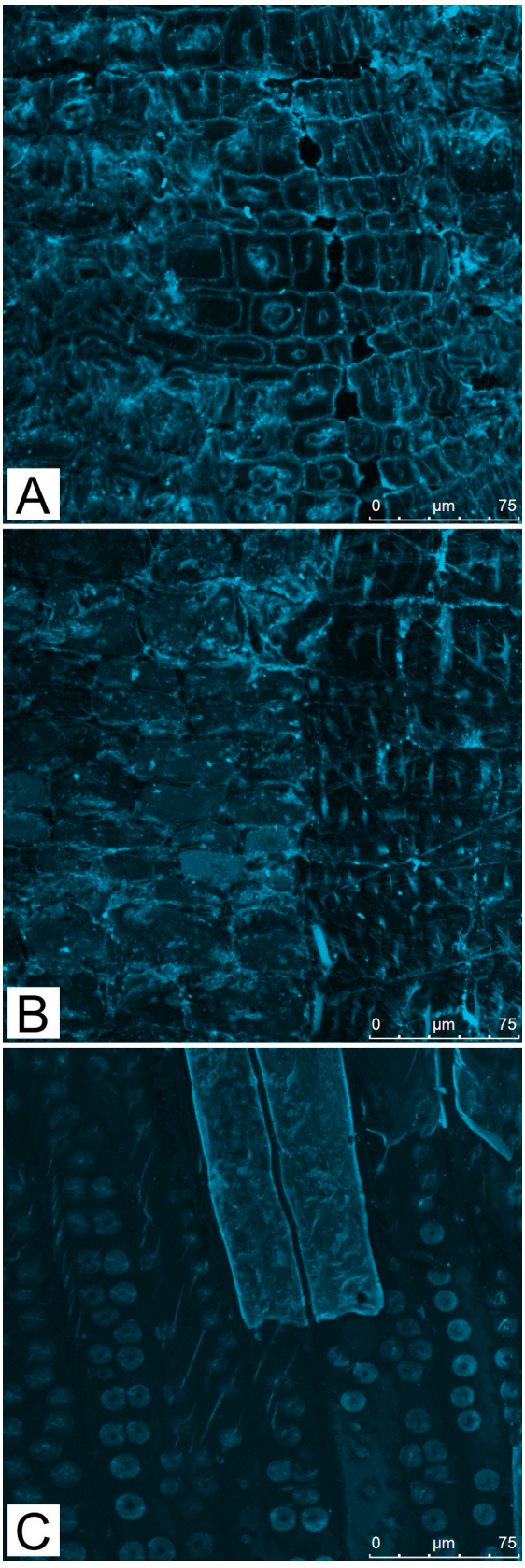
5.9. Thermogravimetry

The various gelification levels of the wood samples studied are reflected by the TGA curves, represented in Fig. 10. The degradation process of cellulose appears at around 300 °C (Singh et al., 2009). The lower amount of cellulose in the fossil samples is tracked by the smaller degradation step. Lower structural carbohydrate content leads to the relative increase of lignin content, which has a natural thermostabilizing and antioxidant effect on wood (Gregorová et al., 2005). It is further modulated by gelification processes, all resulting in a flatter degradation profile above 300 °C (Brebu and Vasile, 2010).

5.10. Elemental analysis, ash yields and Rock-Eval pyrolysis

The content of total organic carbon (TOC) in lignite is relatively uniform, between 48% and 57%. TOC values in fossil wood are very similar to lignite (39–52%). TOC contents in modern wood samples are very similar (45–46%) and slightly lower than in fossil counterparts (Table 4). Total sulphur content (S) in lignite does not exceed 1.24%, reflecting deposition of OM in a freshwater environment (Table 4). Fossil wood has similar S content as lignite, with exception of *Quasisequoioxylon piskowitzense* (Pis) (2.1%), whereas modern wood samples showed lower values. The S contents in fossil wood samples are in a range typical of Miocene samples (0.1–3.6%; Bechtel et al., 2007a). The N contents are also similar in fossil wood and lignite, being higher than in modern wood, with exception of *Sciadopityoxylon wettsteinii* (Table 4). The ratio of TOC to nitrogen (TOC/N) in lignite is high (> 70; Table 4), as expected for terrestrial OM. (Meyers, 1994; Meyers and Ishiwatari, 1993). Ash yield in lignite ranged from 4.6% to 11.4% being two-times higher in the Pis samples. A significant negative correlation between TOC and ash yield ($r = 0.88$; Table 4) was observed, as expected. Wood samples showed notably lower ash yields than lignite with exception of *Quasisequoioxylon piskowitzense* (Pis), which displayed an ash yield of 11.3%, almost identical to Pis lignite. Although the *Sciadopityoxylon wettsteinii* displayed only 0.58% ash, the apparent red colour of the ash (not shown) indicated high Fe level that was also justified by the results of iron contents (Table 3).

Content of extractable organic matter (EOM) of lignite varied from



(caption on next column)

Fig. 8. Confocal laser scanning microscopy (CLSM) images of calcofluor-stained early- and latewood cells. A – Traces of residual cellulose (stronger staining due to calcofluor) associated with thick walled latewood tracheids in transverse section in Welzow-Süd open-cast mine (*Taxodioxylon cryptomerioides*). B – Traces of residual cellulose (much weaker staining due to calcofluor) associated with thick walled latewood tracheids in transverse section in Meuro open-cast mine (*Sciadopityoxylon wettsteinii*). C – Multiseriated, oppositely arranged bordered pits in radial longitudinal section in Piskowitz open-cast mine (*Quasisequoioxylon piskowitzense*). Excitation at 355 nm and emission at 430–550 nm.

104 to 185 mg/g TOC. EOM in two fossil wood samples is higher than in lignite (216 to 330 mg/g TOC), whereas modern wood samples have considerably lower amounts (22–74 mg/g TOC). The EOM of all samples is dominated by polar fraction and asphaltenes, as expected for immature terrestrial OM (e.g. Stojanović and Životić, 2013; Table 4).

The Rock-Eval analysis of lignite samples showed that free hydrocarbons (S1) vary between 9.17 and 13.35 mg HC/g sample; pyrolysate hydrocarbons (S2) range from 55.70 to 90.26 mg HC/g sample; whereas the content of CO_2, generated from oxygenated functional groups (S3), varies between 45.16 and 58.35 mg CO_2/g sample. Values of maximal temperature (T_{max}) range from 376 to 410 °C, indicating an immaturity of samples consistent with huminite reflectance (from 0.32 ± 0.02 to 0.37 ± 0.04% Rr; Kus et al., 2020). Values of the hydrogen index (HI); the S2/S3 ratio (Table 5) and cross plots of HI vs. T_{max}, S2 vs. TOC, and HI vs. OI) (Fig. 11) indicate immature gas-prone Type III kerogen (Peters and Cassa, 1994).

The free hydrocarbons (S1) in fossil (24.05–69.47 mg HC/g sample) and modern wood (37.27–44.73 mg HC/g sample) samples are elevated (Table 5) and much higher than in lignite samples. The modern wood samples have apparently higher pyrolysate hydrocarbons (S2; 145.67–165.24 mg HC/g sample; Table 5) as well as hydrogen index (HI; 324–361 mg HC/g TOC) than their fossil counterparts (S2; 48.71–127.49 mg HC/g sample; HI; 126–247 mg HC/g TOC) and lignite samples (Table 5). The values of maximal temperature (T_{max}) are similar in fossil (342–361 °C) and modern wood (328–338 °C), but lower than in lignite samples. Rock-Eval data of wood samples reflect differences resulting from the early diagenetic alteration of fossil wood samples and are not related to hydrocarbon generation and thermal maturity. High S2, as well as HI value in modern wood samples (Table 5) indicate hydrogen-rich material, such as resin-rich woods, while in fossil wood they imply early diagenetic preservation of woods richer in resin. Results of Rock-Eval pyrolysis of studied samples are like to those reported for coaly source rock (Sykes and Snowdon, 2002).

5.11. *Micro-Fourier transform infrared (micro-FTIR) spectroscopy*

Micro-FTIR spectra were collected in the reflected mode and, as such, represent functional groups distribution at the surface of the sample. These spectra show that the oxygenated group band at 1740 cm^{-1} is clearly defined in all samples, and this band is even more prominent than aromatic C═C band at ~1592 cm^{-1} (Fig. 12). Both the aliphatic stretching region (2800–3000 cm^{-1}) and aliphatic banding region (1350–1500 cm^{-1}) are well-detected and visible. The latter bands in the cellulose and lignin regions have high intensity and look very similar between the samples. A band at 830 cm^{-1}, assigned to lignin, also has similar intensity in the samples. Semi-quantitative analysis of micro-FTIR data shows similarities between the samples regarding the contribution of aliphatic stretching bands in 2800–3000 cm^{-1} and aromatic carbon 1550–1650 cm^{-1} regions, which results in a similar (2800–3000)/1592 ratio (Table 6). The difference is seen in smaller oxygen-containing (carboxyl/carbonyl at 1740 cm^{-1}) band in *Quasisequoioxylon piskowitzense* (Pis), resulting in higher (2800–3000)/1740 ratio. *Taxodioxylon cryptomerioides* (WS) has the greatest cellulose to lignin ratio (6.9), whereas the other two samples show distinctly lower ratio (3.2–4.1).

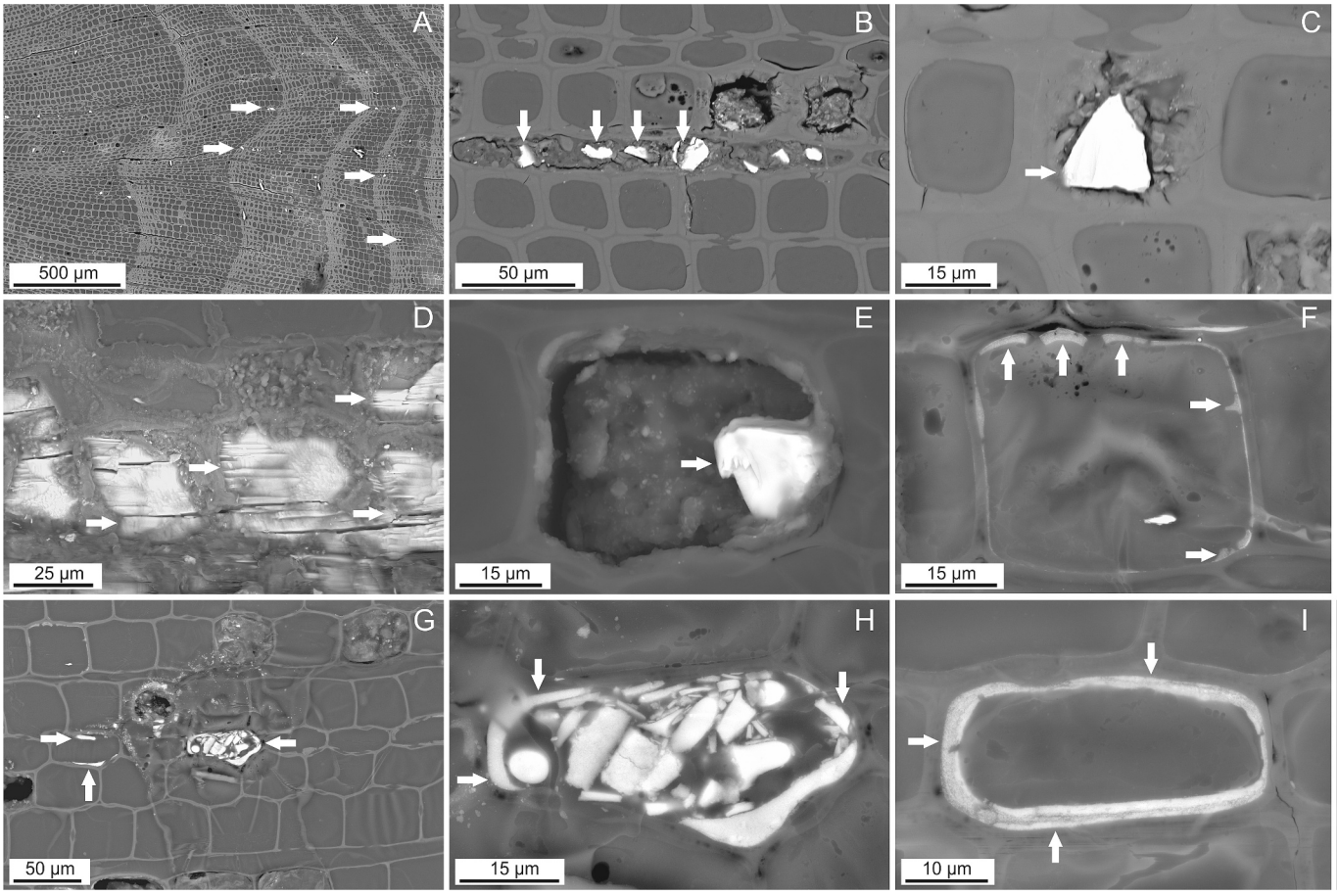


Fig. 9. SEM image of the amorphous opal-A and spherical opal-CT aggregates; A – Transition from earlywood cells to latewood cells. B – Opal-A with detailed microstructure; C – SEM micrograph of opal-CT lepispheres revealing the characteristic spheres consisting of small crystal blades. D to E – Opal-CT blades of spheres with irregularly ragged edges. F to I – Laminar coatings of amorphous silica.

Table 3
Holocellulose, cellulose, total carbon (C) and iron (Fe) contents of fossil and respective modern wood samples.

Sample type	Sample ID	Species	Holocellulose (%)	Kürschner Hoffer cellulose (%)	C (%)	Fe (%)
Fossil wood	LIMS-Nr.: 1708242	*Taxodioxylon cryptomerioides*	37.59	54.31	54.41	1169.0
	LIMS-Nr.: 1708243	*Sciadopityoxylon wettsteinii*	19.96	53.79	53.29	1885.0
	LIMS-Nr.: 1708244	*Quasisequoioxylon piskowitzense*	15.56	53.04	47.86	1043.0
Modern wood	LIMS-Nr.: NA	*Sequoiadendron giganteum*	68.95	51.37	47.45	32.0
	LIMS-Nr.: NA	*Cryptomera japonica*	65.74	47.56	48.42	23.0
	LIMS-Nr.: NA	*Sciadopitys verticillata*	65.36	53.97	48.01	7.6

Legend: NA – non-available information.

In brief, the micro-FTIR data on the fossil wood samples reveal several interesting observations about their chemistry: 1) good preservation of cellulose implying that cellulose bands are more prominent than those of lignin in all spectra; 2) distinct aliphatic hydrogen as shown by aliphatic stretching bands in the 2800–3000 cm^{-1} region, which indicate reducing conditions; and 3) well-preserved oxygenated groups that imply limited microbial degradation of OM.

5.12. Biomarker analysis

5.12.1. Biomarker distributions in lignite

In all Pis samples, biomarker abundances showed the following trend: *n*-alkanes > hopanoids > non-hopanoid triterpenoids > diterpenoids, with exception of Pis 3 sample where diterpenoids slightly dominate over hopanoids and non-hopanoid triterpenoids. WS 1 is characterised by the prevalence of hopanoids over very similar concentrations of non-hopanoid triterpenoids and *n*-alkanes having higher concentration than diterpenoids. In the sample WS 2, biomarker concentrations decrease in the following order: non-hopanoid triterpenoids > *n*-alkanes > hopanoids > diterpenoids. The other detected biomarker compounds, sesquiterpenoids, steroids, fernenes, acyclic isoprenoids, lanosta(eupha) derivatives, methyl esters of fatty acids (detected in Pis 3 sample, only), alkylated 2-methyl-2-(4,8,12-trimethyltridecyl)chromans (MTTCs), and polycylic aromatic hydrocarbons (PAHs) play a subordinate role (Table 7).

In aliphatic fractions of all samples, *n*-alkanes prevail, followed by hopanoids and diterpenoids, while steroids, non-hopanoid triterpenoids, fernenes, sesquiterpenoids, and isoprenoids are present at low concentrations (Fig. 13; Table 8). An exception is WS 1, which is characterised by a higher abundance of hopanoids than *n*-alkanes.

Although non-hopanoid triterpenoids have played a subordinate role in aliphatic fractions, they have prevailed in aromatic fractions of lignite (Fig. 14). The result is consistent with the rapid aromatization of their amyrin precursors during diagenesis in comparison to diterpenoids and

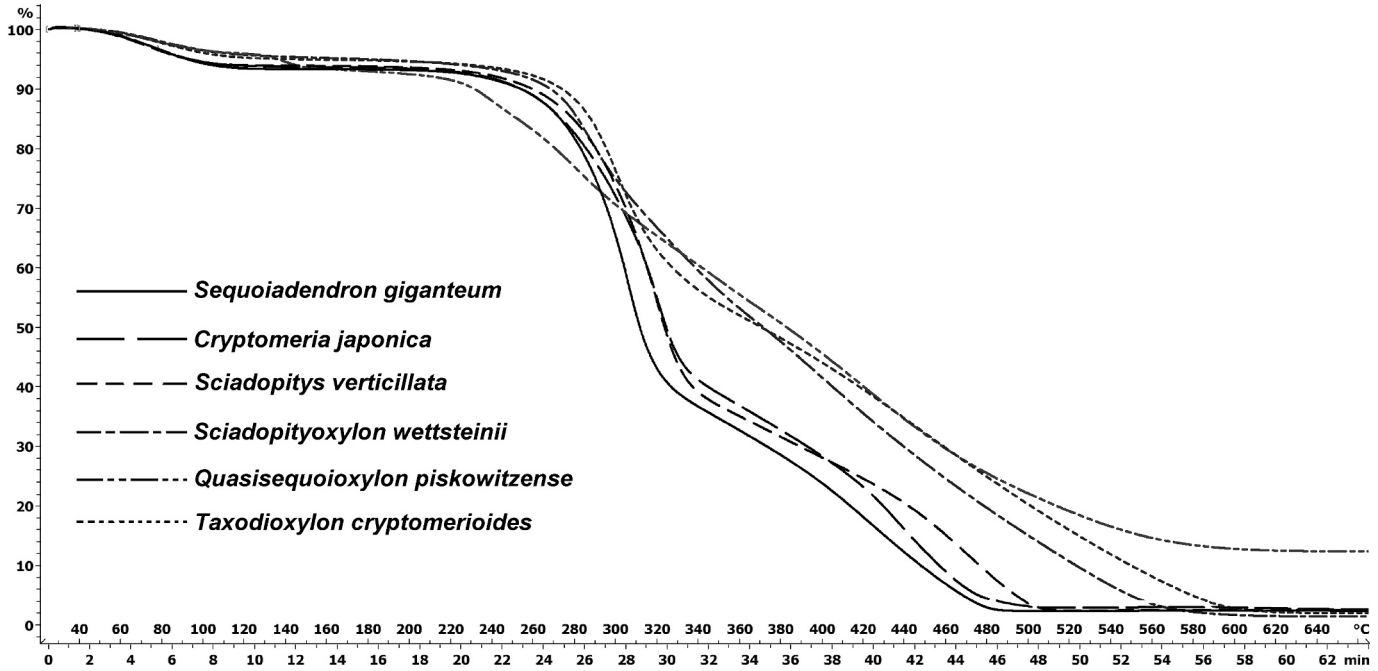


Fig. 10. Thermoanalytical (TGA) curves of the examined modern (*Sequoiadendron giganteum*, *Cryptomeria japonica*, and *Sciadopitys verticillata*) and fossil wood samples (*Sciadopityoxylon wettsteinii, Quasisequoioxylon piskowitzense, Taxodioxylon cryptomerioides*).

Table 4
Bulk geochemical data.

	Sample/ Species	Ash (%)	TOC (%)	N (%)	S (%)	TOC/ N	TOC/ S	EOM (mg/g TOC)	Ali (%)	Arom (%)	Polar + Asp (%)
Lignite	Pis 1	10.66	49.30	0.57	0.73	86.49	67.53	104.15	0.33	0.49	99.18
	Pis 2	11.42	48.17	0.37	0.67	130.19	71.90	143.52	0.53	0.53	98.93
	Pis 3	10.72	53.06	0.55	0.80	96.47	66.33	184.95	0.84	2.37	96.79
	WS 1	4.56	57.20	0.67	1.24	85.37	46.13	118.34	1.60	1.94	96.46
	WS 2	5.63	54.53	0.76	0.90	71.75	60.59	162.96	0.38	1.78	97.84
Fossil wood	*Quasisequoioxylon piskowitzense*	11.30	38.72	1.17	2.10	33.09	18.44	330.19	0.09	0.07	99.84
	Taxodioxylon cryptomerioides	0.76	51.57	0.51	0.68	101.12	75.84	72.27	2.23	0.44	97.33
	Sciadopityoxylon wettsteinii	0.58	51.69	0.09	0.70	574.33	73.84	215.91	0.29	0.58	99.13
Modern wood	*Sequoiadendron giganteum*	0.32	44.92	0.21	0.11	213.90	408.36	26.43	1.35	0.15	98.51
	Cryptomeria japonica	0.44	46.48	0.17	0.14	273.41	332.00	21.88	2.01	0.25	97.74
	Sciadopitys verticilata	0.40	45.80	0.17	0.09	269.41	508.89	73.56	0.26	0.05	99.69

Legend: TOC – Total organic carbon (from elemental analysis); N – Total nitrogen; S – Total sulphur;
EOM – Extractable organic matter; Ali – Aliphatic fraction; Arom – Aromatic fraction; Polar – Polar fraction;
Asp – Asphaltenes; Parameters are given in %, wt. on dry basis.

hopanoids (Nakamura et al., 2010; Stojanović and Životić, 2013). The abundance of other biomarker classes in aromatic fraction decreases in the following order: diterpenoids > hopanoids > sesquiterpenoids > steroids > polycyclic aromatic hydrocarbons (PAHs: fluorene, naphthalene, phenanthrene, fluoranthene, pyrene, chrysene and its methyl-derivatives, benzo(*k*)fluoranthene, benz(*a*)anthracene, and perylene). Exceptions are samples WS 1, which has a higher content of hopanoids than diterpenoids (in accordance with the dominance of these biomarkers in its aliphatic fraction), and WS 2, in which PAHs prevail over steroids, being order of magnitude more abundant than in other samples (Table 9).

In the aliphatic fraction of studied lignite, *n*-alkanes are identified in the C_{15} - C_{35} range. In all samples long-chain *n*-alkanes (C_{26}-C_{33}) are the most abundant, exhibiting notable odd-over even predominance. Mid-chain *n*-alkanes (*n*-C_{21}-C_{25}) and, particularly, short-chain *n*-alkanes ($\leq C_{20}$) are present at lower amounts in comparison with long-chain homologues (Fig. 15; Table 10).

The distribution of hopanoids in the aliphatic fractions of all samples is dominated by C_{31}17α (H)21β(H)22(R) hopane that is often observed in European Miocene lignite (e.g., Stefanova et al., 2005a; Vu et al., 2009; Životić et al., 2013). The other hopanoids present in aliphatic fraction are C_{27} to C_{31} hopanes (C_{28} homologue is absent) with αβ, βα, and ββ configurations and C_{32} ββ hopane, as well as unsaturated C_{27} and C_{30} hopenes having double bond in positions 17(21) and 13(18), respectively (Fig. 16; Table 11). Aromatic hopanoids are represented by series of orphan aromatic hopanoids (bearing an ethyl group at C-21), with one to four aromatic rings, whereas C_{32} and C_{33} benzohopanes cyclised at C-20 are detected in low amounts exclusively in samples Pis 1 and WS 2 (Fig. 14).

Diterpenoids are important constituents of both the aliphatic and aromatic fractions (Figs. 13, 14). 16α(H)-Phyllocladane dominates in the aliphatic fraction of Pis samples, whereas the most abundant diterpanes in the aliphatic fraction of WS 1 and WS 2 are isonorpimarane and norabietane, respectively. Other diterpenoid type constituents of the

Table 5
Parameters derived from the Rock-Eval pyrolysis and huminite reflectance (%Rr) of lignite samples.

	Sample/ Species	TOC* (%)	S1 (mg HC/g sample)	S2 (mg HC/g sample)	S3 (mg CO_2/g sample)	T_{max} (°C)	HI (mg HC/g TOC)	OI (mg CO_2/g TOC)	S2/ S3	%Rr
Lignite	Pis 1	54.07	9.17	86.51	45.17	403	160	84	1.92	0.32 ± 0.02
	Pis 2	38.41	9.62	55.70	55.67	410	145	145	1.00	0.32 ± 0.02
	Pis 3	49.05	13.35	90.26	45.16	391	184	92	2.00	0.32 ± 0.02
	WS 1	37.96	10.04	67.94	51.21	396	179	94	1.91	0.37 ± 0.04
	WS 2	52.89	11.23	82.51	58.35	376	156	110	1.41	0.34 ± 0.03
Fossil wood	*Quasisequoioxylon piskowitzense*	38.72	37.87	48.71	N.M.	361	126	N.C.	N.C.	N.M.
	Taxodioxylon cryptomerioides	51.57	24.05	127.49	N.M.	342	247	N.C.	N.C.	N.M.
	Sciadopityoxylon wettsteinii	51.69	69.47	92.51	N.M.	346	179	N.C.	N.C.	N.M.
Modern wood	*Sequoiadendron giganteum*	44.92	39.77	145.67	N.M.	328	324	N.C.	N.C.	N.M.
	Cryptomeria japonica	46.48	37.27	160.90	N.M.	338	346	N.C.	N.C.	N.M.
	Sciadopitys verticilata	45.80	44.73	165.24	N.M.	335	361	N.C.	N.C.	N.M.

Legend: TOC* – Total organic carbon (from Rock-Eval pyrolysis, %, wt.); S1 – Free hydrocarbons (mg HC/g sample); S2 – Pyrolysate hydrocarbons (mg HC/g sample); HC – Hydrocarbons; S3 – Amount of CO_2 generated from oxygenated functional groups (mg CO_2/g sample); T_{max} – Temperature corresponding to S2 peak maximum (°C); HI – Hydrogen Index = (S2 x 100)/TOC (mg HC/g TOC); OI – Oxygen Index = (S3 x 100)/TOC (mg CO_2/g TOC); N.M. – Not measured; N.C. – Not calculated; %Rr from Kus et al. (2020).

aliphatic fraction are beyerane, norpimarane, pimarane, 16α(H)-kaurane, hibaene, 16β(H)-phyllocladane, isopimaradiene, isopimarane, and isophyllocladene. The aromatic diterpenoids consist of norabieta-6,8,11,13-tetraenes, norabieta-8,11,13-trienes, 16,17-bisnordehydroabietane, dehydroicetexane, dehydroabietane, tetrahydroretene simonellite, retene, sempervirane, totarane, methylretene, and phenolic abietanes. Among aromatic diterpenoids, dehydroicetexane or simonellite prevail in the Pis samples, whereas in the WS lignite, simonellite or retene is the most abundant.

In the aliphatic fraction (Fig. 13), non-hopanoid triterpenoids are represented mainly by tetracyclic des-A-degraded compounds (des-A-olean(12)- and 13(18)-ene, des-A-urs(12)-ene, and des-A-lupane), whereas pentacyclic oleanenes are only detected in Pis 3 and WS 2. In the aromatic fraction both penta- and des-A-tetracylic non-hopanoid triterpenoids occur (Fig. 14). This is in line with the conclusions of Jacob et al. (2007), Stout (1992), and Trendel et al. (1989) that, in difference to hopanoids, the early diagenetic transformation of higher plant triterpenoids preferentially leads to aromatization or degradation of A-ring rather than to formation of unsaturated or saturated pentacyclic compounds. Triaromatic C-ring secotriterpenoids, represented by 8,14-seco-trinor-oleana-1,3,5,7,9,13,15,17-octaene and 8,14-seco-trinor-ursa-1,3,5,7,9,13,15,17-octaene and their tetraaromatic counterparts, des-A-8,14-seco-noroleana-5,7,9,13,15,17-hexaene, and des-A-8,14-seco-norursa-5,7,9,13,15,17-hexaene are also identified in all samples. Among aromatic non-hopanoid triterpenoids, pentacyclic monoaromatic 24,25 dinorlupa-1,3,5(10)-triene dominates in all samples, with the exception of WS 2 lignite enriched in PAHs, where pentacyclic tetraaromatic, 1,2,9-trimethyltetrahydropicene prevails. Furthermore, notable dominance of pentacyclic non-hopanoid triterpenoids over tetracyclic des-A-degraded compounds and 8,14 secotriterpenoids (present in almost identical concentrations) is evident (Table 12).

In all samples, sesquiterpenoids occur at low quantities. Similar result was observed during investigation of other European lignite basins (Đoković et al., 2018; Stefanova et al., 2013). Cadalene prevails in all samples with exception of Pis 3, where the highest concentration is observed for cuparene. Other sesquiterpenoid constituents of the lignite extracts are isocadalene, cadina-1(10),6,8-triene, tetra-, octa- and decahydrocadalenes, dihydro-ar-curcumene, muurolene, cedrane, and eudesmane (Figs. 13, 14).

The acyclic isoprenoids pristane (Pr) and phytane (Ph) are identified in all samples at low amounts (Figs. 13, 15), which is in accordance with well-known fact that in terrestrial immature OM, isoprenoid precursors are still bounded into the macromolecular matrix (Dzou et al., 1995; Vu et al., 2009) or present as functionalised compounds (Fabiańska and Kurkiewicz, 2013; Zdravkov et al., 2011). Considering above mentioned data and multiple sources of these isoprenoids, an interpretation of the Pr/Ph ratio (Didyk et al., 1978) as redox proxy in lignite, is not recommended.

Steroids are detected in the studied samples at low concentrations being typical for lignite, since higher plants synthesise small amounts of steroid compounds. In aliphatic fractions they are represented by C_{27}-C_{29} (Δ^2-, Δ^4 and Δ^5-) sterenes (Fig. 17), showing notable prevalence of C_{29} homologues, as expected (Table 8), whereas in the aromatic fraction only 4-methyl-24-ethyl-19-norcholesta-1,3,5(10)-triene is detected (Fig. 14).

Lanosta(eupha) derivatives represented by lanosta(eupha)-pentaene and lanosta(eupha)-hexaene are detected in the aromatic fractions of all samples (Table 10). These compounds possess euphane or tirucallane structure, widespread in angiosperm plants (Mishra et al., 2000; Wang et al., 2003), and their presence coincides with high concentrations of non-hopanoid triterpenoids (Tables 7, 9). 5,8-Dimethyl- + 7,8-dimethyl MTTC and 5,7,8-trimethyl MTTC are present in samples Pis 1, Pis 2, and WS 2, whereas a series of fatty acids methyl esters ranging from C_{24} to C_{34} is exclusively observed in Pis 3 sample (Tables 7, 9).

5.12.2. *Biomarker distributions in wood samples*

In wood samples, biomarker hydrocarbon classes are represented by diterpenoids, sesquiterpenoids, *n*-alkanes, and isoprenoids. Very low amounts of steroids and hopanoids are detected in fossil wood, whereas non-hopanoid triterpenoids and lanosta(eupha) derivatives are only identified in the sample *Taxodioxylon cryptomerioides* (WS). Contents of diterpenoids, sesquiterpenoids, steroids, and isoprenoids are comparable in lignite and fossil wood samples, whereas concentrations of other biomarker classes are notably lower in the latter. Modern wood samples have a lower content of biomarkers than fossil counterparts (Table 7).

Diterpenoids notably prevailed in all wood samples. They comprise norisopimaradiene, isopimaradienes, pimaradienes, abietadienes, norabietane, pimarane, phyllocladane, abietane, rimuane, dihydorimuene, 16α(H)-kaurane, kaurene, 16,17-bisnordehydroabietane, hibaene, 1-metilbisnorabietatriene, simonellite, totarane, and sempervirane.

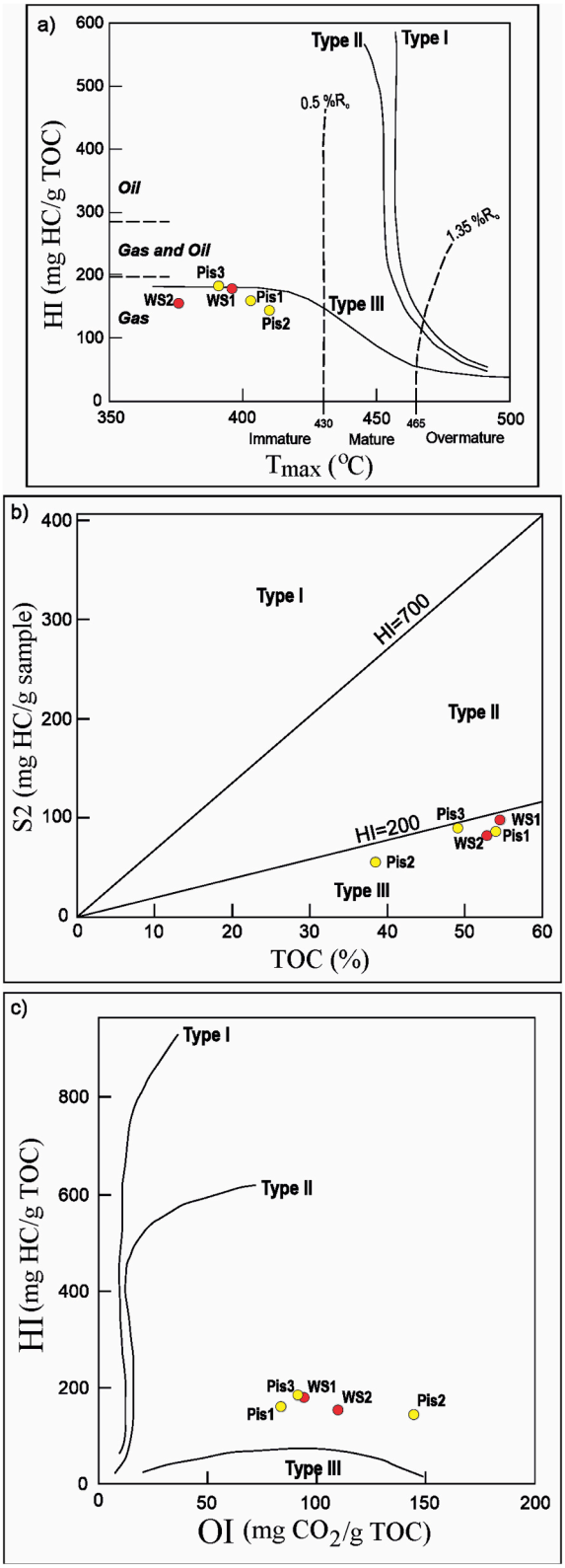


Fig. 11. Diagrams derived from Rock-Eval pyrolysis of lignite samples: a) HI vs. T_{max}; b) S2 vs. TOC; c) HI vs. OI. Legend: TOC – Total organic carbon (from Rock-Eval pyrolysis); HI – Hydrogen Index = (S2 x 100)/TOC (mg HC/g TOC); S2 – Pyrolysate hydrocarbons (mg HC/g sample); T_{max} – Temperature corresponding to S2 peak maximum (°C); OI – Oxygen Index = (S3 x 100)/TOC (mg CO_2/g TOC).

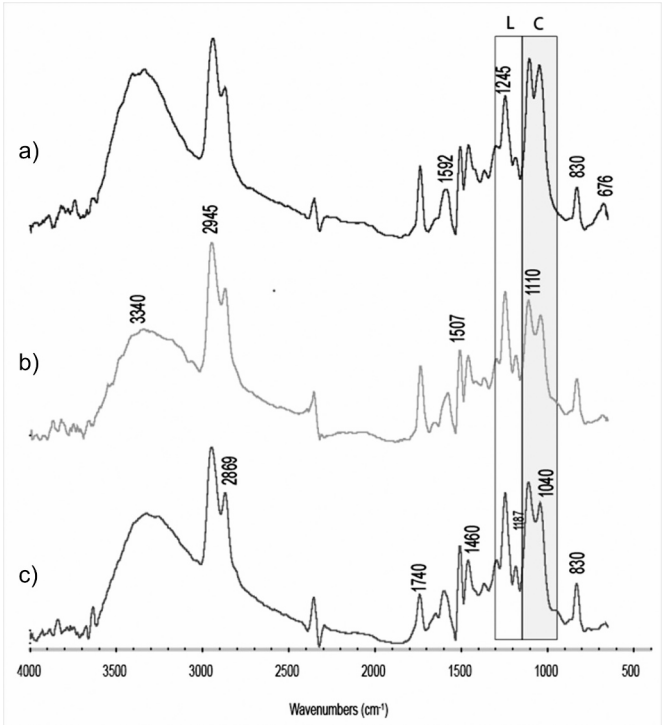


Fig. 12. Micro-FTIR spectra of the fossil wood samples: (a) *Taxodioxylon cryptomerioides*, (b) *Sciadopityoxylon wettsteinii*, (c) *Quasisequoioxylon piskowitzense*. Each spectrum is the average spectrum based on 10 analyses. L – lignin region; C – cellulose region.

Aliphatic diterpenoids sharply prevail over aromatic counterparts, which are detected in extremely low amounts (as minor components) in *Quasisequoioxylon piskowitzense* (Pis), *Taxodioxylon cryptomerioides* (WS), *Cryptomeria japonica*, and *Sequoiadendron giganteum*. The most abundant diterpenoid in *Sciadopityoxylon wettsteinii*, *Quasisequoioxylon piskowitzense* (Pis), and *Sequoiadendron giganteum* is 16α(H)-phyllocladane; norpimarane prevails in *Taxodioxylon cryptomerioides*; whereas abietadienes dominate in *Cryptomeria japonica* and *Sciadopitys verticilata*. Sesquiterpenoid distributions in fossil wood samples *Quasisequoioxylon piskowitzense* (Pis) and *Taxodioxylon cryptomerioides* (WS) comprise longifolane, cedrane, numerous isomers of cadinenes (isopropyl, dimethyl-octahydronaphthalenes), drimane, cuparene, and cadalene. Sesquiterpenoids are not detected in *Sequoiadendron giganteum*. Modern wood of *Cryptomeria japonica* comprises muurolene and its isomers, calamenene, 4-isopropyl-4,7-dimethyl-1,2-dihydro-naphthalene, and cadalaene. Sesquiterpenoid assemblage in *Sciadopitys verticilata* is reperesented by cuprenene, α-cedrene, longipinene, bisabolene, cuparene, and cadalene, whereas in *Sequoiadendron giganteum*, only muurolene and cadalene are detected Figs. 18, 19).

Steroids, only detected in fossil wood samples, are represented by C_{29} sterenes and steradiene. Among hopanoids C_{31} αβ(*R*)-hopane and BCD triaromatic hopanoid are identified in *Taxodioxylon cryptomerioides* (WS), whereas C_{30} hop-17(21)-ene is detected in *Quasisequoioxylon piskowitzense* (Pis) and *Sciadopityoxylon wettsteinii*.

Isoprenoids in wood samples are represented by pristane and phytane. *n*-Alkanes are absent or almost absent in fossil wood samples, whereas in modern wood they are detected in range from C_{21} or C_{23} to C_{31} with sharp prevalence of odd homologues and maximum at C_{25} (Fig. 18).

5.13. Stable carbon isotope ($\delta^{13}C$) analysis of fossil wood

The $\delta^{13}C$ values of four fossil wood (*Quasisequoioxylon piskowitzense* (Pis), *Taxodioxylon cryptomerioides* (WS), and *Sciadopityoxylon wettsteinii*

Table 6
Semi-quantitative micro-FTIR analysis of fossil wood samples.

Sample type	Species	2800-3000 cm^{-1}	1700–1800 cm^{-1}	1650–1550 cm^{-1}	(2800–3000)/1740	(2800–3000)/1592	Cellulose/Lignin
Fossil wood	*Quasisequoioxylon piskowitzense*	40.8	4.2	5.7	9.7	7.2	4.1
	Taxodioxylon cryptomerioides	40.1	6.5	5.9	6.2	6.8	6.9
	Sciadopityoxylon wettsteinii	39.7	7.2	5.4	5.5	7.3	3.2

Legend: Each value is based on ten spectra. In the cellulose/lignin ratio, cellulose includes bands at 1040 and 1110 cm^{-1}, while lignin comprises bands at 1187 and 1245 cm^{-1} (Fig. 12). All values are based on integration areas of the bands.

(M)) samples were analyzed in this study. The obtained $\delta^{13}C$ values range from −24.6 ‰ to −20.3 ‰ (Fig. 21). The $\delta^{13}C$ increases from Pis open-cast mine with −24.6 ‰ for *Quasisequoioxylon piskowitzense* to the most positive value of −20.3 ‰ for *Sciadopityoxylon wettsteinii* in M open-cast mine. The $\delta^{13}C$ values for *Taxodioxylon cryptomerioides* in WS open-cast mine vary between −22.1 ‰ to −21.9 ‰. There is no trend observed as there is insufficient data for its adequate resolution.

6. Discussion

6.1. Detection of high-cellulose contents – In-situ fossil stumps and trunks

With the aid of various imaging techniques explored in this study, the presence of cellulose is confirmed by its characteristic birefringence observed under crossed polars in the xylitic tissue of cell walls of *Taxodioxylon cryptomerioides*, *Sciadopityoxylon wettsteinii*, and *Quasisequoioxylon piskowitzense*. According to Stout and Spackman (1987), the arrangement of cellulose micelles is responsible for the characteristic anisotropic effect of an undulate and helical nature viewed under cross-polarised illumination. In general, cellulose in primary lignocellulosic plant materials is unlikely to survive during humification at a peat stage; thus, a low to moderate alteration of chemical molecular structure of the investigated cellulosic framework has to be invoked. Calcofluor staining aided in the detection of cellulose in fossil wood samples, indicating traces of residual cellulose related to thick-walled latewood tracheids in all three samples. Although it remains unclear whether calcofluor staining can also be applied to fossil material, its presence in cell walls would support the presence of cellulose characteristic birefringence occurring in cell walls. Calcofluor white stain excited with a 405 nm laser line resulted in blue fluorescence of cellulosic walls (Donaldson and Bond, 2005; Kitin et al., 2010). The presence of cellulose in xylem cell walls is a consequence of either a lack of or a hindering of fungal degradation by an extant fungal species. Differentiated delignification and/or concurrent decay of lignin- and cellulose-rich components were absent, as general soft rot features together with additional anatomical changes in the examined tissue were non-existent.

6.2. Determination of high contents of cellulose – In-situ fossil stumps and trunks

The cellulose content of fossil wood can be variable depending on the age, environment, type, and extent of degradation. The holocellulose content determined in the studied fossil wood points toward anomalously high-cellulose values ranging between 15.56% and 37.59% (Table 3), and these values are comparable with those reported for Miocene fossil wood samples (1.4 to 43.1%) (Schleser et al., 1999; Bechtel et al., 2002, 2007a; Hámor-Vidó et al., 2010). Similarly, elevated to anomalously high levels of holocellulose contents were reported for other Miocene matrix and/or xylite-rich lignite samples in Europe. Correspondingly, Hámor-Vidó et al. (2010) reported high-cellulose contents (18.2 to 41.2%) of Taxodiaceae fossil trees investigated in the Bükkalja Lignite Formation outcropping at Bükkábrány open-cast mine, Hungary. Marynowski et al. (2013) reported high-cellulose values (4.5% and 34.4%) for Miocene Lubstów lignite deposit, Poland. Havelcová et al. (2013) ascertained higher cellulose content from telohuminite, presumably of *Glyptostroboxylon* and *Taxodioxylon* investigated in the Miocene "Stump Horizon" of the Bílina open-cast mine, Most Basin, Czech Republic. Marynowski et al. (2019) established an abundant (holo)cellulose content in Miocene *Piceoxylon piceae* and other unassigned fossil wood samples collected from the Konin area, Jóźwin IIB, Drzewce, and the Jaroszów open-cast mine, Poland. Lücke et al. (1999) reported higher cellulose content of Middle Miocene Taxodiaceae remains in Garzweiler Seam (horizon 6E in local stratigraphy is equivalent to the Garzweiler seam and latest Serravallian) in the Hambach open-cast mine, where its values range from 30 to 45% (dry weight) with single extreme values of 4.2 and 54.9%. Bechtel et al. (2003b) determined high-cellulose contents (10.6 to 35.8%) from the Pliocene gymnosperm fossil wood (xylite) from Slovenia. There are also examples of pre-Miocene (Eocene) coalified wood logs with similarly anomalous cellulose content (48%) (Hatcher and Breger, 1982). In addition, Morey et al. (1983) investigated cellulose contents of several fossil woods by different physical methods, pointing out that cellulose measured by X-ray diffraction exceeded 60% for several European lignite.

6.3. Sources of OM in lignite

6.3.1. Implications from diterpenoids and non-hopanoid triterpenoids

The presence of diterpenoids (Di) and non-hopanoid triterpenoids (Tri) in relatively high concentrations in all samples (Tables 7–9) shows that both gymnosperms and angiosperms contributed to the precursor OM. However, the Di/(Di + Tri) ratio < 0.5 (Table 12; Bechtel et al., 2003b) suggests a greater impact of angiosperms in all samples with exception of Pis 3, where contents of Di and Tri are similar. A gradual increase of the Di/(Di + Tri) ratio from Pis 1 to Pis 3 (Table 12) can be attributed to enhanced impact of gymnosperms and/or more intense degradation of angiosperms' tissues that are generally more prone to degradation than gymnosperms (Hatcher and Clifford, 1997). Very similar concentrations of hopanoids (Table 7) that are considered as indicators of bacterial activity and microbial diagenetic OM degradation in Pis 1 and 2 samples suggest higher contribution of gymnosperms to the latter. On the other hand, notable rise in concentration of hopanoids in Pis 3 (Table 7) may imply that increase of the Di/(Di + Tri) ratio in this sample (Table 12) did not result from greater impact of gymnosperms only, but possibly also from more intense degradation of angiosperm-derived OM and/or changes in the relative height of the ground water table, pH, and climatic settings (Dehmer, 1995). The prevalence of Tri over Di independently on hopane concentration in WS samples clearly indicates prevalence of angiosperms over gymnosperms in precursor OM (Tables 7, 12).

The presence of tricyclic diterpenoids with abietane, pimarane, and isopimarane skeletons, as well as tetracyclic ones (phyllocladane, bayerane, kaurane) indicates the impact of following families to precursor OM: Pinaceae, Cupressaceae (particularly Taxodioideae, i.e., formerly recognised Taxodiaceae), and Phyllocladaceae (Otto and Wilde, 2001; Stefanova et al., 2005b). Cuparene is specific for

Table 7
Total concentrations of identified biomarker classes (µg/g TOC) in aliphatic and aromatic fractions.

	Sample/ Species	Sesquiterpenoids	Diterpenoids	Non-hopanoid triterpenoids	*n*-Alkanes	Hopanoids	Steroids	Fernenes	Isoprenoids	Lanosta(eupha) derivatives	PAHs	MTTCs	Fatty acids methyl esters
Lignite	Pis 1	0.83	13.50	71.68	121.74	105.05	3.79	N.D.	2.78	5.29	2.08	0.20	N.D.
	Pis 2	0.70	35.49	69.13	150.8	113.57	3.03	N.D.	1.66	4.94	2.68	0.07	N.D.
	Pis 3	13.29	484.54	301.51	605.29	434.88	14.90	2.72	5.90	40.28	3.74	N.D.	117.67
	WS 1	39.48	494.12	781.36	732.73	1112.41	7.69	5.65	10.53	48.28	5.48	N.D.	N.D.
	WS 2	16.03	98.58	497.21	203.76	137.22	10.92	2.36	1.90	1.78	20.50	0.28	N.D.
Fossil wood	*Quasisequoioxylon piskowitzense*	1.81	61.12	N.D.	N.D.	0.16	0.22	N.D.	0.45	N.D.	N.D.	N.D.	N.D.
	Taxodioxylon cryptomerioides	16.39	333.91	19.73	N.D.	2.53	4.91	N.D.	N.D.	2.16	N.D.	N.D.	N.D.
	Sciadopityoxylon wettsteinii	N.D.	993.10	N.D.	6.70	0.48	6.41	N.D.	7.90	N.D.	N.D.	N.D.	N.D.
Modern wood	*Sequoiadendron giganteum*	0.16	5.07	N.D.	4.64	N.D.	N.D.	N.D.	1.55	N.D.	N.D.	N.D.	N.D.
	Cryptomeria japonica	3.22	14.05	N.D.	4.38	N.D.	N.D.	N.D.	1.27	N.D.	N.D.	N.D.	N.D.
	Sciadopitys verticilata	3.31	39.25	N.D.	7.48	N.D.	N.D.	N.D.	1.80	N.D.	N.D.	N.D.	N.D.

Legend: MTTC – 2-Methyl-2-(4,8,12-trimethyltridecyl)chroman; PAHs – Polycylic aromatic hydrocarbons; N.D. – Not detected.

Cupressaceae (Haberer et al., 2006; Otto and Wilde, 2001), whereas presence of dehydroicetexane is also indicative for Cupressaceae, particularly its subfamily Cupressoideae (Nytoft et al., 2019). Totarane and phenolic abietanes (ferruginol, 6,7 dehydroferruginol, showing the highest concentrations in Pis 2) are indicative for Cupressaceae. Differences in amounts of individual diterpenoids may be attributed to different contribution of conifer families. The decrease of dehydroicetexane content and the tetracyclic/tricyclic diterpanes ratio (Table 12) indicate a decreasing contribution of Cupressaceae and increased input of Pinaceae to precursor OM of WS samples in comparison to Pis samples. In addition, order of magnitude higher content of dehydroicetexane in Pis 3 than in other samples, accompanied with prevalence of cuparene among sesquiterpenoids, may imply that the higher Di/(Di + Tri) ratio in this sample (Table 12) results from increased impact of Cupressaceae.

Non-hopanoid triterpenoids are not specific for precursor angiosperm plant community. Nevertheless, their abundance in studied samples depicts Middle Miocene angiosperm palaeovegetation (oak-laurel forest, palms, Ericaceae, etc.) and reed sweet-grass (*Glyceria maxima*) in the studied area (Kus et al., 2020 and references therein). Certain earlier studies suggest that elevated abundance of lupane derivatives could be indicative for contribution of Betulaceae (Hayek et al., 1989; Regnery et al., 2013). Considering the abundant lupane derivatives in the studied samples, we can speculate that Betulaceae contributed to the precursor OM. This is particularly related to WS 1 sample where the content of pentacyclic monoaromatic non-hopanoid terpenoids with a lupane skeleton prevails over those with oleanane/ursane skeleton by an order of magnitude.

6.3.2. *Implications from n-alkanes*

The *n*-alkane distributions (Figs. 13, 15; Table 10) associated with the CPI values (Carbon Preference Index; Bray and Evans, 1961) higher than 4 in all lignite samples indicate a significant contribution of epicuticular waxes. Enhanced concentrations of plant wax *n*-alkanes found in lignite coincide with abundant angiosperm-derived triterpenoids (Table 7), as also observed by Bechtel et al. (2019). Moreover, it is in line with differences in *n*-alkane abundances of recent species, which have lower contents of *n*-alkanes in several conifer species compared to angiosperms (Diefendorf et al., 2011; Lane, 2017). All samples showed very low abundance of short-chain *n*-alkane homologues (C_{15}–C_{20}), reflecting very small impact of algae and plankton in relation to plant material. However, differences in abundance of mid-chain *n*-alkanes (C_{21}–C_{25}) are evident (Table 10). Samples Pis 1 and particularly, Pis 2 are characterised by elevated content of mid-chain homologues and consequently higher Paq ratio (Ficken et al., 2000) that can be related to elevated contribution of emergent aquatic macrophytes and/or *Sphagnum* sp. However, analysis of modern plant lipids demonstrated that some terrestrial plants (including several conifer species) might also be important source of these biomarkers with maxima at *n*-C_{23} or *n*-C_{25} (Bush and McInerney, 2013). This is also documented in the current study, since all investigated modern wood samples showed *n*-alkane maximum at *n*-C_{25}, followed by *n*-C_{23}.

Previous investigations showed that OM derived from trees and shrubs usually has higher concentrations of *n*-C_{27} and *n*-C_{29} in relation to other homologues (Bi et al., 2005; Ficken et al., 2000; Rieley et al., 1991). On the other hand, grasses and mosses usually show the maximum at *n*-C_{31} that prevails in studied samples with exception of WS 1, where *n*-C_{31} and *n*-C_{29} homologues are identified in similar amounts. Furthermore, samples differ according to the second *n*-alkane maximum, which is *n*-C_{29} in Pis 1 and WS 2, *n*-C_{25} in Pis 2, and *n*-C_{33} in Pis 3. The results indicate somewhat greater impact of herbaceous peat-forming plants than woody vegetation that is in concordance with observed prevalence of angiosperms derived OM over conifer organic material. The elevated contents of *n*-C_{31} and *n*-C_{33} homologues were also proposed as indicator of species growing in a warmer climate (Cranwell, 1973; Duan and He, 2011; Poynter et al., 1989). On the other hand,

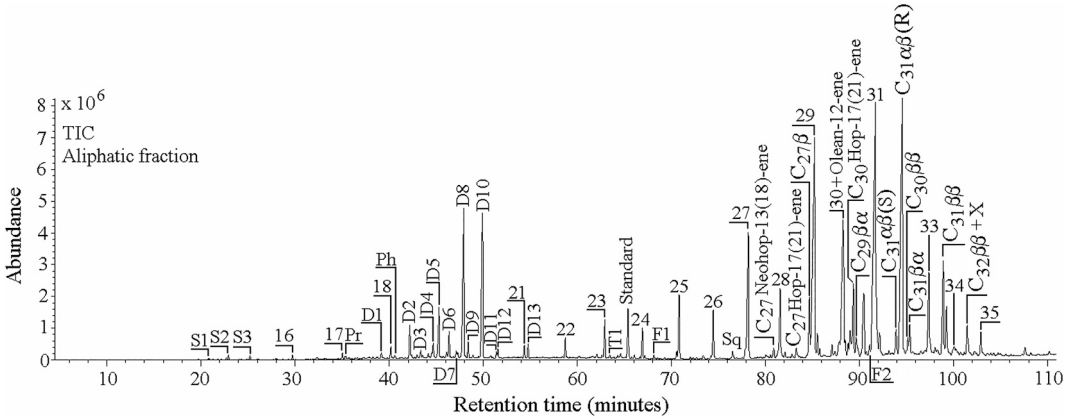


Fig. 13. Total ion current (TIC) of lignite aliphatic fraction (sample WS 2).
Peak assignments: *n*-Alkanes are labelled according to their carbon number; Pr – Pristane;
Ph – Phytane; S1 – 1H-3a,7-methanoazulene -octahydro-3,6,8,8-tetramethyl (cedrane);
S2–7-Isopropyl-1,4a-dimethyl-decahydronaphthalene (selinane); S3–1,2,3,4-Tetrhydrocadalene (calamenene); D1 – Bisnorpimarane; D2–19-Norabietatriene;
D3–19-Norabietatetraene; D4 –Isopimaradiene; D5 – Isonorpimarane; D6 – Norpimarane;
D7 – Isophyllocladene; D8 – Fichtelite; D9 – Pimarane; D10 – 16α(H)-Phyllocladane;
D11 – Dehydroicetexane; D12 – Dehydroabietane; D13 – Simonellite; T1 – Des-A-olean-12-ene; F1 – Des-A-fern-9(11)-ene; Sq – Squalane; F2 –Fern-8-ene; α and β designate configuration at C_{17} in C_{27} hopanes; ββ, βα, and αβ designate configurations at C_{17} and C_{21} in C_{29}-C_{32} hopanes; (R) and (S) designate configuration at C_{22} in hopanes; C_{27} neohop-13(18)-ene – C_{27} 22,29,30-trisnorneohop-13(18)-ene; C_{27} hop-17(21)-ene – C_{27} 22,29,30-trisnorhop-17(21)-ene; X – Unknown compound co-eluting with C_{32} ββ hopane; Standard – Deuterated *n*-tetracosane.

Table 8
Total concentrations of identified biomarker classes (μg/g TOC) in aliphatic fraction.

	Sample/Species	Aliphatic sesquiterpenoids	Aliphatic diterpenoids	Aliphatic non-hopanoid triterpenoids	*n*-Alkanes	Aliphatic hopanoids	Aliphatic steroids	Aliphatic fernenes	Isoprenoids
Lignite	Pis 1	N.D.	8.67	0.17	121.74	100.57	1.98	N.D.	2.78
	Pis 2	0.25	7.31	0.68	150.8	109.46	N.D.	N.D.	1.66
	Pis 3	8.04	426.53	8.07	605.29	414.58	6.22	2.72	5.90
	WS 1	20.76	475.71	18.42	732.73	974.02	7.69	5.65	10.53
	WS 2	0.60	59.19	28.02	203.76	111.34	2.03	2.36	1.90
Fossil wood	*Quasisequoioxylon piskowitzense*	1.81	59.00	N.D.	N.D.	0.16	0.22	N.D.	0.45
	Taxodioxylon cryptomerioides	7.68	327.73	N.D.	N.D.	1.72	4.91	N.D.	N.D.
	Sciadopityoxylon wettsteinii	N.D.	990.12	N.D.	6.70	0.48	6.41	N.D.	7.90
Modern wood	*Sequoiadendron giganteum*	0.12	5.01	N.D.	4.64	N.D.	N.D.	N.D.	1.55
	Cryptomeria japonica	2.25	13.84	N.D.	4.38	N.D.	N.D.	N.D.	1.27
	Sciadopitys verticilata	2.87	39.25	N.D.	7.48	N.D.	N.D.	N.D.	1.80

Schwark et al. (2002) reported an increase in *n*-C_{31} during the cold periods, as a result of a rapid decrease in deciduous trees and extensive development of grasslands. However, considering the established palaeoclimate data in Federal Republic of Germany during Middle Miocene (Bruch et al., 2007; Madelaine et al., 2007), the prevalence of *n*-C_{31} in studied samples can be attributed to warm climate.

6.3.3. *Implications from hopanoids*

Hopanoids represent important constituents of EOM (Tables 7–9). The result documents a significant contribution of prokaryotic bacterial biomass to the precursor OM. The hopanoid distribution in aliphatic fraction of samples is notably dominated by C_{31} αβ(R) hopane (> 80%, with exception of WS 2, where proportion of this hopanoid is 64%; Table 11). According to the measured $\delta^{13}C$ values of C_{31} αβ(R) hopane in lignite (Mitrović et al., 2016; Pancost et al., 2007), heterotrophic bacteria that consumed higher-plant-derived OM was proposed as the main source of this hopanoid. Hopanoids containing up to 30 carbon atoms, present in the studied samples, may have additional sources, like ferns, lichens, and mosses. Unsaturated hopenes are detected in the studied samples in low amounts (Table 11), however it is noteworthy to mention that WS samples have an order-of-magnitude higher proportion of hopenes with double bonds in position 17(21) and 13(18) than the Pis lignite. Due to the relatively low amount of sulphur in the studied lignite (Table 4), the impact of sulphate reducing bacteria as a possible source of C_{30} hop-17(21)-ene (Wolff et al., 1992) can be excluded, with exception of WS 1 sample. Therefore, C_{30} hop-17(21)-ene in samples most probably originated from diagenetic isomerisation of C_{30} hop-22 (29)-ene (diploptene; Volkman, 1986; Wakeham, 1990), which was found in ferns, mosses, lichens, fungi and hopanoid-containing bacteria (Bottari et al., 1972; Ourisson et al., 1979). Since fernenes are identified in WS lignite, whereas perylene (fungal indicator) was absent (Tables 7, 9), the elevated contents of 17(21)-hopene and particularly, 13(18)-hopene (Table 10), in these samples can be attributed to impact of ferns. Furthermore, a typical characteristic of WS 2 is apparently the higher proportion of C_{27} and C_{29} hopanes with ββ-configuration than in other samples (Table 11). $C_{27}17\beta(H)$- and $C_{29}17\beta(H)21\beta(H)$ hopanes could originate from heterotrophic bacteria, but also from chemoautotrophic and methanotrophic bacteria (Mitrović et al., 2016; Neunlist and Rohmer, 1985; van Winden et al., 2012). On the other hand, enhanced content of C_{27} and C_{29} homologues may be indicative of rather oxidizing

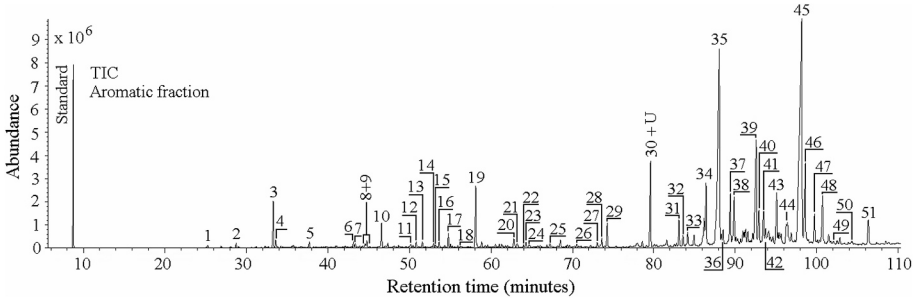


Fig. 14. Total ion current (TIC) of lignite aromatic fraction (sample WS 2).
Peak assignments: 1–1,2,3,4-Tetrhydrocadalene (calamenene); 2 – Cadina-1(10),6,8-triene;
3–1,6-Dimethyl-4-isopropyl-naphthalene (cadalene); 4–1,6-Dimethyl-3-isopropyl-naphthalene (isocadalene); 5 – Phenanthrene; 6–16,17-Bisnorsimonellite; 7–19-Norabietatetraene;
8–9-Methylphenanthrene; 9–1-Methylphenanthrene; 10 –Norsimonellite;
11–1,7-Dimethylphenanthrene; 12 – Fluoranthene; 13 – C3-phenanthrene; 14 – Pyrene;
15–1,2,3,4-Tetrahydroretene; 16 – Benzo(*b*)naptho(2,1d)-furan; 17 – Simonellite;
18 – Totarane; 19 – Retene; 20 – Dehydroferruginol; 21 – Ferruginol; 22 – Des-A-8,14-seco-noroleana-5,7,9,13,15,17- hexaene; 23–2-Methylretene; 24 – Des-A-8,14-seco-norlupa-5,7,9,13,15,17-hexaene; 25 – Chrysene + Triphenylene; 26 – Pentamethyldodecahydrochrysene; 27 – Methylchrysene; 28 – Des-A-trinorursa-5,7,9,11,13,15,17-heptaene (3,4,7-trimethyl-1,2,3,4-tetrahydrochrysene); 29 – Des-A-trinoroleana-5,7,9,11,13,15,17-heptaene (3,3,7-trimethyl-1,2,3,4-tetrahydrochrysene); 30–5,8-Dimethyl- + 7,8-dimethyl MTTC (MTTC – 2-methyl-2-(4,8,12-trimethyltridecyl)chroman); U – Unknown compound co-eluting with dimethyl-MTTC; 31 – Pentanorlupa-1,3,5(10)-triene; 32–8,14-Seco-trisnoroleana(ursa)-1,3,5,7,9,13,15,17-octaene; 33–8,14-Seco-trisnor-oleana(ursa)-1,3,5,7,9,13,15,17-octaene; 34 – Dinoroleana(ursa)-pentaene; 35–24,25-Dinoroleana-1,3,5(10),13(18)-tetraene; 36 – Trisnoroleana(ursa)-1,3,5(10),12-tetraene; 37–24,25 Dinorursa-1,3,5(10),12-tetraene; 38–24,25 Dinorlupa-1,3,5(10)-triene; 39 – Tetranoroleana-1,3,5(10),6,8,11,13-heptaene (2,2,4a,9-tetramethyl-1,2,3,4,4a,5,6,14b-octahydropicene); 40 – Tetranorursa-1,3,5(10),6,8,11,13-heptaene (1,2,4a,9-tetramethyl-1,2,3,4,4a, 5,6,14b-octahydropicene); 41 – BCD-ring triaromatic hopane;
42–4-Methyl, 24-ethyl, 19-norcholesta-1,3,5(10)-triene; 43 – Tetranoroleana-1,3,5(10),6,8,11,13-heptaene, isomer; 44 – ABCD-ring tetraaromatic hopane; 45 – Pentanorursa-1,3,5(10),6,8,11,13,15,17(18)-nonaene (1,2,9-trimethyl-1,2,3,4-tetrahydropicene);
46 – Pentanoroleana-1,3,5(10),6,8,11,13,15,17(18)- nonaene (2,2,9-trimethyl-1,2,3,4-tetrahydropicene); 47 – Pentanoroleana(ursa)-decaene (trimethyl-1,2 dihydropicene);
48 – Pentanoroleana(ursa)-decaene (trimethyl-1,2 dihydropicene); 49 – C_{32} Benzohopane;
50 – C_{33} Benzohopane; 51 –Pentanoroleana(ursa)-undecaene (trimethylpicene);
Standard – Deuterated naphthalene.

Table 9
Total concentrations of identified biomarker classes (μg/g TOC) in aromatic fraction.

	Sample/ Species	Aromatic sesquiterpenoids	Aromatic diterpenoids	Aromatic non-hopanoid triterpenoids	Aromatic hopanoids	Aromatic steroids	Lanosta (eupha) derivatives	MTTCs	Perylene	PAHs	Fatty acids methyl esters
Lignite	Pis 1	0.83	4.83	71.51	4.48	1.81	5.29	0.20	0.25	2.08	N.D.
	Pis 2	0.44	28.18	68.45	4.11	3.03	4.94	0.07	0.83	2.68	N.D.
	Pis 3	5.25	58.01	293.44	20.30	8.67	40.28	N.D.	N.D.	3.74	117.67
	WS 1	18.72	18.40	762.95	138.39	N.D.	48.28	N.D.	N.D.	5.48	N.D.
	WS 2	15.42	39.40	469.19	25.88	8.89	1.78	0.28	N.D.	20.50	N.D.
Fossil wood	*Quasisequoioxylon piskowitzense*	N.D.	2.12	N.D.	N.D.	N.D.	N.D.	N.D.	N.D.	N.D.	N.D.
	Taxodioxylon cryptomerioides	8.71	6.18	19.73	0.81	N.D.	2.16	N.D.	N.D.	N.D.	N.D.
	Sciadopityoxylon wettsteinii	N.D.	2.98	N.D.	N.D.	N.D.	N.D.	N.D.	N.D.	N.D.	N.D.
Modern wood	*Sequoiadendron giganteum*	0.04	0.06	N.D.	N.D.	N.D.	N.D.	N.D.	N.D.	N.D.	N.D.
	Cryptomeria japonica	0.27	0.21	N.D.	N.D.	N.D.	N.D.	N.D.	N.D.	N.D.	N.D.
	Sciadopitys verticilata	0.44	N.D.	N.D.	N.D.	N.D.	N.D.	N.D.	N.D.	N.D.	N.D.

Legend: For abbreviations see the legend of Table 7.

palaeoconditions.

The presence of unsaturated hopenes and domination of ββ-isomers in range C_{27}, C_{29}-C_{30} over αβ-hopanes is consistent with an immature stage of OM. The ratio of 17β(H)21β(H) to (17β(H)21β(H) + 17α(H)21β(H)) C_{30} hopanes (Table 11) is within range proposed for lignite, (Mackenzie et al., 1981) or even higher, indicating deposition of OM in primarily reducing environment (Marynowski and Zatoń, 2010). The latter is further supported by apparent prevalence of saturated hopanes over unsaturated hopenes (Fig. 16).

6.3.4. *Implications from perylene*

Perylene that is commonly present in immature terrestrial OM (Grice et al., 2009; Itoh et al., 2012; Mitrović et al., 2016; Zhang et al., 2014) is detected in small concentration only in samples Pis 1 and Pis 2 (Table 9). Since it is generally considered as indicator of conifer fossil wood degradation by wood-degrading fungi (Kohzu et al., 2005; Marynowski et al., 2013), the absence or low amount of this biomarker may be indicative for low fungal activity (consistent with low amount of fusinite; Kus et al., 2020).

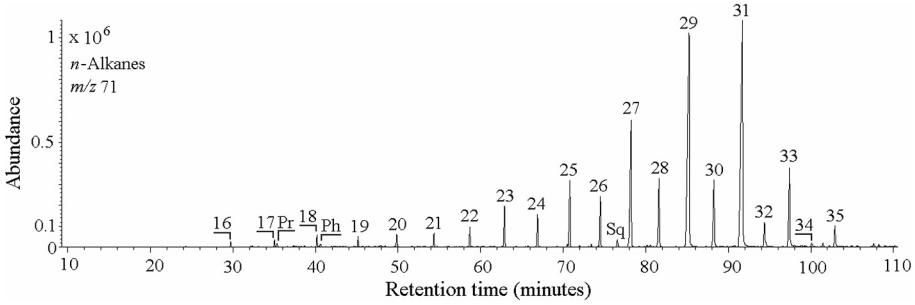


Fig. 15. GC–MS mass chromatogram of *n*-alkanes, *m/z* 71, in lignite (sample WS 2). For peak assignments, see the legend of Fig. 13.

Table 10
The values of the parameters calculated from the distributions of *n*-alkanes and isoprenoids.

	Sample/Species	*n*-Alkane maximum	$CPI_{23–33}$	*n*-C_{15} – *n*-C_{20} (%)	*n*-C_{21} – *n*-C_{25} (%)	*n*-C_{26} – *n*-C_{33} (%)	Paq	*n*-C_{31}/*n*-C_{27}	*n*-C_{31}/*n*-C_{29}	Pr/Ph
Lignite	Pis 1	*n*-C_{31}	5.75	2.89	20.34	76.77	0.22	6.21	2.32	0.55
	Pis 2	*n*-C_{31}	5.88	2.39	34.47	63.14	0.44	4.21	1.71	0.85
	Pis 3	*n*-C_{31}	6.68	2.08	12.80	85.12	0.15	8.36	2.23	0.68
	WS 1	*n*-C_{29}	7.34	1.79	7.97	90.24	0.07	3.09	0.75	0.59
	WS 2	*n*-C_{31}	4.67	2.48	9.88	87.64	0.10	2.64	1.11	1.15
Fossil wood	*Quasisequoioxylon piskowitzense*	N.C.	N.C.	N.C.	N.C.	N.C.	N.C.	N.C.	N.C.	0.39
	Taxodioxylon cryptomerioides	N.C.	N.C.	N.C.	N.C.	N.C.	N.C.	N.C.	N.C.	N.C.
	Sciadopityoxylon wettsteinii	*n*-C_{18}	N.C.	N.C.	N.C.	N.C.	N.C.	N.C.	N.C.	0.91
Modern wood	*Sequoiadendron giganteum*	*n*-C_{25}	3.64	6.21	64.55	29.24	0.85	0.16	0.47	0.85
	Cryptomeria japonica	*n*-C_{25}	4.47	4.82	62.63	32.55	0.71	0.59	0.83	0.52
	Sciadopitys verticilata	*n*-C_{25}	2.41	7.49	58.59	33.92	0.73	0.26	0.25	1.68

Legend: $CPI_{23–33}$ – Carbon Preference Index determined for distribution of *n*-alkanes C_{23}-C_{33}, $CPI_{23–33} = 1/2$ x [Σodd(*n*-C_{23} - *n*-C_{33})/Σeven(*n*-C_{22} - *n*-C_{32}) + Σodd(*n*-C_{23} - *n*-C_{33})/Σeven(*n*-C_{24} - *n*-C_{34})] (Bray and Evans, 1961);
n-C_{15} – *n*-C_{20} (%) = (Σ *n*-C_{15} – *n*-C_{20}) x 100/Σ of total *n*-alkanes;
n-C_{21} – *n*-C_{25} (%) = (Σ *n*-C_{21} – *n*-C_{25}) x 100/Σ of total *n*-alkanes;
n-C_{26} – *n*-C_{33} (%) = (Σ *n*-C_{26} – *n*-C_{33}) x 100/Σ of total *n*-alkanes;
Paq = (*n*-C_{23} + *n*-C_{25})/(*n*-C_{23} + *n*-C_{25} + *n*-C_{29} + *n*-C_{31}) (Ficken et al., 2000);
n-Alkanes were quantified from mass chromatogram *m/z* 71;
Pr/Ph = Pristane/Phytane (Didyk et al., 1978);
N.C. – Not calculated due to the absence of compounds.

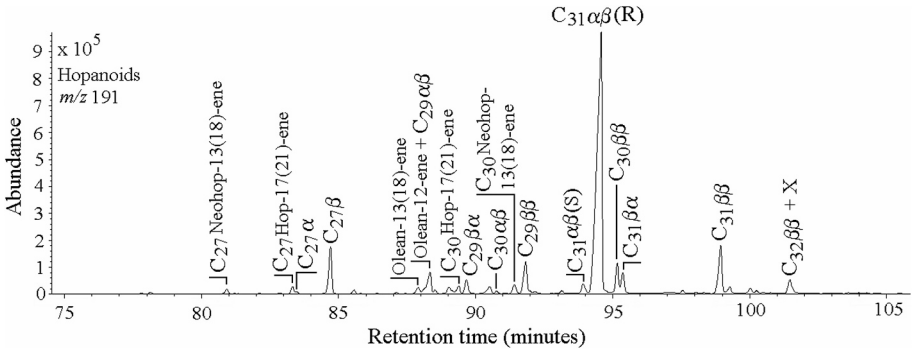


Fig. 16. GC–MS mass chromatogram of hopanoids, *m/z* 191, in lignite (sample WS 2). For peak assignments, see the legend of Fig. 13.

6.3.5. General implications for palaeovegetation

The obtained results imply impact of forested and reed-mire vegetation, with prevalence of the latter, associated with dominance of angiosperm-derived triterpenoids over conifer diterpenoids. Conifer precursor families are mainly represented by Cupressaceae and Pinaceae. A slight input of aquatic macrophytes and ferns is also evident, whereas microbial derived hopanoids played an important role in the precursor biomass. The main differences between WS and Pis lignite are expressed by higher dehydroicetexane content, Paq index, and the tetracyclic/tricyclic diterpanes ratio, as well as by lower contents of non-hopanoid triterpenoids, total hopenes (particularly those with double bond at 13(18)-position), and fernenes in the latter one. Mentioned results indicate decreasing contribution of Cupressaceae and emergent macrophyta, associated with increased input of Pinaceae, angiosperms, and ferns to precursor OM of WS in comparison to the Pis lignite, thus may imply change to slightly drier conditions in WS open-cast mine (Kasiński and Słodkowska, 2016; Worobiec et al., 2021). In general, the biomarker signatures are consistent with the results of palaeobotanical studies, indicating Pinaceae (*Piceoxylon pseudotsugae, Pinus), Erica* species (*Cyrilla*), reed sweet-grass, shrubs, Cupressaceae sensu lato

Table 11
The values of parameters calculated from distributions of hopanoids and sterenes.

	Sample/Species	$C_{31}\alpha\beta$(R) (%)	Unsaturated hopenes (%)	$C_{27}\beta$ Hopane x 100/ (C_{27} + ΣC_{29}-C_{31})$\beta\beta$ Hopanes (%)	$C_{29}\beta\beta$ Hopane x 100/ (C_{27} + ΣC_{29}-C_{31})$\beta\beta$ Hopanes (%)	$C_{30}\beta\beta$ Hopane x 100/ (C_{27} + ΣC_{29}-C_{31})$\beta\beta$ Hopanes (%)	$C_{31}\beta\beta$ Hopane x 100/ (C_{27} + ΣC_{29}-C_{31})$\beta\beta$ Hopanes (%)	$C_{31}\alpha\beta$(S) Hopane/ $C_{31}\alpha\beta$(S + R) Hopanes	$C_{30}\beta\beta$ Hopane/ $C_{30}(\beta\beta + \alpha\beta)$ Hopanes	ΣAliphatic hopanoids/ ΣAromatic hopanoids	pH	C_{27} Sterenes (%)	C_{28} Sterenes (%)	C_{29} Sterenes (%)
Lignite	Pis 1	80.77	0.22	25.69	19.39	17.66	37.26	0.01	0.87	22.45	3.40	1.48	13.17	85.34
	Pis 2	85.39	0.31	20.11	13.49	15.47	50.93	0.03	0.88	26.63	3.37	4.26	8.47	87.27
	Pis 3	85.46	0.17	21.32	15.43	13.77	49.48	0.02	0.88	20.42	3.38	3.18	8.99	87.83
	WS 1	86.11	1.23	14.18	14.57	11.50	59.76	0.01	0.93	7.04	3.41	2.64	6.59	90.77
	WS 2	63.98	1.74	28.97	22.27	17.41	31.35	0.03	0.92	4.30	3.66	1.68	5.40	92.92
Fossil wood	*Quasisequoioxylon piskowitzense*	N.C.	100	N.C.	N.C.	N.C.	N.C.	N.C.	N.C.	N.C.	N.C.	0.00	0.00	100
	Taxodioxylon cryptomerioides	100	N.C.	N.C.	N.C.	N.C.	N.C.	N.C.	N.C.	2.12	N.C.	0.00	0.00	100
	Sciadopityoxylon wettsteinii	N.C.	100	N.C.	N.C.	N.C.	N.C.	N.C.	N.C.	N.C.	N.C.	0.00	0.00	100

Legend: β designates configuration at C_{17} in hopanes; ββ and αβ designate configurations at C_{17} and C_{21} in hopanes;
(R) and (S) designates configuration at C_{22} in hopanes;
$C_{31}\alpha\beta$(R) (%) = $C_{31}\alpha\beta$(R) hopane x 100/Σ of total aliphatic hopanoids;
Unsaturated hopenes (%) = ΣUnsaturated hopenes x 100/Σ of total aliphatic hopanoids;
pH = [5.22 x $C_{31}\beta\beta$-hopane/C_{31} ($\beta\beta$ + $\alpha\beta$R)-hopanes] + 3.11 (Inglis et al., 2018);
Aliphatic hopanoids were quantified from mass chromatogram *m/z* 191;
C_{27} Sterenes (%) = 100 x $C_{27}(\Delta^2 + \Delta^4 + \Delta^5)$-Sterenes/Σ($C_{27}$-$C_{29}$)$(\Delta^2 + \Delta^4 + \Delta^5)$-Sterenes;
C_{28} Sterenes (%) = 100 x $C_{28}(\Delta^2 + \Delta^4 + \Delta^5)$-Sterenes/Σ($C_{27}$-$C_{29}$)$(\Delta^2 + \Delta^4 + \Delta^5)$-Sterenes;
C_{29} Sterenes (%) = 100 x $C_{29}(\Delta^2 + \Delta^4 + \Delta^5)$-Sterenes/Σ($C_{27}$-$C_{29}$)$(\Delta^2 + \Delta^4 + \Delta^5)$-Sterenes;
Sterenes were quantified from mass chromatogram *m/z* 215;
N.C. – Not calculated due to the absence of compounds;
Modern wood samples are not listed in the table, because they do not contain hopanoids and steroids.

Table 12
The values of parameters calculated from the distributions of diterpenoids and non-hopanoid triterpenoids.

	Sample/Species	Di/(Di + Tri)	Tetracyclic Di/ Tricyclic Di	Dehydroicetexane (μg/g TOC)	Phenolic abietanes (μg/g TOC)	1-Ar ring Di (μg/g TOC)	2-Ar ring Di (μg/g TOC)	3-Ar ring Di (μg/g TOC)	1-Ar ring Di/ (1 − +2 − +3-Ar rings) Di	ΣAliphatic diterpenoids/ ΣAromatic diterpenoids
Lignite	Pis 1	0.16	1.38	1.03	0.24	2.23	1.54	0.82	0.49	1.80
	Pis 2	0.34	1.75	2.79	10.52	2.98	13.68	1.00	0.17	0.26
	Pis 3	0.62	2.48	27.43	0.24	35.14	21.82	0.82	0.61	7.35
	WS 1	0.39	0.11	2.59	N.D.	11.17	5.96	1.28	0.61	25.85
	WS 2	0.17	0.63	0.70	4.41	4.27	12.8	17.92	0.12	1.50
Fossil wood	*Quasisequoioxylon piskowitzense*	N.C.	1.58	N.D.	N.D.	N.D.	2.12	N.D.	N.C.	27.83
	Taxodioxylon cryptomerioides	0.94	0.27	N.D.	N.D.	2.40	3.78	N.D.	0.39	53.05
	Sciadopityoxylon wettsteinii	N.C.	1.02	N.D.	N.D.	2.98	N.D.	N.D.	N.C.	332.40
Modern wood	*Sequoiadendron giganteum*	N.C.	0.66	N.D.	N.D.	N.D.	0.06	N.D.	N.C.	77.82
	Cryptomeria japonica	N.C.	0.38	N.D.	N.D.	0.12	0.09	N.D.	0.56	65.80
	Sciadopitys verticilata	N.C.	0.21	N.D.	N.D.	N.D.	N.D.	N.D.	N.C.	N.C.
	Sample/Species	**T1 (μg/g TOC)**	**T2 (μg/g TOC)**	**T3 (μg/g TOC)**	**T1/T3**	**1-Ar ring T1 (μg/g TOC)**	**3-Ar ring T1 (μg/g TOC)**	**4-Ar ring T1 (μg/g TOC)**	**1-Ar ring T1/ (1 − +3 − +4-Ar rings) T1**	
Lignite	Pis 1	67.05	2.16	2.31	29.01	34.80	22.08	6.72	0.55	
	Pis 2	65.54	1.17	1.74	37.71	43.08	16.32	5.88	0.66	
	Pis 3	285.33	4.10	4.02	70.94	198.91	74.66	9.05	0.70	
	WS 1	719.94	35.66	7.35	97.98	425.82	198.55	86.36	0.60	
	WS 2	448.6	9.11	11.49	39.05	167.26	63.23	208.32	0.38	
Fossil wood	*Quasisequoioxylon piskowitzense*	N.D.	N.D.	N.D.	N.C.	N.D.	N.D.	N.D.	N.C.	
	Taxodioxylon cryptomerioides	17.31	N.D.	2.42	7.14	15.70	1.61	N.D.	0.91	
	Sciadopityoxylon wettsteinii	N.D.	N.D.	N.D.	N.C.	N.D.	N.D.	N.D.	N.C.	
Modern wood	*Sequoiadendron giganteum*	N.D.	N.D.	N.D.	N.C.	N.D.	N.D.	N.D.	N.C.	
	Cryptomeria japonica	N.D.	N.D.	N.D.	N.C.	N.D.	N.D.	N.D.	N.C.	
	Sciadopitys verticilata	N.D.	N.D.	N.D.	N.C.	N.D.	N.D.	N.D.	N.C.	

Legend: Di/(Di + Tri) = ΣDiterpenoids/(ΣDiterpenoids + ΣNon-hopanoid triterpenoids);
Tetracyclic Di/Tricyclic Di = (Σ of tetracyclic aliphatic diterpenoids with beyerane, phyllocladane and kaurane skeleton))/(Σ of tricyclic aliphatic diterpenoids with isopimarane, pimarane and abietane skeleton);
1-Ar ring Di – Total aromatic diterpenoids with one aromatic ring;
2-Ar ring Di – Total aromatic diterpenoids with two aromatic rings;
3-Ar ring Di – Total aromatic diterpenoids with three aromatic rings;
T1 – Total pentacyclic aromatic non-hopanoid triterpenoids;
T2 – Total 8,14-seco aromatic non-hopanoid triterpenoids;
T3 – Total tetracyclic des-A-degraded aromatic non-hopanoid triterpenoids;
1-Ar ring T1 – Total pentacyclic aromatic non-hopanoid triterpenoids with one aromatic ring;
3-Ar ring T1 – Total pentacyclic aromatic non-hopanoid triterpenoids with three aromatic rings;
4-Ar ring T1 – Total pentacyclic aromatic non-hopanoid triterpenoids with four aromatic rings;
N.D. – Not detected; N.C. – Not calculated due to the absence of compounds.

(*Cryptomeria*, *Quasisequoia*), accompanied with greater amount of *Pinus* in WS than in the Pis facies (Kus et al., 2020).

6.4. Sources of OM in fossil wood

6.4.1. Implications from $\delta^{13}C$

The $\delta^{13}C$ values of four fossil wood samples analyzed in this study were compared with the $\delta^{13}C$ values of living and recently deceased trees from the Holocene (n = 1174) and subfossil wood from the Neogene (n = 68) (after Lukens et al., 2019 and references therein; Fig. 21). This large $\delta^{13}C$ dataset includes, among others, Miocene fossil wood samples from the Hambach open-cast in Federal Republic of Germany, the Lubstów deposit in Poland, the Oberdorf lignite seam and the Zillingdorf lignite deposit in Austria (Bechtel et al., 2002, 2003a, c, Bechtel et al., 2007a, 2007b; Poole et al., 2006; van Bergen and Poole, 2002). According to published data, in both the Holocene and Neogene (on average) gymnosperms had higher $\delta^{13}C$ values (from −25.9 to −21.3 ‰) than angiosperms (from −29.3 to −22.7 ‰). The wood fossils analyzed in this study yield $\delta^{13}C$ values ranging from −24.6 ‰ to −20.3 ‰ that are consistent with Neogene gymnosperm trees. In general, higher $\delta^{13}C$ values, particularly in *Taxodioxylon cryptomerioides* and *Sciadopityoxylon wettsteinii* in comparison to gymnosperm samples shown in Fig. 21, suggest good preservation of cellulose, since it was reported that cellulose decomposition is usually associated with the progressive depletion of wood in ^{13}C (Bechtel et al., 2008; Benner et al., 1987).

6.4.2. Implications from biomarker distributions

Biomarker assemblages in fossil wood samples that are characterised by sharp prevalence of diterpenoids and the presence of conifer derived sesquiterpenoids clearly confirmed gymnosperm sources (Figs. 18, 19). Differences in $\delta^{13}C$ values (Fig. 21) and abundance of individual diterpenoid compounds resulted from variable contribution of individual conifer taxa.

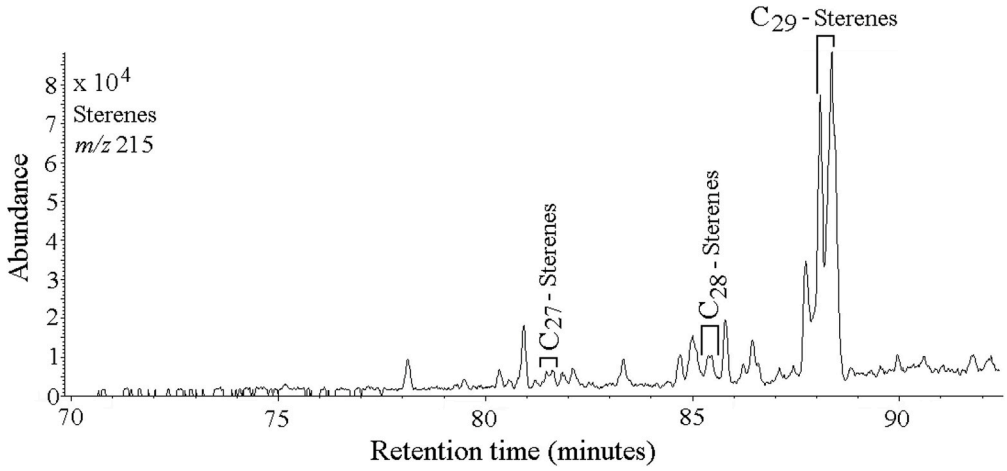


Fig. 17. GC–MS mass chromatogram of sterenes, *m/z* 215, in lignite (sample WS 2). For peak assignments, see the legend of Fig. 13.

Comparison of biomarker distributions in lignite and fossil wood indicates similarities between samples originating from the same location. 16α(H)-Phyllocladane is the most abundant diterpenoid in the Pis lignite and *Quasisequoioxylon piskowitzense*, whereas compounds with pimarane and abietane skeleton prevail in WS lignite and *Taxodioxylon cryptomerioides*. Concentrations of sesquiterpenoids and steroids are higher in *Taxodioxylon cryptomerioides* than in *Quasisequoioxylon piskowitzense*, consistent with greater amount of these biomarker classes in WS in comparison to Pis lignite. The presence of low amounts of non-hopanoid triterpenoids in *Taxodioxylon cryptomerioides* can be attributed to inherent (native) impurity, consistent with prevalence of these biomarkers in the WS lignite (Table 7). Mentioned similarities indicate that biomarker assemblages in lignite can be used for estimation of palaeoconditions, which are responsible for good preservation of cellulose in fossil wood samples.

Furthermore, distributions of diterpenoids and sesquiterpenoids, as well as fatty acids (Figs. 18–20) in fossil and modern wood samples are also similar. The main difference is reflected through a higher amount of saturated diterpenoid hydrocarbons with pimarane and abietane skeleton in fossil wood than in modern one, where corresponding unsaturated dienes prevail. This can be attributed to hydrogenation reactions and implies reducing conditions.

6.4.3. Implications from Micro-FTIR

Micro-FTIR spectra collected from the examined fossil wood samples indicate bands in the cellulose and lignin regions of remarkable high intensity and well- comparable similarity (Fig. 12). Semi-quantitative analysis of micro-FTIR data suggests presence of cellulose in all samples and its well-preserved status. It has been shown that *Taxodioxylon cryptomerioides* has the highest cellulose to lignin ratio (6.9; Table 6), and, thus, the highest content of cellulose among the investigated samples.

Micro-FTIR, FTIR, or ATR-FTIR methods have commonly been applied as qualitative and semi-quantitative tools to identify chemical functional groups, differentiate between softwoods and hardwoods, and to evaluate the degree of degradation of fossil wood samples. These techniques enable to investigate chemical alterations in OM by comparison of the presence or the absence of specific bands as well as band intensities. FTIR fossil wood spectra display a characteristic fingerprint region at 800–1700 cm^{-1} and a large OH band (2900–3400 cm^{-1}) and allow to assign specific bands to cellulose, α-cellulose, hemicellulose, or lignin (Fig. 12). An extensive assignment of FTIR bands is presented in Faix (1991, 1992), Pandey (1999), and Schwanninger et al. (2004). In general, the coalification process induces profound changes to the molecular components in fossil OM. For sub-fossil samples, the hemicellulose FTIR bands at 1740 and 1220 cm^{-1}, the cellulose bands at 1370, 1160 cm^{-1}, and the lignin bands at 1510 and 1260 cm^{-1} have been proposed. Marynowski et al. (2023) documented similarly a shoulder with complex band at 1710–1740 cm^{-1} and assigned the band to the presence of pectin and/or hemicelluloses in Miocene and Eocene xylite from Borków and Niedźwiada quarries. Additionally, Marynowski et al. (2023) also assigned a similar band at 1367 cm^{-1} to cellulose and various types of hemicelluloses (xyloglucan, galactomannan, and mannan). Further, a characteristic and again well-comparable cellulose band at 1160 cm^{-1} was suggested to represent C—O and C–OH stretching vibrations. In the present study, the broad peak at 3340 cm^{-1} is distinctive for stretching vibration of the hydroxyl group in polysaccharides. This peak may also comprise inter- and intramolecular hydrogen bond vibrations in cellulose. The band at 2869 cm^{-1} is characteristic to C—H stretching vibration in polysaccharides. Typical bands assigned to cellulose were observed in the region of 1740–830 cm^{-1}.

Analytical studies performed on fossil and sub-fossil wood indicate in many cases a preferential hydrolytic removal of polysaccharides, while the lignin moieties display only slight changes. Studies such as these by Uçar et al. (2005) confirm the labile nature of polysaccharides by investigating two fossil trunks of *Sequoiadendron giganteum* excavated in a coal mine located about 20 km west of Bosporus. In that study, the respective FTIR spectra pointed toward more saturated groups, a higher aromaticity, and the presence of more condensed units in the case of fossil milled wood lignins (MWLs). As presence and preservation of cellulose in fossil gymnosperms can vary widely in the geologic record, studies revealing abnormalities existing in specific molecular groups and prevailing in well-preserved fossil wood samples are increasingly important As such, Wolfe et al. (2012) documented well-preserved cellulose of fossil wood of *Metasequoia* genus buried in the 53.3 ± 0.6 Ma Panda kimberlite pipe of the Lac de Gras field in the Slave province, Northwest Territories, Canada. The performed FTIR study on early Eocene (Ypresian) fossil wood indicated major absorption peaks including CH_2 deformation (900 cm^{-1}) and CH_3 skeletal vibration (1375 cm^{-1}), testifying at the same time to the presence of α-cellulose. The yielded spectra are different from those of hemi- and holocellulose. Other cases of astonishingly well-preserved fossil wood are reported from the neighbouring Diavik kimberlite A-154, A-418 pipes, and from the Ekati Panda kimberlite pipe of the same Lac de Gras kimberlites (Hook et al., 2015). The ATR-FTIR spectra of fossil wood samples (genus *Piceoxylon*; age 53.3 ± 0.6 Ma) from Ekati Panda kimberlite showed many ATR-FTIR peaks diagnostic of lignin (e.g., 1600, 1512, and 1265 cm^{-1}) and α-cellulose (e.g., 1029, 1058, 1105, and 1161 cm^{-1}).

In conclusion, micro-FTIR allowed for the delineation of semi-quantitative changes in molecular structure of the *in-situ* fossil wood. The successfully applied method confirms the presence of well-preserved cellulose and supports the hypothesis of limited microbial

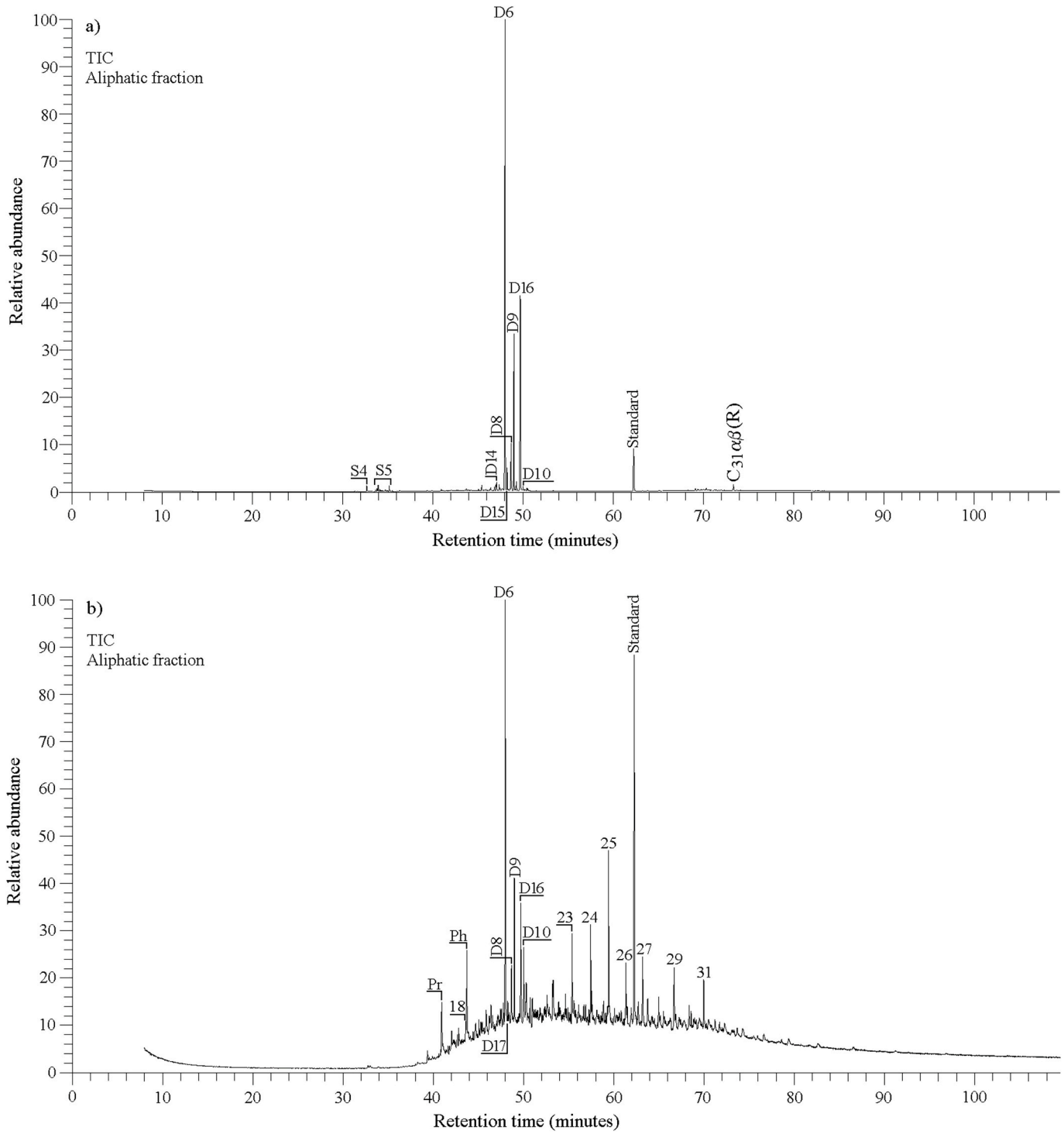


Fig. 18. Total ion current (TIC) of aliphatic fraction: (a) fossil wood – *Taxodioxylon cryptomerioides*, (b) modern wood – *Cryptomeria japonica*.
Peak assignments: S4 – α-Cedrene; S5 – Hydrogenated cadinenes and muurolenes - isopropyl (1 or 4) dimethyl (4,7 or 1,6) octahydronaphthalenes; D14 – Nor-abietane; D15 – Beyerane;
D16 – Abietane; D17 – Pimaradiene; *n*-Alkanes are labelled according to their carbon number; Standard – Squalane; for other peak assignments, see the legend of Fig. 13.

degradation of OM.

6.5. Depositional environment and palaeoclimate

6.5.1. General implications from lignite bulk parameters

In lignite, total S and TOC contents demonstrated good positive correlation ($r = 0.92$; Table 4), whereas a negative correlation between sulphur and ash yield ($r = -0.89$; Table 4) is observed, suggesting that sulphur is mostly associated (incorporated) with OM. The data indicate that peatification occurred in a reducing environment and also may imply a limited concentration of iron in the water body. The high TOC/S ratios (> 10) and TOC around 50% (Table 4), are consistent with terrestrial palaeoenvironment (Berner and Raiswell, 1984).

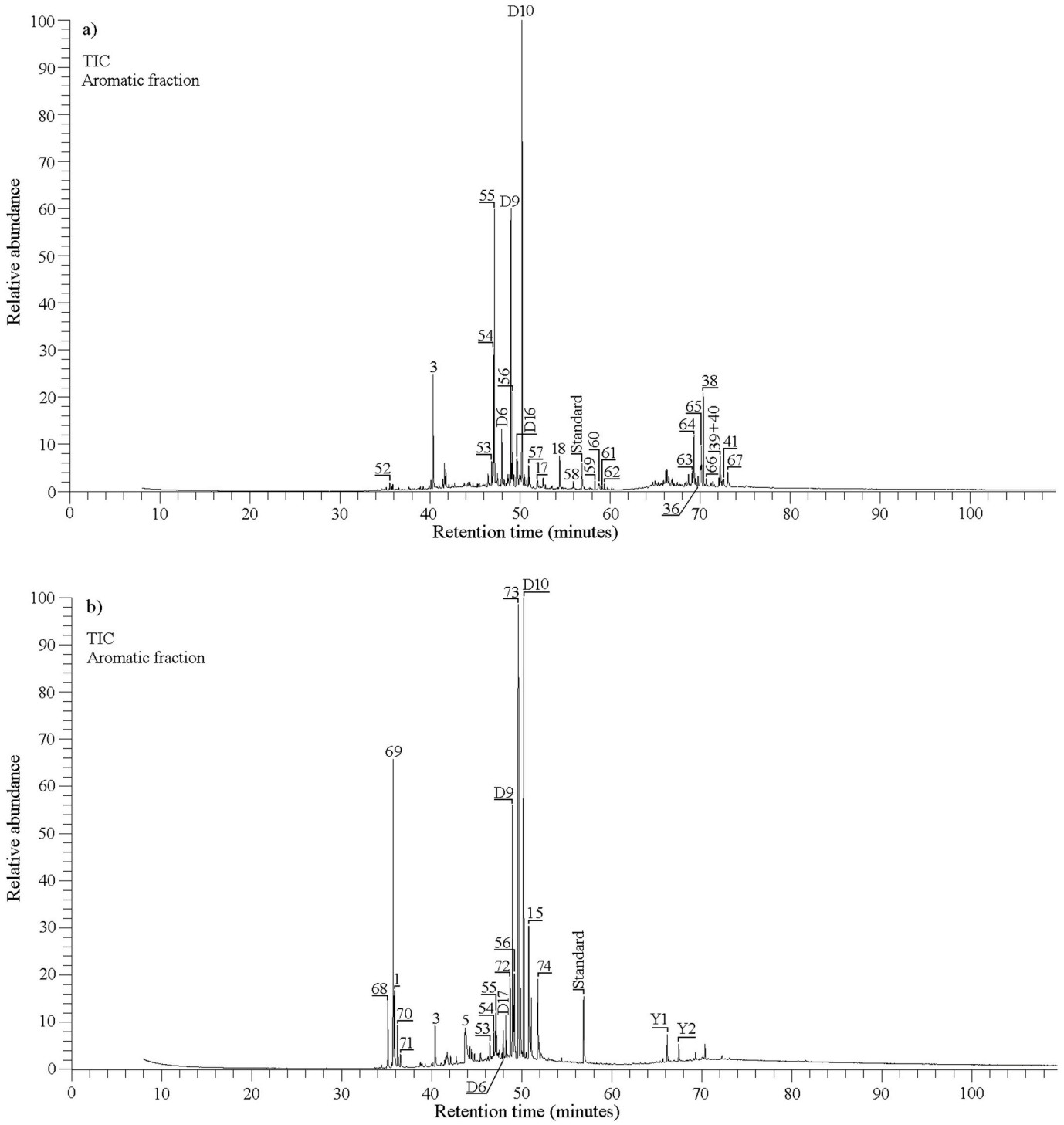


Fig. 19. Total ion current (TIC) of aromatic fraction of fossil wood – (a) *Taxodioxylon cryptomerioides* and (b) modern wood – *Cryptomeria japonica*.
Peak assignments: 52 – Cuparene; 53–16,17-Bisnordehydroabietane; 54 – Hibaene;
55 – Hibaene isomer; 56 – Rimuene; 57–1-Metilbisnorabietatriene; 58 – Sempervirane;
59 – Pentamethyldecahydrochrysene; 60–3,3,7,12a-tetramethyl-1,2,3,4,4a,11,12,12a-octahydrochrysene; 61–3,4,7,12a-tetramethyl-1,2,3,4,4a,11,12,12a-octahydrochrysene;
62 – Des-A-26,27-dinolupa-5,7,9,11,13-pentaene; 63 – C_{29} Sterene; 64 – Dinor-oleana-1,3,5(10),12-tetraene; 65 – C_{29} Steradiene; 66 – Lanostaeuphapentaene;
67 – Lanostaeuphahexaene; 68 – α-Muurolene; 69 and 70 – Muurolene isomers (hexahydrocadalenes); 71–4-Isopropyl-4,7-dimethyl-1,2-dihydro-naphthalene;
72 – Bisnordehydroabietane isomer; 73 – Abietadiene; 74 – Dihydroretene;
Y1 and Y2 – Unknown isomers (M^+ =?, basic peaks 205, 121 and 81); Standard – 11′-binaphthyl; For other peak assignments, see the legends of Figs. 13 and 14.

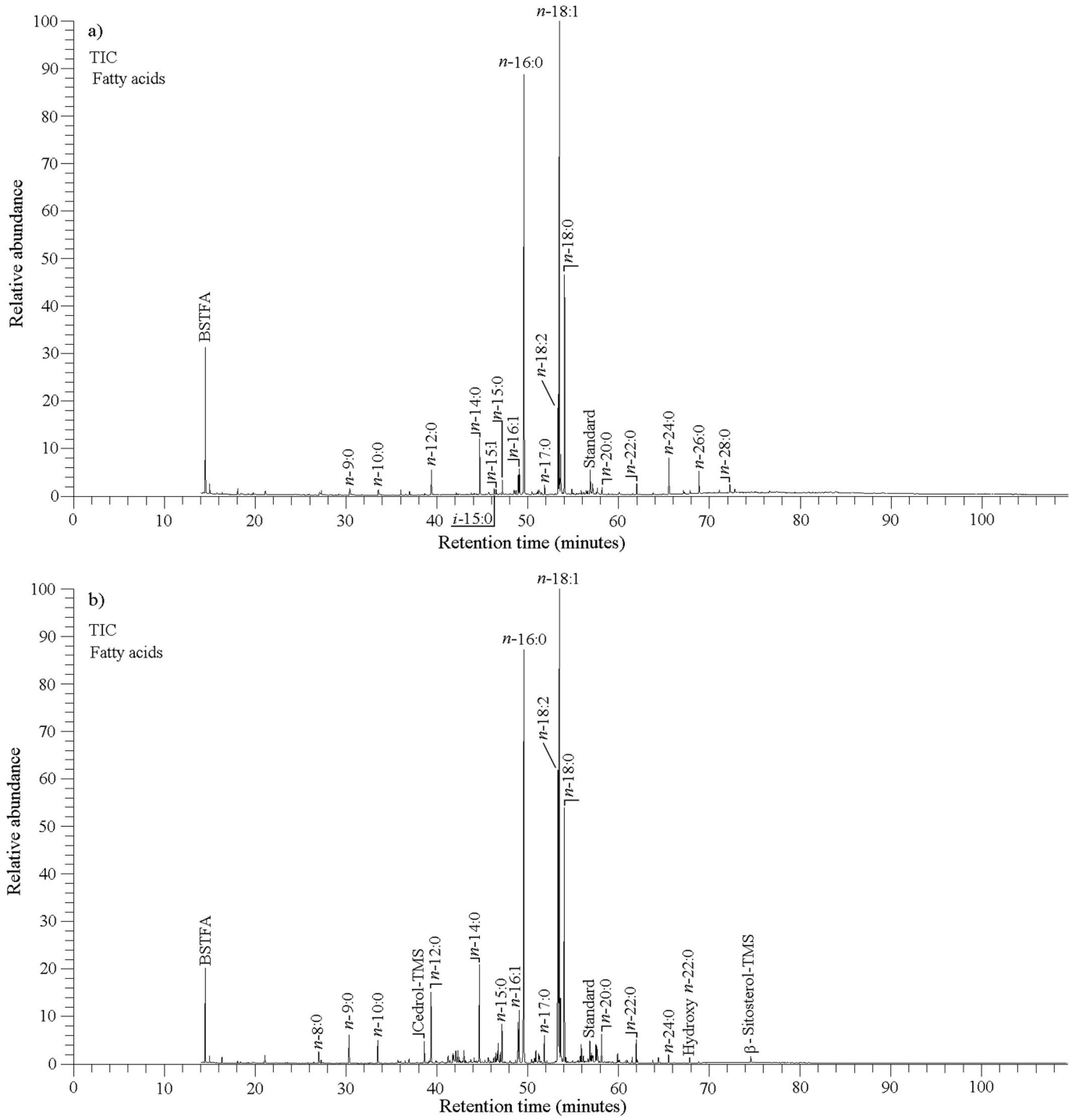


Fig. 20. Total ion current (TIC) of fatty acids, derivatised as trimethylsilyl (TMS) esters of (a) fossil wood – *Taxodioxylon cryptomerioides* and (b) modern wood – *Cryptomeria japonica*.
Peak assignments: BSTFA – *N,O*-bis(tri methylsilyl)trifluoroacetamide; Fatty acids are denoted as x:y, with x indicating number of carbon atoms and y giving the number of double bonds; structural isomers are denoted by prefixes, *n* – normal and *i* – iso; Standard – 11′-binaphthyl.

6.5.2. *The Piskowitz open-cast mine*

The biomarker data of Pis 1 and Pis 2 samples are similar (Tables 7–12). The prevalence of *n*-alkanes and hopanoids over diterpenoids and non-hopanoid triterpenoids coincides with prevalence of densinite among huminite group macerals (Kus et al., 2020), indicating water-saturated depositional environment with a stable groundwater table. The dominance of angiosperm-derived biomarkers over conifer-derived diterpenoids is considered to reflect the angiosperm-dominated vegetation in the precursor biomass, as indicated by palaeobotanical data. Concerning the generally lower resistance of angiosperm biomass to degradation, limited degradation under a stable water table and reducing conditions are implied. The above mentioned data are further supported by prevalence of pentacyclic monoaromatic non-hopanoid triterpenoids over counterparts with greater number of aromatic rings (Table 12). Despite relatively abundant hopanoids, the bacterial degradation was rather limited, as reflected in the notable domination of pentacyclic aromatic non-hopanoid triterpenoids over tetraclyclic ones (T1/T3); low amount of triaromatic retene derivatives

in relation to contents of mono- and diaromatic diterpenoids (Table 12); high CPI (Table 10); high values of the $C_{30}\beta\beta/(C_{30}\beta\beta + C_{30}\alpha\beta)$ hopane ratio (Table 11); and, although having limited validity for lignite, the Pr/Ph ratio < 1 (Table 10). This is in line with Tissue Preservation Index (TPI) slightly above 1 and Gelification Index (GI), in range 1.5–2.0 (Kus et al., 2020), which indicate low degree of aerobic OM degradation and its fast deposition (Diessel, 1986, 1992).

The Pis 3 sample is characterised by higher concentrations of all biomarkers in comparison to Pis 1 and Pis 2 (Table 7), consistent with greater TOC and EOM contents (Table 4). The Pis 3 sample is the only exception in the studied sample set that has Di/(Di + Tri) ratio > 0.5 (i.e., 0.6; Table 12), which indicates slightly higher contribution of conifers over angiosperms. Furthermore, it differs from Pis 1 and Pis 2 by the higher amount of long chain *n*-alkanes, lower Paq, higher CPI, and higher tetracyclic Di/tricyclic Di ratio (Tables 10, 12). Considering the prevalence of dehydroicetexane among aromatic diterpenoids and cuparene among sesquiterpenoids in this sample, associated with almost identical ash yield and sulphur content in all Pis lignite samples, the observed differences in the Pis 3 sample can be attributed to elevated impact of woody vegetation, particularly those derived from Cupressaceae. The result is consistent with slightly higher TPI in Pis 3 sample in comparison to Pis 1 and 2 (Kus et al., 2020). Despite enhanced content of hopanoids in Pis 3 than in Pis 1 and Pis 2 lignite, low degree of diagenetic aromatization is reflected by a notable increase of contents of the monoaromatic diterpenoids and monoaromatic pentacyclic non-hopanoid triterpenoids vs. their counterparts with greater number of aromatic rings, the T1/T3 ratio and the ratio of aliphatic vs. aromatic diterpenoids (Table 12). These findings, as well as the high $C_{30}\beta\beta/(C_{30}\beta\beta + C_{30}\alpha\beta)$ hopane ratio (Table 11) and low Pr/Ph < 1 (Table 10) argue for a reducing environment.

Briefly, the obtained data suggest that Pis lignite is formed in permanently water-logged mire with stable water level (table) under reducing, mesotrophic conditions. Based on the uniform ash yields (≈ 11%; Table 4) in the Pis samples, periodical flooding can be assumed.

6.5.3. The Welzow-Süd open-cast mine

Despite richness in microbial communities (the highest hopanoid concentration in the studied sample set), degree of aromatization of diterpenoids and non-hopanoid triterpenoids in WS 1 is similar or lower than in Pis lignite, suggesting reducing conditions. High CPI and $C_{30}\beta\beta/(C_{30}\beta\beta + C_{30}\alpha\beta)$ hopane ratio, and low Pr/Ph (< 0.6) support this interpretation (Tables 10, 11). High amount of total hopanoids, prevailing over the concentrations of all other biomarker classes (Table 7), associated with the highest content of C_{30} 17(21) hopene in studied sample set may imply some impact of sulphate-reducing bacteria (Wolff et al., 1992) that coincides with a slight increase of sulphur (Table 4) in the WS 1 sample. Anaerobic microbial activity under high water level is further supported by low TPI ≈ 0.5 and GI ≈ 10 (Diessel, 1986, 1992; Kus et al., 2020).

The WS 2 sample is characterised by the prevalence of angiosperm-derived non-hopanoid triterpenoids over *n*-alkanes and hopanoids, which dominated in the other samples (Tables 7–9). Furthermore, this sample has higher degree of aromatization of both diterpenoids and non-hopanoid triterpenoids (Table 12), associated with elevated concentration of PAHs (Tables 7, 9), greater proportion of C_{27}- and C_{29} ββ hopanes (Table 11), and Pr/Ph slightly higher than 1 (Table 10). The results suggest a lowering of the water level and peatification in transitional/slightly oxic environment. The enhanced aromatization of WS 2, concerning the same maturity level in addition to increased Eh settings, can be also partly attributed to post-depositional erosion and/or palaeo-wildfires. Comparing to the Pis open-cast mine, the obtained results suggest enhanced fluctuation of water level and/or post-depositional events in WS. Very low amount of ash in both WS samples (Table 4), being characterisitic in xylite-rich lignite, suggests that mire was isolated from siliciclastic input.

6.5.4. Implications from $\delta^{13}C$

The $\delta^{13}C$ of known taxa can enable a reconstruction of environmental and climatic change (van Bergen and Poole, 2002; Lukens et al., 2019). The $\delta^{13}C$ values (−25.4 to −23.1‰) obtained from the Early Miocene Oberdorf fossil gymnosperm wood of the Köflach-Voitsberg coal district, Austria (Bechtel et al., 2002), and $\delta^{13}C$ values (−25.1 to −22.7‰) sourced from the late Miocene (Pannonian) fossil gymnosperm wood of the Hausruck lignite district, Austria (Bechtel et al., 2003a) are, in general, only slightly lower than $\delta^{13}C$ values (−24.6 to −20.3‰) recorded in this study for Miocene fossil gymnosperm wood collected from the 2nd MFH. Similarly, partially lower $\delta^{13}C_{wood}$ values for gymnosperm wood (−25.7 to −22.8‰) were also reported by Bechtel et al. (2007a) for the Middle Miocene fossil wood of Poland and $\delta^{13}C$ (−24.9 to −22.5‰) for the Late Miocene fossil wood in Austria (Bechtel et al., 2007b). A very similar scenario is present for *Taxodioxylon* sp. The $\delta^{13}C$ values (−23.7 to −22.2‰) of *Taxodioxylon* sp. reported by Poole et al. (2006)) for Middle Miocene of Federal Republic of Germany are partially lower than $\delta^{13}C$ values (−22.1 to −21.9‰) of *Taxodioxylon cryptomerioides* recorded for the Middle Miocene of the 2nd MFH in the study area.

Concluding, the reconstructed carbon isotope record for fossil wood for the Middle Miocene of the Lusatia lignite mining district, Federal Republic of Germany, displays a deviation within the lignite facies of *Marcoduria* (M-facies) for different gymnosperm taxa. Nevertheless, the obtained results are in general agreement with corrected $\delta^{13}C$ reported for lignite (Bechtel et al., 2008). The latter generally co-varies with approximations related to mean annual temperature reported for the Paleogene to Neogene (Krutzsch et al., 1992; Eissmann, 1994; Blumenstengel et al., 1996; Bruch, 1998; Haas et al., 1998; Kolcon and Sachsenhofer, 1999).

As seen in the compilation of available data (Fig. 21), angiosperm and gymnosperm samples of Neogene age are higher in $\delta^{13}C$ as compared to Holocene wood. As Holocene vegetation differs from Miocene flora, differences in isotopic fractionation between different species must be taken into account. Variations in $\delta^{13}C$ of CO_2, available to the plants, are considered to be of minor importance, as $\delta^{13}C$ variations of 2.5‰ are within the range of variability observed in plants within a habitat, and can be explained without invoking variations in

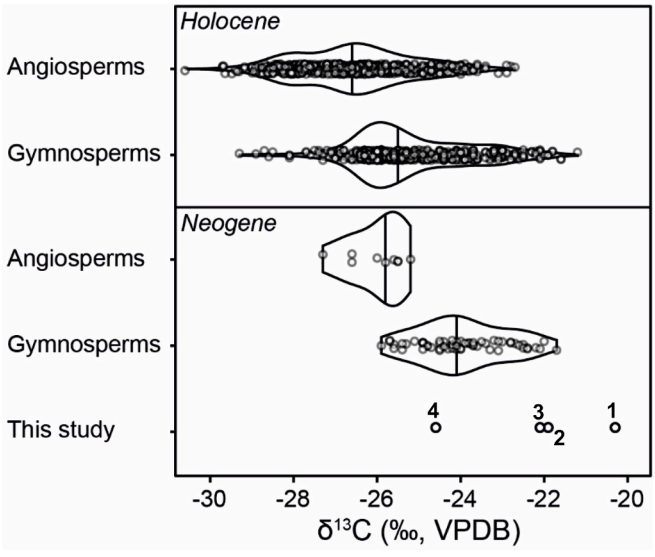


Fig. 21. Violin plots of $\delta^{13}C$ values of wood fossils from this study compared with trees from the Holocene and Neogene (after Lukens et al., 2019). Violins are mirrored kernel density functions with medians shown as vertical bars. Legend: 1 – *Sciadopityoxylon wettsteinii*; 2 – *Taxodioxylon cryptomerioides*; 3 – *Taxodioxylon cryptomerioides* (additional sample); 4 – *Quasisequoioxylon piskowitzense*.

$\delta^{13}C$ of CO_2 (Diefendorf et al., 2019; Inglis et al., 2019). The obtained differences in $\delta^{13}C$ may be interpreted to have been caused by water availability to the plants, due to the adjustment of stomatal aperture to minimise water loss (van Bergen and Poole, 2002; Bechtel et al., 2008; Jahren and Sternberg, 2008; Diefendorf and Freimuth, 2017; Diefendorf et al., 2019). However, wide-spread peat accumulation during the Neogene, argues against less humid conditions in comparison to the Holocene. Therefore, the differences in $\delta^{13}C$ data of Holocene and Neogene wood and lignite are most likely related to differences in mean annual air temperatures.

6.6. Implications for preservation of cellulose within the in-situ fossil stumps and trunks

The *in-situ* occurrence of fossil stumps and trunks preserved in lignite-bearing strata is a common feature in the geological record (Mosbrugger et al., 1994; Hámor-Vidó et al., 2010; DiMichele and Falcon-Lang, 2011; Mustoe et al., 2019, and references therein). As such, fossilization of naturally preserved secondary xylem can occur under diverse geological conditions, including, among others, rapid and catastrophic burial in the course of tsunamis or storm surge, subsidence due to tectonic events or earthquakes, river or lake flooding, tidal sedimentation, sandbar or sand dune migration, crevasse-splay deposition, slumps and landslides, sea-level rise, early diagenetic mineralization, diminished oxygenation, and lack of bacterial or fungal degradation. Thus, the resulting forms of preservation can vary from mummified, coalified, or petrified wood tissue.

Coalified woody tissue is, in general, composed of transformation products of lignin such as catechols, phenols, and napthols (Poole et al., 2006). Fossil lignin-cellulose-hemicellulose complexes are typically structurally and chemically modified with the progressive loss of hemicellulose and cellulose and retention of some lignin (Stankiewicz et al., 1998). Despite recent advances, understanding of the role of cellulose and lignin in preservation of fossil tree trunks is deficient. Spackman et al. (1976) inferred for the Everglades-Mangrove swamp-marsh complex of southern Florida in Georgia, USA that the extracted hemicellulose is not exclusively a plant-only-related hemicellulose but it also contains fungal and bacterial polysaccharides. The primarily extracted hemicellulose (glucose, xylose) from cell walls of higher plants and obtained from surface peat differed significantly in constituents from the hemicellulose extracted from peat at lower depths. The latter contained much less glucose and xylose. Instead, uronic acids and other neutral sugars such as rhamnose appeared in significant concentrations. This suggests that microbial polysaccharides provide an important input to the total sum of polysaccharides of hemicellulose as supported by Exarchos and Given (1977) as well as Lucas et al. (1988). In the context of geological record, substantial not-lignified cellular material can be preserved as argued by Cohen and Spackman (1977), Bates and Hatcher (1989), Bates et al. (1991), Fengel (1991), Moers et al. (1994), Yang et al. (2005), and Lechien et al. (2006). As a result, the preserved α-cellulose can be slightly altered chemically without depolymerization, according to Given (1984), Given et al. (1984), Hámor-Vidó et al. (2010), and Hook et al. (2015). The lack of destructed cellular morphology is accompanied by the evidence that cellulose can survive in some peats as presented by Given et al. (1984).

Cellulose in the examined fossil wood samples of *Taxodioxylon cryptomerioides*, *Sciadopityoxylon wettsteinii*, and *Quasisequoioxylon piskowitzense* was detected by incident light microscopy, CLSM-induced calcofluor staining, and cellulose analyses. The techniques employed herein testify unequivocally to the presence of well-preserved cellulose in the examined xylite of the M-facies (more differentiated into MCy-facies, MSc-facies, and MQu-facies). Besides the studied *in-situ* fossil tree stumps and trunks occurring in open-cast mines of WS, M, and Pis, also other former open-cast mines were reported to hold similar occurrences. Gothan (1922, 1926) was first to notice the occurrence of cellulose in xylite-rich lithotype of Miocene lignite exploited in the Lusatia Wilhelmsglück coalfield at Klettwitz (Lower Lusatia, Federal Republic of Germany). Other cellulose-rich lignite was reported to occur in the Weidmannsheil coalfield in the vicinity of Klettwitz (Angel and Scharizer, 1932). Following the occurrence of other cellulose-rich lignite in the Lusatia lignite mining district, Potonié (1895) and Gothan and Benade (1930) introduced new terms of “Sapperit” and “Faserlignite”, i.e., fibrous xylites for the occurrence of cellulose-rich lignite at megascopic scale. In addition, Gothan and Benade (1930) pointed to their specific defibration, durability, high flexibility, and specific high elasticity. The authors associated these properties with bast or inner bark of conifer wood tissue. The rows of bast cells formed thin bast plates, which became weathered, eroded, or frayed upon disintegration. The corresponding cellulose-rich xylites were composed of over 30% cellulose and were macroscopically characterised by a white or light colour. The delineated cellulose-rich “Faserlignite” in the 2nd MFH of the Middle Miocene were also identified and classified in the Berzdorf and Zittau Olbersdorf open-cast mines. The macroscopic appearance of the trunks and cellulose-rich “Faserlignite” was also detected in the Niemtsch open-cast mine in the wood trunk-rich horizons of the M-facies, displaying only some insignificant changes, lacking signs of humification or fusinitisation. The volume of macerated wood tissue, composed dominantly of cellulose, decreases significantly in the upper portion of the respective examined wooden trunk (Schneider, 1969a).

Apart from macroscopically described cellulose-enriched xylites, microscopic research studies were also conducted. Jurasky (1938a, 1938b) reported on transmitted-light microscopy methods which enabled the identification of cellulose in xylites. The method used double refraction of micellar structures viewed under polarised-light microscopy. Sapperit displays a whitish-blue illumination under fluorescence irradiation (Roselt, 1978). This supports results obtained in this study by means of transmitted light microscopy. Microscopically, in polished sections, the cellulose-rich cell walls are characterised by fibrous structure, low reflectance (Rr <0.10%), anisotropy effects in transmitted light, and a strong yellow fluorescence (Schneider, 1995). In order to differentiate the cellulose-rich from cellulose-poor cell walls, Schneider (1998) called the cellulose-rich cell walls “cellinite”, being comparable to “dark textinite A". The latter is the established and approved term (Sýkorová et al., 2005). Schneider (1998) designated a “cellinite deadline” to illustrate the phenomenon of cellulose-rich “Faserlignite,” marking at the same time the degradation limit of cellulose.

The *in-situ* preserved cellulose-rich xylites constituting the examined wood trunks were collected from the wood trunk-rich horizons of the MCy-facies, for example, *Cryptomeria-conferta* bog facies identified within the Middle Miocene 2nd MFH (Dolezych, 2005). The M-facies, for example, *Marcoduria* bog facies in the Pis, Klettwitz, Schlabendorf, Plessa-Lauch, Niemtsch, Scado, Spreetal, and Burghammer open-cast mines in the Lusatia lignite mining district, is composed of both the *Marcoduria* species together with the *Sequoia* leaves (Schneider, 1966, 1969b). Later, Schneider (2004) established the S-facies (*Sequoia* open canopy-woodland facies), which is dominated by remains of *Sequoia* and successively located between the K-facies and A-facies (see above, paragraph 2.0).The abundance of cellulose-rich “Faserlignite”, i.e., fibrous lignite, in the Pis open-cast mine is characteristic of the younger lignite-bearing strata of the 2nd MFH but not for all strata (Heinicke, 1905). In the submerged shoots of the *Marcoduria* roots within the MSc-facies, “*Sciadopitys* bog facies”, the parenchyma tissue cells of roots were separated from the vascular bundles by zig zag (*germ.*: Zick-Zack) running bundle sheath. The vascular bundles contained among other thick cell-walled parenchymatic cells, known as aerenchymas, supporting, as such, oxygen transport and humic colloidal solutions, while in the parenchyma tissues of the roots reducing conditions prevailed. After the death of tree, the transport routes of oxygen transport and humic colloidal solutions remain preserved in the aerenchymas, resulting in the coagulation of humocollinite (levi- and porigelinite) as shown by Schneider (1984).

It has been suggested that processes of cellulose decomposition and transformation of lignin both start at the early phase of wood transformation at peatification stage and that both processes can occur simultaneously (Hatcher, 1988; Senftle et al., 1986; Stout et al., 1988). Within the development of peat, the process of decay vs. preservation of fallen and surface vegetation shifted more toward preservation of at least cellulose-rich plant material (Hower et al., 2013, 2021). High preservation of cellulose and minimal modification of lignin for the sample studied suggest that the conditions were very favourable for wood preservation. Several factors can contribute to such high preservation. Low Eh and pH of the environment favour the preservation of cellulose and lignin, resulting in minimal wood transformation (Francis, 1961; Teichmüller and Teichmüller, 1968; O'Keefe et al., 2013). Another factor suggested is the sparsity of microorganisms that can attack cellulose and cleave the glycosidic bonds within the cellulose chains (Kirk, 1973; Eriksson and Wood, 1985). In addition, avoidance of bacterial and fungi attacks in the uppermost oxidation zone of the peat layer, as well as fast burial into its deeper, more reducing zone, was adopted by Schneider (1966, 1969a, 1995) to account for the occurrence of a considerable amount of cellulose in the *in-situ* preserved wooden stumps. Protection of the wood by conifer resins, i.e. terpene resins sensu Hower et al. (2021) could also contribute to excellent wood preservation. This suggestion can be related to the possible exudation of resin by coniferous species (Cupressaceae s.l. and Pinaceae) formed as a result of changing climatic conditions, environment/depositional conditions, fire, or disease, due to, for example, microbial infection or fungal invasion. The associated fungal relation with resins is given by Hower et al. (2010, 2013). Also, O'Keefe et al. (2013) and references therein provided an extensive account of fungal association with resins and its role in fungal attacks. While Cupressaceae are less resinous today, they are thought to be the source plants for some Cretaceous and younger amber deposits. On the other hand, Pinaceae resin does not preserve well, and so it is rare in the fossil record (Seyfullah et al., 2018). By comparison, present-day abundance of "traumatic resin canals," into which resin is secreted by the adjacent xylem cells, is well-reported in the Okefenokee mire-marsh complex of Georgia (Spackman et al., 1976). Anaerobic conditions will also exert a certain effect on the preservation potential of cellulose. According to Hedges et al. (1985), holocellulose (i.e. hemicellulose and cellulose) of wood is in theory preferentially degraded relative to lignin, with hemicellulose degrading faster than cellulose under natural anaerobic conditions. Therefore, hemicellulose can be preserved for thousands of years, the cellulose in general millions of years, and the lignin can still be identified after hundreds of millions of years. Lignin can be anaerobically degraded to some extent by bacteria (Benner et al., 1984; Colberg and Young, 1982, 1985). The degree of lignin breakdown also has been shown to be associated with the proportion of fungal hyphae in peat bogs, indicating that saprophytic fungi may be significant contributors to lignin decomposition and depletion of cellulose (Hower et al., 2011; Dai et al., 2020; and references therein). In contrast, under aerobic conditions, lignin as a phenolic polymer of complex structure can be preserved in the presence of molecular oxygen, as shown by Crawford (1981) and Zeikus et al. (1982).

The selective removal and alteration of the chemical structure of wood will depend correspondingly on the respective sedimentary environment (e.g., Blanchette, 1991; van Bergen et al., 1994; Poole et al., 2006), reflecting high-amplitude temporal fluctuations in oxygen and nutrients, soil wetness, etc. In general, it is plausible that oscillating and/or lowering the water table during sedimentation processes gave rise to water-saturated conditions at least to a certain extent in a marine or otherwise brackish-to lacustrine-reducing environment. A high water table could have contributed to the preservation of the wood (Hower et al., 1990). A similar account was revealed in a study of peat sediments from the vast low-lying plain Everglades-Mangrove mire complex of southern Florida in Georgia, USA (Spackman et al., 1976, 1988). Lack or low-range and low degree of degradation of some carbohydrates and thus, only a partial decomposition of lignin can be envisaged in both the hypoxic bottom-water conditions and in deeper layers of the sediment column. Microbial decomposition of OM during early diagenesis may be initially evoked by sulfate-reduction mechanisms in the shallow subsurface. A present-day example of degradation and decomposition of at least part of OM is related to formation and accumulation of a gelatinous, mineral-rich sediment called "liver mud" (*germ.*: Lebermudde) in mangrove ponds of the Everglades-Mangrove mire-marsh complex (Spackman et al., 1976).

Yet another mechanism, which has to be considered is erosion and deterioration of volcanic and granodiorite protoliths. Lowering of the water table during the wet-dry cycles and initiation of weathering of the surrounding tuff- and rhyolite-dominated acidic volcanic rocks may have led to deterioration of the vitreous matrix of tuffs and acidification of the meteoric waters (Lang, 1920, and references therein). The related source of volcanic and granodiorite protoliths is the Lausitz Volcanic Field and especially the Stolpen Volcano, with today's remnants of scoria ash tuff found between the granodioritic frame and the basaltic lava body (Tietz et al., 2018). The Stolpen Volcano is located just south of the studied open-cast mines. The related $^{40}K/^{39}Ar$-isotopic ages point to 25.3 ± 0.5 Ma (Pfeiffer et al., 1984). Similarly, the typical $^{40}Ar/^{39}Ar$ and $^{40}K/^{40}Ar$ -derived isotopic age determinations in the Lausitz Volcanic Field suggest an age of the volcanic deposits between 35 and 23 Ma (Büchner et al., 2015b). In addition, the associated erosion of saprolites on the Lausitz granodiorite and deterioration of the matrix led to formation of the Middle Miocene kaolinite-rich clays. The δD and $\delta^{18}O$ values of the kaolinite-rich clay fractions from various lithologies indicate kaolinization at temperatures of ~15 ± 5 °C from meteoric waters that were isotopically heavier than present-day meteoric waters. In summary, the sedimentary environment of the altered granodiorite and tuffs was characterised by a low pH and did not experience hydrothermal activity. The evidence reported in literature suggests that the presence of granodiorite and volcanic glass in the protoliths of residual clay minerals were a prerequisite for the formation of kaolinite at low pH conditions. It can be envisaged that repeated wet-dry cycling signifies deterioration of these protoliths. This is supported by the sea-level rise due to eustatically-controlled transgression of a high system track, and it also explains the prevalence of the M-facies (*Marcoduria*-Facies) and the lithotype flaser-stratified lignite seam (Süss and Rammler, 1965; Schneider, 1966, 1969a, 1969b). According to Weyland (1957), the M-facies points toward dry forest flora together with a fast and substantial subsidence.

Deterioration of both granodiorite and the vitreous matrix of tuffs was caused by (1) percolation or recharge of peat-sourced humic and fulvic acid-rich waters, or by (2) weathering processes, leading to formation of kaolin. The contemporaneously occurring aqueous alteration of silicate minerals (feldspar and other aluminum silicates) in granodiorite deposits or volcanic glass during the deterioration can lead directly to silica being released to an aqueous solution as monosilicic acid $Si(OH)_4$ and to its *in-situ* precipitation. This provides a possible explanation for the occurrences of opal-A and opal-CT in the studied samples. For the first time, detected occurrences of opal-A and opal-CT in non-permineralised fossil trunks and stumps by means of SEM and CLSM point toward a repeated precipitation of amorphous silica from supersaturated aqueous solutions. The examined SEM images display the comparative morphological features of precipitated amorphous silica ($SiO_2 \bullet nH_2O$). The precipitation of amorphous silica is also confirmed and documented by Schneider (2010) to occur in small, lanceolate leaflets of *Silicophyllum heerlenense*, a dicotyledonous plant of unknown affiliation. The specimen was found in the so-called Fuchsrote Kohle ("Foxy Red Coal") of the under-seam of the Pis open-cast mine and in the 2nd MFH in the Jänschwalde open-cast mine (Süß, 1959; Dolezych and Schneider, 2006; Schneider, 2010). The suggested mode of formation of amorphous silica is in line with hypotheses reported by Eißmann (1968) and Meinel (1986). Other sources of silica precipitation are listed in Standke (2010). These include: (1) quartz grains subjected to lowering

of the silica-enriched groundwater level during humid warm conditions (Hohl, 1957), (2) sands of the barren measures without a large lateral transport (Haage, 1966), and (3) water transport (Radtke, 1966). During the ongoing diagenesis, the precipitated amorphous silica opal-A can be either gradually transformed to opal-CT, opal-C, and eventually to quartz, or it can originate as a result of direct crystallization from dissolved silica in seawater (Cady et al., 1996; Liesegang et al., 2018). The herein reported results show that along with precipitated amorphous silica in tissues of the secondary xylem, there is also a well-documented presence of microcrystalline opal-CT beaded-lepispheres. Thus, a preservation of a gradual transformation from amorphous silica to opal-related forms can be evoked. The amorphous silica might be formed either by aqueous alteration of silicate minerals or by a release of silicic acid into an aqueous environment and its subsequent precipitation by abiogenic processes (Marin-Carbonne et al., 2014). Opal-A may form from both organic and inorganic sources. Opal-A of biogenic origin develops from Si stored in plants and aquatic organisms. Opal-A of inorganic origin precipitates from supersaturated solutions. In general, the precipitation of opal-A is dependent on the degree of supersaturation, ionic strength, and fluid pH value. At ambient conditions and pH <2 to 3, the solubility of amorphous silica is at its maximum, and on pH 7 at its minimum (Iler, 1979). Its solubility also depends on the solution chemistry. In a warm to tropical climate, during weathering, tannins and similar catechol-like substances increase silica solubility significantly. On the contrary, in a cold climate, aqueous aluminum, Na^{+}, K^{+}, Mn^{2+}, Mg^{2+}, Ca^{2+}, etc., represent silica dissolution inhibitors.

Given the presence of both silica species opal-A and opal-CT in the examined fossil wood samples, the alternating solubility of Si in water becomes apparent. The driving force behind these oscillations in Si saturations seems to be controlled by the pore water pH. It is therefore suggested that a relatively early penetration by amorphous silica-saturated solutions of xylitic woody tissue during an early stage of peat formation can account for (1) the particularly well-preserved morphology of fossil wood and (2) the extremely high content of cellulose. This is further reinforced by Siever and Scott (1963) as well as by Stein (1982), who suggested that hydrogen bonds begin to form between the silicic acid sourced from the interstitial pore solution and the hydroxyl groups sourced from the preserved cellulose and lignin.

The authors speculate that xylitic woody tissues were prevented from becoming permineralised, i.e., silicified during later diagenetic processes. In course of the pH variation, dissolution of opal-A species points in general to silica-supersaturated solutions, from which opal-CT can precipitate in preference to quartz. The solubility of amorphous silica increases greatly at pH >9. Therefore, the relatively low number of both silica species in the examined fossil woods indicates that either the respective coating and infilling of opal-A and opal-CT were present but not widespread, or that fluid-mediated and mineral dissolution accounting for removal of silica took place in alkaline conditions. The source of alkaline and fluid-mediated and subsequent mineral dissolutions can be generally related to an influence of a slightly alkaline (pH of 8.0 to 8.4) sea water. Consequently, the associated removal of opal-A and opal-CT can be related and attributed to: (1) deposition of stratigraphically younger transgressive marine strata, (2) influence of subtidal channels present in Middle Miocene interstrata, and (3) steep-sided and distinctly U-shaped subglacial channels formed during Pleistocene glaciations. As for (1) deposition of the overlaying and stratigraphically younger transgressive marine strata, the associated meteoric overprint could have impacted the peat strata, leading to removal of silica species. Considering (2) the influence of subtidal channels present in Middle Miocene interstrata, their formation represents another source for oxygenated sea waters in 2nd MFH (Standke, 2006) and removal of silica precipitates. The (3) source of oxygenated waters, which affected the lignite-bearing 2nd MFH, is steep-sided and distinctly U-shaped subglacial channels incised by an erosion during Pleistocene glaciations (Gothan, 1926; Piotrowski et al., 1999; Kühner, 2009).

The micro-FTIR data and content of holocellulose (Table 3) reveal good (*Quasisequoioxylon piskowitzense* (Pis) and *Sciadopityoxylon wettsteinii* (M)) to excellent (*Taxodioxylon cryptomerioides* (WS)) preservation of cellulose in fossil wood samples. Considering the detailed interpretation of biomarker assemblages given in previous sections, it can be presumed that preservation of cellulose in fossil wood samples was governed by reducing conditions, i.e., low Eh of the environment. The Middle Miocene climate in the studied area was warm (Bruch et al., 2007; Madelaine et al., 2007) and humid, with relatively uniform amount of precipitation during the whole year. The continuous precipitation and warm calm climate may have resulted in formation of water temperature gradient (higher temperature of water in surface) that allowed stratification of the water body and development of reducing conditions even at relatively low depths. Thus, it can contribute to OM preservation, since it is well documented that anaerobic bacteria degrade OM slower in comparison to aerobic bacteria. Based on the very low ash yields (Table 1) in WS samples, a nutrient-poor oligotrophic mire can be presumed. Somewhat higher values of this parameter in Pis samples (Table 1) indicate periodical flooding associated with moderate supply of mineral matter that probably caused more intense degradation of OM, which is reflected through lower content of holocellulose and the cellulose to lignin ratio in *Quasisequoioxylon piskowitzense* than *Taxodioxylon cryptomerioides*. Better preservation of cellulose in *Taxodioxylon cryptomerioides* from the WS open-cast mine, in addition to Eh settings, can be attributed to fluctuation of water level, associated with weathering of the surrounding tuff- and rhyolite-dominated acidic volcanic rock. Such weathering process may cause lowering of pH values. The pH was estimated based on the C_{31} $\beta\beta/(\beta\beta + \alpha\beta)$ hopane ratio in lignite samples (Table 8; it was impossible to calculate this parameter for fossil wood due to the absence of C_{31} $\beta\beta$- or both, C_{31} $\beta\beta$- and $\alpha\beta$- hopane) using the equation proposed by Inglis et al. (2018). The obtained results (pH in range 3.37–3.66; Table 11) indicate quite acidic conditions. Such pH values can be found in low latitude (tropical) ombrotrophic peatlands (bogs sensu Inglis et al., 2018) of Southeast Asia (Anshari et al., 2010; Inglis et al., 2018; Ishikura et al., 2018; Murayama and Bakar, 1996; Page et al., 2006) and/or in raised bogs (Økland et al., 2001). The latter argues for ombrotrophic rather than minerotrophic mire and accounts for its low fertility and buffering by humic acids. This is in line with very low ash yields in WS lignite. However, moderate to high hopanoid concentrations in lignite (Table 4) indicate that acidity is probably overestimated here by proposed equation, consistent with conclusion derived from investigation of the Konin lignite (Bechtel et al., 2019). Nevertheless, the calculated pH value, along with low sulphur and low degree of diagenetic aromatization of diterpenoids and triterpenoids indisputably argue for a limited bacterial activity under acidic conditions during peatification (Casagrande, 1987) and, therefore, a high degree of OM preservation.

In contrast to lignite, all fossil wood samples contain minor hopanoids (0.16–2.53 μg/g TOC; Table 4), consistent with acidic environment, also indicating negligible post-depositional microbial degradation of OM. Limited microbial degradation of OM can be also caused by protection of the wood by conifer resins, particularly due to the fact that fossil Cupressaceae, which contribution has been well confirmed, was more resinous than modern varieties, representing the source plant of some Cretaceous and younger amber deposits (Seyfullah et al., 2018). Perylene is absent in fossil wood remains, WS and Pis 3 lignite, whereas it was detected in very low concentration (0.25–0.83 μg/g TOC; Table 6) in Pis 1 and Pis 2, consistent with negligible amount of funginite (Kus et al., 2020). This is in accordance with observations of Benner et al. (1987) and Bechtel et al. (2007a) that cellulose decomposition occurs mainly under aerobic conditions as a result of fungal, and to some extent bacterial, activity. The negative relationship between contents of EOM and cellulose/holocellulose (Tables 3, 4), reported also by Bechtel et al. (2020), suggests biogeochemical formation of lipids in the wood during gelification and cellulose decomposition. However, the relative enrichment of EOM due to the depletion of fossil wood in cellulose and (partly) lignin cannot be excluded.

In general, palaeovegetation and palaeoenvironment in Pis and WS open-cast mines were similar to those reported by Bechtel et al. (2019) and Widera et al. (2021) for the First Lusatian lignite seam of the Konin Basin (Poland), whereas cellulose content in *Quasisequoioxylon piskowitzense* (Pis) and *Sciadopityoxylon wettsteinii* (WS) is comparable to the cellulose richest fossil wood remains from the same area (Bechtel et al., 2020). This is in line with observation that the Neogene lignite seams from Poland continue into adjacent areas of Federal Republic of Germany (Widera et al., 2008), resulting in a similarity between the Middle Miocene lignite seams in south-eastern Federal Republic of Germany and the first Mid-Polish Lignite Seam (MPLS-1) from the Konin Basin of the same age.

As for the palaeoclimatic implications, the Miocene was largely governed by Miocene Climatic Optimum, a warming event, which was relatively well-constrained by land and ocean surface palaeotemperatures (You et al., 2009). While the Miocene Climatic Optimum is interpreted to represent a global long-term warm interval, in Europe (Wiesa location), mid-latitude regions were subjected to a subtropical palaeoclimate. Regionally, as in case of Lusatia (Wiesa, Federal Republic of Germany), Kunzmann et al. (2022) classified the Neogene and Paleogene flora in central and eastern Federal Republic of Germany into Early-Middle Miocene Younger Mastixioideae flora (Mai, 2000) and from the Paleogene, mainly Eocene into Older Mastixioideae flora. The late Early Miocene Wiesa flora fall into the Younger Mastixioideae flora. Based on new approach of Phytogeographic Reference Region Assessment (PRRA), Kunzmann et al. (2022 and the references therein) provided important insights into the palaeoclimate at the Wiesa site during Miocene and with this at the neighbouring M, Pis, and WS open-cast mines. According to the Köppen-Trewartha classification system, the palaeoclimate was characterised by subtropical and humid conditions, with mean annual temperature (MAT) of ca. 18 °C or slightly lower, with warmest month mean temperature (WMMT) above 25 °C, and coldest month mean temperature (CMMT) between 7 and 9 °C. The growing season during the beginning of Miocene Climatic Optimum (MCO) lasted almost all year. After Kunzmann et al. (2022), the mean annual precipitation (MAP) values for the Wiesa flora site are consistently above 1000 mm. Seasonality in precipitation is revealed by palaeobotanical approaches of Climate Leaf Analysis Multivariate Program (CLAMP), CA (Coexistence Approach), and Isopore Approach (IA)/ Overlapping Distribution Analysis (ODA). The Wiesa floral assemblages and palaeoclimatic conditions were associated with fluvio-alluvial settings located in costal lowlands. It can be implied that similar palaeoclimate conditions prevailed during Middle Miocene (Brieske Formation) and, thus during formation of the 2nd MFH.

Concluding, palaeoenvironmental, and palaeovegetation reconstruction of the Miocene M, Pis, and WS area was established using detailed biomarker analyses, micro-FTIR data, and stable carbon isotope ($\delta^{13}C$) methods. The reconstruction supported in addition by palaeoclimate records revealed a mixed forested and reed-mire vegetation, with predominance of reed-mire vegetation. The higher contribution of angiosperms compared to gymnosperms in precursor lignite OM was established based on contents of diterpenoids and non-hopanoid triterpenoids. Furthermore, biomarker assemblages indicated that conifer precursor families were mainly represented by Cupressaceae and Pinaceae. Although not substantial, a characteristic input of aquatic macrophytes and ferns was evident. It can be suggested that reducing conditions (low Eh) prevailed during the peatification associated with a stable water level, while transitional/slightly oxic environment appear to be: (1) partially linked with lowering of the water level and (2) partially attributed to post-depositional erosion and/or palaeo-wildfires. The fluctuating water table implies periodical flooding events as well as a moderate input of detrital material. More acidic (low pH) conditions are attributable to weathering of the surrounding tuff- and rhyolite-dominated acidic volcanic rock. Their prevalence is largely accentuated during lowering of the water level. As such, preservation of OM in peatland occurred during both the reducing conditions (low Eh) at water highstand and during acidic conditions (low pH) at water lowstand. The associated palaeoenvironmental conditions exerted a decisive influence on the aerobic fungal degradation and bacterial activity, hampering or limiting their degree and extent. In addition, it is suggested that Cupressaceae-derived resins provided in part an additional protection of the wood. In support of the palaeoclimatic conditions, preservation of cellulose in the *in-situ* fossil tree stumps and trunks of *Quasisequoioxylon piskowitzense* (Pis), *Sciadopityoxylon wettsteinii* (M), and *Taxodioxylon cryptomerioides* (WS) species was governed by a dynamic interplay of fluctuating water table, the input of acidified runoff from the eroded and deteriorated volcanic as well as granodiorite protoliths of Lusatia, and the respective autochthonous taphocoenosis.

7. Conclusion

A multidisciplinary research study was conducted to investigate the high-cellulose contents in non-petrified fossil wood samples, representing *Taxodioxylon cryptomerioides* from the Welzow-Süd (WS) open-cast mine (1. Flözbank, lignite seam Nr. 2, M-facies); *Sciadopityoxylon wettsteinii* from the Meuro (M) open-cast mine (2. Flözbank, lignite seam Nr. 2, M-facies); and *Quasisequoioxylon piskowitzense* from the Piskowitz (Pis) open-cast mine, collected from Miocene lignite seams of the Lusatia lignite mining district, Saxony, Federal Republic of Germany.

1. Optical microscopy, CLSM, and calcofluor-stained CLSM examined the optical appearance of cellulose, opal-A, opal-CT, and xylite, as well as the optical properties of xylitic tissue as related to fluorescence spectroscopy of middle lamellas and cell walls of secondary xylem. Results from optical microscopy show extremely well-preserved xylitic tissue characterised by well-developed structural integrity, hampered occasionally by microcracks in cell walls of latewood. The secondary cell walls display a triple zonation of variable lateral extent and thickness, and the so-called PP cells. We suggest that the increased appearance of PP cells may be due to the plant's defense reactions, one of which may be related to wound periderm formation. Results on optical appearance of cellulose in transmitted light demonstrate presence of birefringent and optically anisotropic cell walls of extremely well-preserved tissue with a characteristic undulation phenomenon, supporting undoubtedly the presence of cellulose in huminite. This is further supported by calcofluor-stained CLSM indicating traces of residual cellulose associated with thick-walled latewood tracheids in all samples. In addition, the presence of cellulose is further confirmed by very high holocellulose contents in the examined fossil wood samples.
2. Optical properties determined via CLSM indicate a correspondence between fluorescence emission colour and emission intensity, with the pale fluorescent middle lamellas depicting areas of relatively higher intensity of emission signals. Laser-induced fluorescence spectroscopy indicated a presence of two peaks, with maximum fluorescence intensity of epoxy resin denoting slightly shorter wavelength than the red peak of absorption of the secondary peak associated with fluorescent xylitic tissues.
3. With SEM examination, the presence of opal-A and opal-CT in cells of secondary xylem tissues was confirmed. In addition, opal-A was also observed by CLSM, denoting a characteristic laminar coating in early- and latewood cells. The multilayered lining is dissected and largely fragmented, however not affecting secondary cell walls themselves, as detected in SEM. Opal-CT occurrences are, on contrary, associated with blades, revealing typical irregularly ragged edges and forming crystals that appear as aggregates of spherical lepispheres. The mineralization of Miocene fossil wood adds to a growing body of evidence suggesting a multistage process for wood silicification.
4. The Rock-Eval data revealed subtle differences in source material of the examined organic matter of lignite, reflecting at the same time their early diagenetic preservation rather than hydrocarbon

potential or stage of coalification. The hydrogen-rich material ascertained by S2 and HI values of fossil wood samples suggests resin-rich woods contributing to their early diagenetic preservation.

5. Changes in chemical composition of fossil wood of *Quasisequoioxylon piskowitzense* (Pis open-cast mine), *Sciadopityoxylon wettsteinii* (M open-cast mine), and *Taxodioxylon cryptomerioides* (WS open-cast mine) were analysed with micro-FTIR. The spectra interpretation showed that changes can be observed in hydroxyl groups as well as in C—O and C—H functional groups of polysaccharides and lignin. The study confirmed well-preserved cellulose and hemicellulose bands, with the latter being present at 1740 cm^{-1} and 1245 cm^{-1}. The ring stretching vibration at 1110 cm^{-1} and 1040 cm^{-1} are characteristic for cellulose. The aromatic skeletal vibration at 1507 cm^{-1} is a characteristic peak of lignin. The absorption bands in the cellulose and lignin regions display high intensity and bear a very similar appearance between the analysed samples. The greatest cellulose to lignin ratio was reported for fossil wood of *Taxodioxylon cryptomerioides* from the WS. The aliphatic stretching region (2800–3000 cm^{-1}) and the aliphatic banding region (1350–1500 cm^{-1}) are remarkable.
6. The biomarker assemblages show relatively similar compositions in studied Pis and WS lignite. Contribution of forested and herbaceous vegetation, with prevalence of the latter is indicated, associated with dominance of angiosperm-derived triterpenoids over conifer diterpenoids. Conifer precursor families are represented mainly by Cupressaceae and Pinaceae. A slight input of aquatic macrophytes, mosses, and ferns is also evident, whereas microbial derived hopanoids played an important role in the precursor biomass. The main differences between WS and Pis lignite are expressed by higher dehydroicetexane content, Paq index, and the tetracyclic/tricyclic diterpanes ratio, as well as by lower contents of non-hopanoid triterpenoids, total hopenes, and fernenes in latter one. This indicates decreasing contribution of Cupressaceae and emergent macrophyta, associated with increased input of Pinaceae, angiosperms, and ferns to precursor OM of WS in comparison to the Pis lignite, thus may imply change to somewhat drier conditions in the WS open-cast mine. The Pis lignite formed in permanent wetland swamp with stable water table under reducing, mesotrophic conditions. For WS samples, a nutrient-poor oligotrophic mire can be presumed. Biomarker patterns of WS 1 indicate sedimentation of OM under high water level and reducing settings, whereas WS 2 was formed under transitional/slightly oxic conditions. The obtained results suggest more pronounced fluctuation of water level and/or post-depositional events in the WS than in Pis open-cast mine. Biomarker assemblages that are characterised by sharp prevalence of diterpenoids, the presence of conifer-derived sesquiterpenoids, and $\delta^{13}C$ clearly confirmed gymnosperm sources of fossil wood samples. Comparison of biomarker distributions in lignite and fossil wood indicates similarities between samples originating from the same open-cast mine. Therefore, biomarker assemblages in lignite were used for estimation of palaeconditions, which favoured good preservation of cellulose in fossil wood samples, observed based on holocellulose content and micro-FTIR derived cellulose/lignin ratio > 3. Distributions of diterpenoids and sesquiterpenoids, as well as fatty acids in modern and fossil wood samples are also similar. The main difference is reflected through higher amount of saturated diterpenoid hydrocarbons with pimarane and abietane skeleton in fossil wood than in modern one, where corresponding unsaturated dienes prevail, resulted from hydrogenation reactions, thus implies reducing conditions. This is also evident from numerous biomarker ratios in lignite. In addition to reducing environment, preservation of cellulose in fossil wood was also governed (controlled) by absence/extremely low aerobic fungal degradation, the limited bacterial activity due to the acidic conditions, and good protection of the wood by Cupressaceae-derived resins. The biomarker assemblages in lignite showed very good agreement with palaeobotanical and petrographic data (Kus et al., 2020 and references therein), and provide reasonable explanations for cellulose preservation in the fossil wood, thus confirming their applicability and relevance for determination of sources and depositional environment of sedimentary OM, including complex geological and tectonic areas.
7. The analysed fossils wood samples yield $\delta^{13}C$ values chemotaxonomically consistent with Neogene gymnosperm trees. In general, higher $\delta^{13}C$ values, particularly in *Taxodioxylon cryptomerioides* (WS open-cast mine) and *Sciadopityoxylon wettsteinii* (M open-cast mine) are recorded in comparison to published analyses of gymnosperm samples. This suggests possible relation between $\delta^{13}C$ and cellulose preservation, since previous literature data also reported that cellulose decomposition is usually associated with the progressive depletion of $\delta^{13}C$ in wood.
8. Preservation of high-cellulose contents of the *in-situ* fossil stumps and trunks described as MCy-facies, such as *Cryptomeria-conferta* bog facies, occurred in the Second Lusatian lignite seam (2nd MFH). Our results demonstrate unequivocally the presence of cellulose in examined fossil wood samples and we interpret the high content of cellulose as due to a number of the following factors: high-amplitude temporal fluctuations in the water table, and thus, (1) percolation or recharge of peat-sourced humic acid-rich and fulvic acid-rich waters causing weathering of the surrounding protoliths of tuff- and rhyolite-dominated acidic volcanic and the Lausitz granodiorite and (2) the resulting contemporaneous formation of both the Middle Miocene kaolinite-rich clays at low pH conditions and aqueous alteration of volcanic-related silicate minerals, which lead to a release of silica ions and their precipitation from saturated solutions into the examined woody tissues. The associated low Eh and pH of the environment, sparsity of cellulose-degrading microorganisms, avoidance of bacterial attacks, presence of protective conifer resins, and anaerobic conditions were the resultant or subsequent cause of the fluctuations in the water table and the associated weathering of the protoliths of tuff- and rhyolite-dominated acidic volcanic and the Lausitz granodiorite.

The obtained results allow for (1) a valuable contribution toward the understanding of the presence of extremely high-cellulose contents in the *in-situ* fossil Miocene stumps and trunks and for (2) better understanding of the processes hampering effective fossilization (petrification) of fossil wood processes. The application of multimethod studies through (1) cellulose detection and content determination in secondary xylem tissues, (2) optical characterization of preservation state of wood cell structure in xylite, (3) optical properties of huminite, and (4) opal A and opal-CT detection as linings and fillings enabled researchers to narrow down the most feasible scenario. Finally, the current study demonstrates the applicability of geochemical, micro-FTIR spectroscopy, and stable carbon isotope ($\delta^{13}C$) methods to investigate the *in-situ* deposited and cellulose-enriched fossil tree stumps and trunks. It also reveals that exhaustive palaeoenvironmental and palaeovegetation reconstruction of the Miocene Meuro (M), Piskowitz (Pis), and Welzow-Süd (WS) leads to understanding of the exceptional preservation of high-cellulose contents in fossil wood and their association with formation of kaolin deposits.

CRediT authorship contribution statement

J. Kus: Writing – review & editing, Writing – original draft, Validation, Methodology, Investigation, Data curation, Conceptualization. **M. Dolezych:** Writing – review & editing, Methodology, Investigation, Conceptualization. **W. Schneider:** Investigation. **J.C. Hower:** Writing – review & editing, Validation, Methodology, Conceptualization. **T. Hofmann:** Writing – review & editing, Methodology, Investigation. **E. Visiné Rajczi:** Writing – review & editing, Investigation. **A. Bidló:** Writing – review & editing, Investigation. **B. Bolodár-Varga:** Writing – review & editing, Investigation. **R.F. Sachsenhofer:** Writing – review &

editing, Investigation. **A. Bechtel:** Writing – review & editing, Investigation. **K. Stojanović:** Writing – review & editing, Visualization, Methodology, Investigation. **D. Životić:** Writing – review & editing, Methodology, Investigation. **I. Kojić:** Writing – review & editing, Investigation. **M. Mastalerz:** Writing – review & editing, Investigation. **T. Graupner:** Investigation. **W.E. Lukens:** Investigation, Writing – review & editing. **L. Donaldson:** Investigation, Writing – review & editing.

Declaration of competing interest

The authors declare that they have no known competing financial interests or personal relationships that could have appeared to influence the work presented in this paper.

Data availability

Data will be made available on request.

Acknowledgments

The article is published with the permission of Federal Institute for Geosciences and Natural Resources (BGR), Hannover, Federal Republic of Germany. The study was partly financed by the Ministry of Science, Technological Development and Innovation of Republic of Serbia (Contract number: 451-03-47/2023-01/200168 and 451-03-47/2023-01/200288). The authors are very thankful to the following persons, who contributed samples used for investigations and figures in this study: Dr. Jochen Rascher from the GEOmontan, Freiberg, Federal Republic of Germany and Dr. Ulrich Pietzarka from the Botanical Garden of Tharandt at the Technical University Dresden, Federal Republic of Germany. The authors express their sincere gratitude to two anonymous Reviewers and the Editor for their prompt review and for providing insightful comments that improved the quality of the manuscript.

References

Angel, F., Scharizer, R., 1932. Grundriß der Mineralparagenese. Springer, Wien, 296 pp.

Anshari, G.Z., Afifudin, M., Nuriman, M., Arianie, L., Susana, R., Nusantara, R.W., Sugardjito, J., Rafiastanto, A., 2010. Drainage and land use impacts on changes in selected peat properties and peat degradation in West Kalimantan Province, Indonesia. Biogeosciences 7, 3403–3419. https://doi.org/10.5194/bg-7-3403-2010.

Bardet, M., Pournou, A., 2015. Fossil wood from the Miocene and Oligocene epoch: chemistry and morphology. Magn. Reson. Chem. 53, 9–14. https://doi.org/10.1002/mrc.41439.

Barghoorn, E.S., 1952. Degradation of plant tissues in organic sediments. J. Sediment. Petrol. 22, 34–41. https://doi.org/10.1306/D42694AE-2B26-11D7-8648000102C1865D.

Bates, A.L., Hatcher, P.G., 1989. Solid-state ^{13}C NMR studies of a large fossil gymnosperm from the Yallourn Open Cut, Latrobe Valley, Australia. Org. Geochem. 14, 609–617. https://doi.org/10.1016/0146-6380(89)90040-5.

Bates, A.L., Hatcher, P.G., Lerch, H.E., Cecil, C.B., Neuzil, S.G., Supardi, 1991. Studies of a peatified angiosperm log cross-section from Indonesia by nuclear magnetic resonance spectroscopy and analytical pyrolysis. Org. Geochem. 17, 37–45. https://doi.org/10.1016/0146-6380(91)90038-L.

Bechtel, A., Sachsenhofer, R.F., Gratzer, R., Lücke, A., Püttmann, W., 2002. Parameters determining the carbon isotopic composition of coal and fossil wood in the Early Miocene Oberdorf lignite seam (Styrian Basin, Austria). Org. Geochem. 33, 1001–1024. https://doi.org/10.1016/S0146-6380(02)00054-2.

Bechtel, A., Gruber, W., Sachsenhofer, R.F., Gratzer, R., Lücke, A., Püttmann, W., 2003a. Depositional environment of the Late Miocene Hausruck lignite (Alpine Foreland Basin): insights from petrography, organic geochemistry, and stable carbon isotopes. Int. J. Coal Geol. 53, 153–180. https://doi.org/10.1016/S0166-5162(02)00194-5.

Bechtel, A., Sachsenhofer, R.F., Markic, M., Gratzer, R., Lücke, A., Püttmann, W., 2003b. Paleoenvironmental implications from biomarker and stable isotope investigations on the Pliocene Velenje lignite seam (Slovenia). Org. Geochem. 34, 1277–1298. https://doi.org/10.1016/S0146-6380(03)00114-1.

Bechtel, A., Reischenbacher, D., Sachsenhofer, R.F., Gratzer, R., Lücke, A., 2007a. Paleogeography and paleoecology of the upper Miocene Zillingdorf lignite deposit (Austria). Int. J. Coal Geol. 69, 119–143. https://doi.org/10.1016/j.coal.2006.03.001.

Bechtel, A., Widera, M., Sachsenhofer, R.F., Gratzer, R., Lücke, A., Woszczyk, M., 2007b. Biomarker and stable carbon isotope systematics of fossil wood from the second Lusatian lignite seam of the Lubstów deposit (Poland). Org. Geochem. 38, 1850–1864. https://doi.org/10.1016/j.orggeochem.2007.06.01.

Bechtel, A., Gratzer, R., Sachsenhofer, R.F., Gusterhuber, J., Lücke, A., Püttmann, W., 2008. Biomarker and carbon isotope variation in coal and fossil wood of Central Europe through the Cenozoic. Palaeogeogr. Palaeoclimatol. Palaeoecol. 262, 166–175. https://doi.org/10.1016/j.palaeo.2008.03.005.

Bechtel, A., Widera, M., Woszczyk, M., 2019. Composition of lipids from the First Lusatian lignite seam of the Konin Basin (Poland): Relationships with vegetation, climate and carbon cycling during the mid-Miocene Climatic Optimum. Org. Geochem. 138, 103908 https://doi.org/10.1016/j.orggeochem.2019.103908.

Bechtel, A., Widera, M., Lücke, A., Groß, D., Woszczyk, M., 2020. Petrological and geochemical characteristics of xylites and associated lipids from the First Lusatian lignite seam (Konin Basin, Poland): Implications for floral sources, decomposition and environmental conditions. Org. Geochem. 140, 104052 https://doi.org/10.1016/j.orggeochem.2020.104052.

Benner, R., Maccubbin, A.F., Hodson, R.E., 1984. Anaerobic biodegradation of the lignin and polysaccharide components of ligno-cellulose and synthetic lignin by sediment microflora. Appl. Environ. Microbiol. 47, 998–1004. https://doi.org/10.1128/aem.47.5.998-1004.1984.

Benner, R., Fogel, M.L., Sprague, E.K., Hodson, R.E., 1987. Depletion of 13C in lignin and its implications for stable carbon isotope studies. Nature 329, 708–710. https://doi.org/10.1038/329708a0.

Berner, R.A., Raiswell, R., 1984. C/S method for distinguishing freshwater from marine sedimentary rocks. Geology 12, 365–368. https://doi.org/10.1130/0091-7613(1984)12<365:CMFDFF>2.0.CO;2.

Bi, X., Sheng, G., Liu, X., Li, C., Fu, J., 2005. Molecular and carbon and hydrogen isotopic composition of n-alkanes in plant leaf waxes. Org. Geochem. 36, 1405–1417. https://doi.org/10.1016/j.orggeochem.2005.06.001.

Biester, H., Knorr, K.-H., Schellekens, J., Basler, A., Hermanns, Y.-M., 2014. Comparison of different methods to determine the degree of peat decomposition in peat bogs. Biogeosciences 11, 2691–2707. https://doi.org/10.5194/bg-11-2691-2014.

Blanchette, R.A., 1991. Delignification by wood-decay fungi. Annu. Rev. Phytopathol. 29, 381–398.

Blumenstengel, H., Krutzsch, W., Volland, L., Knoth, W., Knuth, G., 1996. Revidierte Stratigraphie tertiärer Ablagerungen im südlischen Sachsen-Anhalt Teil 1: Raum Halle-Merseburg. In: Hallesches Jahrbuch der Geowissenschaften, vol. 1. Reihe B, Beiheft. Landesamt für Geologie und Bergwesen, Sachsen-Anhalt, Halle/Saale, p. 101.

Bönisch, R., 1990. Zur Verbreitung von *Cathaya roselti* Schneider im 2. Lausitzer Flöz (Untermiozän). Z. Geol. Wiss. 18 (10), 889–896.

Bottari, F., Marsili, A., Morelli, I., Pacchiani, M., 1972. Aliphatic and triterpenoid hydrocarbons from ferns. Phytochemistry 11, 2519–2523. https://doi.org/10.1016/S0031-9422(00)88528-3.

Bracewell, J.M., Robertson, G.W., Williams, B.L., 1980. Pyrolysis mass spectroscopy studies of humification in a peat and a peaty podzol. J. Anal. Appl. Pyrolysis 2, 53–62. https://doi.org/10.1016/0165-2370(80)80045-3.

Bray, E.E., Evans, E.D., 1961. Distribution of n-paraffins as a clue to recognition of source beds. Geochim. Cosmochim. Acta 22, 2–15. https://doi.org/10.1016/0016-7037(61)90069-2.

Brebu, M., Vasile, C., 2010. Thermal degradation of lignin – A Review. Cellul. Chem. Technol. 44, 353–363.

Bruch, A., 1998. Palynologische Untersuchungen im Oligozän Sloweniens – Paläoumwelt und Paläoklima im Ostalpenraum. Tübinger Mikropaläontologische Mitteilungen 8, 1–193.

Bruch, A.A., Uhl, D., Mosbrugger, V., 2007. Miocene climate in Europe – patterns and evolution a first synthesis of NECLIME. Palaeogeogr. Palaeoclimatol. Palaeoecol. 253, 1–7. https://doi.org/10.1016/j.palaeo.2007.03.030.

Büchner, J., Tietz, O., Viereck, L., Abratis, M., Suhr, P., 2014. The Lausitz Volcanic Field – link between volcanoes of Bohemia (CZ) and Silesia (PL). Schriftenreihe der Deutschen Gesellschaft für Geowissenschaften 85, 436.

Büchner, J., Tietz, O., Suhr, P., Loges, A., Franz, G., 2015a. Cenozoic Lausitz Volcanism and its Basement. In: Röhling, H.-G. (Ed.), GeoBerlin 2015. Exkursionsführer/Excursion guide, vol. 255. Exkursionsführer und Veröffentlichungen der Deutschen Gesellschaft für Geowissenschaften, pp. 17–34.

Büchner, J., Tietz, O., Viereck, L., Suhr, P., Abratis, M., 2015b. Volcanology, geochemistry and age of the Lausitz Volcanic Field. Int. J. Earth Sci. 104, 2057–2083. https://doi.org/10.1007/s00531-015-1165-3.

Büchner, J., Suhr, P., Tietz, O., 2017. Das Lausitzer Vulkanfeld unter besonderer Berücksichtigung der Guttauer Vulkangruppe. In: Schulze, P., Gerschel, H., Suhr, P. (Eds.), Maare, Rohstoffe und Bergbaufolgen in der sächsischen Oberlausitz, vol. 258. Exkursionsführer und Veröffentlichungen der Deutschen Gesellschaft für Geowissenschaften, pp. 89–122.

Bush, R.T., McInerney, F.A., 2013. Leaf wax *n*-alkane distributions in and across modern plants: Implications for paleoecology and chemotaxonomy. Geochim. Cosmochim. Acta 117, 161–179. https://doi.org/10.1016/j.gca.2013.04.016.

Cady, S.L., Wenk, H.-R., Dowing, K.H., 1996. HRTEM of microcrystalline opal in chert and porcelanite from the Monterey Formation, California. Am. Mineral. 81, 1380–1395. https://doi.org/10.2138/am-1996-11-1211.

Casagrande, D.J., 1987. Sulphur in peat and coal. In: Scott, A.C. (Ed.), Coal and Coal-Bearing Strata: Recent Advances, vol. 32. Geological Society, London, Special Publications, pp. 87–105.

Chen, Y., Mastalerz, M., Schimmelmann, A., 2012. Characterization of chemical functional groups in macerals across different coal ranks via micro-FTIR spectroscopy. Int. J. Coal Geol. 104, 22–33. https://doi.org/10.1016/j.coal.2012.09.001.

Cohen, A.D., Spackman, W., 1977. Phytogenetic organic sediments and sedimentary environments in the Everglades Mangrove Complex of Florida; Part II: The origin,

description and classification of the peats of southern Florida. Palaeontogr. Abt. B 162, 71–114.
Colberg, P.J., Young, L.Y., 1982. Biodegradation of lignin-derived molecules under anaerobic conditions. Can. J. Microbiol. 28, 886–889. https://doi.org/10.1139/m82-132.
Colberg, P.J., Young, L.Y., 1985. Anaerobic degradation of soluble fractions of [^{14}C-lignin] lignocellulose. Appl. Environ. Microbiol. 49, 345–349. https://doi.org/10.1128/aem.49.2.345-349.19855.
Cranwell, P.A., 1973. Chain-length distribution of n-alkanes from lake sediments in relation to post-glacial environmental change. Freshw. Biol. 3, 259–265. https://doi.org/10.1111/j.1365-2427.1973.tb00921.x.
Crawford, R.L., 1981. Lignin Biodegradation and Transformation. John Wiley & Sons, New York, Chichester, p. 170.
Dai, S., Bechtel, A., Eble, C.F., Flores, R.M., French, D., Graham, I.T., Hood, M.M., Hower, J.C., Korasidis, V.A., Moore, T.A., Püttmann, W., Wei, Q., O'Keefe, J.M.K., 2020. Recognition of peat depositional environments in coal: A review. Int. J. Coal Geol. 219, 103383 https://doi.org/10.1016/j.coal.2019.103383.
De Putter, T., Roche, M., Dupuis, C., Fairon-Demaret, M., Nicaise, D., Roblain, D., Thonart, P., 1996. Taphocoenosis of Miocene taxodiaceous wood from the Entre-Sambre-et-Meuse cryptokarsts (southern Belgium). Neues Jahrbuch für Geologie und Palaöntologie 202, 259–268. https://doi.org/10.1127/njgpa/202/1996/2599.
Dehmer, J., 1995. Petrological and organic geochemical investigation of recent peats with known environments of deposition. Int. J. Coal Geol. 28, 111–138. https://doi.org/10.1016/0166-5162(95)00016-X.
Deutsche Stratigraphische Kommission (STD), 2016. Stratigraphische Tabelle von Deutschland. Deutsche Stratigraphische Kommission, Deutsches GeoForschungsZentrum Potsdam. https://www.stratigraphie.de/std/Bilder/5_2.pdf.
Didyk, B.M., Simoneit, B.R.T., Brassell, S.C., Eglinton, G., 1978. Organic geochemical indicators of paleoenvironmental conditions of sedimentation. Nature 272, 216–222. https://doi.org/10.1038/272216a0.
Diefendorf, A.F., Freimuth, E.J., 2017. Extracting the most from terrestrial plant-derived n-alkyl lipids and their carbon isotopes from the sedimentary record: A review. Org. Geochem. 103, 1–21. https://doi.org/10.1016/j.orggeochem.2016.10.016.
Diefendorf, A.F., Freeman, K.H., Wing, S.L., Graham, H.V., 2011. Production of n-alkyl lipids in living plants and implications for the geologic past. Geochim. Cosmochim. Acta 75, 7472–7485. https://doi.org/10.1016/j.gca.2011.09.028.
Diefendorf, A.F., Leslie, A.B., Wing, S.L., 2019. A phylogenetic analysis of conifer diterpenoids and their carbon isotopes for chemotaxonomic applications. Org. Geochem. 127, 50–58. https://doi.org/10.1016/j.orggeochem.2018.11.007.
Diessel, C.F.K., 1986. The correlation between coal facies and depositional environments. In: Proceedings of 20th Symposium of Department of Geology. University of New Castle, New South Wales, pp. 11–22.
Diessel, C.F.K., 1992. Coal-bearing Depositional Systems. Springer Verlag, Berlin, p. 721.
DiMichele, W.A., Falcon-Lang, H.J., 2011. Pennsylvania "fossil forests" in growth position (T^0 assemblages): origin, taphonomic biases and palaeoecological significance. J. Geol. Soc. Lond. 168, 585–605. https://doi.org/10.1144/0016-76492010-103.
DIN 22020-2: 1998. Rohstoffuntersuchungen im Steinkohlenbergbau - Mikroskopische Untersuchungen an Steinkohle, Koks und Briketts - Teil 2: Herstellung von Körnerschliffen und Stückschliffen. Investigations of raw material in hard-coal-mining - Microscopical examination of hard coal, coke and briquettes - Part 2: Preparation of polished surface from lump material and particulate blocks, Beuth, Berlin, Germany, 4 pp.
Đoković, N., Mitrović, D., Životić, D., Bechtel, A., Sachsenhofer, R.S., Stojanović, K., 2018. Petrographic and biomarker analysis of xylite-rich coal from the Kolubara and Kostolac lignite basins (Pannonian Basin, Serbia). Geol. Carpath. 69, 51–70. https://doi.org/10.1515/geoca-2018-0004.
Dolezych, M., 2005. Koniferenhölzer im Lausitzer Flöz und ihre ökologische Position. LLP Contribut. Series 19, 1–339.
Dolezych, M., 2011. Taxodiaceous woods in Lusatia (Central Europe), including curiosities in their nomenclature and taxonomy, with a focus on *Taxodioxylon*. Japanese J. Historical Botany 19 (1–2), 25–46. https://doi.org/10.34596/hisbot.19.1-2_25.
Dolezych, M., Schneider, W., 2006. Inkohlte Hölzer und *Cuticulae dispersae* aus dem 2. Miozänen Flözhorizont im Tagebau Welzow (Lausitz). Taxonomie und vergleichende feinstratigraphisch-fazielle Zuordnung. Z. Geol. Wiss. 34 (3–4), 165–259.
Dolezych, M., Schneider, W., 2007. Taxonomie und Taphonomie von Koniferenhölzern und Cuticulae dispersae im 2. Lausitzer Flözhorizont (Miozän) des Senftenberger Reviers. Palaeontogr. Abt. B 276 (1–3), 1–95.
Donaldson, L.A., Bond, J., 2005. Fluorescence Microscopy of Wood (CD ROM). Rotorua, Scion, New Zealand.
Drobniak, A., Mastalerz, M., 2006. Chemical evolution of Miocene wood: Example from Belchatow brown coal deposit, Central Poland. Int. J. Coal Geol. 66, 157–178. https://doi.org/10.1016/j.coal.2005.06.004.
Duan, Y., He, J., 2011. Distribution and isotopic composition of n-alkanes from grass, reeds and tree leaves along a latitudinal gradient in China. Geochem. J. 45, 199–207. https://doi.org/10.2343/geochemj.1.0115.
Dzou, L.I.P., Noble, R.A., Senftle, J.T., 1995. Maturation effects on absolute biomarker concentration in a suite of coals and associated vitrinite concentrates. Org. Geochem. 23, 681–697. https://doi.org/10.1016/0146-6380(95)00035-D.
Eißmann, L., 1968. Überblick über die Entwicklung des Tertiärs in der Leipziger Tieflandsbucht (Nordwestsachsen). Sächsische Heimatblätter 14, 25–37.
Eissmann, L., 1994. Leitfaden der Geologie des Präquartärs im Saale-Elbe-Gebiet. DEUQUA Tagung 1994, Leipzig. Altenberger naturwissenschaftliche Forschung 7, 11–53.
Eissmann, L., 2002. Tertiary geology of the Saale–Elbe Region. Quat. Sci. Rev. 21 (11), 1245–1274.
Erdei, B., Dolezych, M., Hably, L., 2009. The buried Miocene forest at Bükkábrány (Hungary). Rev. Palaeobot. Palynol. 155, 69–79.
Eriksson, K.E., Wood, T.M., 1985. Biodegradation of cellulose. In: Higuchi, T. (Ed.), Biosynthesis and Biodegradation of Wood Components. Academic Press, New York, pp. 469–503.
Escher, D., Gerschel, H., Geißler, M., Hartmann, A., Rascher, J., Rascher, M., Richter, L., Wittwer, S., 2020. Lithofazieskarten Tertiär Lausitz 1. 50.000 (LKT50 Lausitz). Sächsisches Landesamt für Umwelt, Landwirtschaft und Geologie, Dresden, p. 89.
Espitalié, J., Deroo, G., Marquis, F., 1985. La pyrolyse Rock-Eval et ses applications. Deuxiéme partie. Revue de l'Institut Francais du Petrole 40, 755–784. https://doi.org/10.2516/ogst:198504.
Exarchos, C., Given, P.H., 1977. Cell wall polymers of higher plants in peat formation: The role of microorganisms. In: Given, P.H., Cohen, A.D. (Eds.), Interdisciplinary Studies of Peat and Coal Origins, vol. 7. Geological Society of America Microform Publication, pp. 122–141.
Fabbri, D., Torri, C., Simoneit, B.R.T., Marynowski, L., Rushdi, A.I., Fabiańska, M.J., 2009. Levoglucosan and other cellulose and lignin markers in emissions from burning of Miocene lignites. Atmos. Environ. 43, 2286–2295. https://doi.org/10.1016/j.atmosenv.2009.01.030.
Fabiańska, M.J., Kurkiewicz, S., 2013. Biomarkers, aromatic hydrocarbons and polar compounds in the Neogene lignites and gangue sediments of the Konin and Turoszów Brown Coal Basins (Poland). Int. J. Coal Geol. 107, 24–44. https://doi.org/10.1016/j.coal.2012.11.008.
Fairon-Demaret, M., 1992. A propos de la découverte de *Juniperoxylon pachyderma* (Göppert) Kräusel 1949 dans le Tertiaire de Bioul (Entre-Sambre-et-Meuse). Ann. Soc. Geol. Belg. 115, 333–339.
Faix, O., 1991. Classification of lignins from different botanical origins by FT-IR Spectroscopy. Holzforschung 45 (S), 21–28. https://doi.org/10.1515/hfsg.1991.45.s1.21.
Faix, O., 1992. Fourier transform infrared spectroscopy. In: Lin, S.Y., Dence, C.W. (Eds.), Methods in Lignin Chemistry. Springer Verlag, Berlin, pp. 83–109.
Feiler, W., Sschneider, W., 1987. Ergebnisse der Laborbrikettierung und -verkokung typischer Faziesproben aus dem Tagebau Welzow-Süd. Neue Bergbautechnik 17 (4), 147–151.
Fengel, D., 1991. Aging and fossilization of wood and its components. Wood Sci. Technol. 25, 153–177. https://doi.org/10.1007/BF00223468.
Fengel, D., Wegener, G., 1989. Distribution of the components within the wood cell wall. In: Wood – Chemistry, Ultrastructure, Reactions. Walter de Gruyter Verlag, Berlin, pp. 217–239.
Ficken, K.J., Li, B., Swain, D.L., Eglinton, G., 2000. An n-alkane proxy for the sedimentary input of submerged/floating freshwater aquatic macrophytes. Org. Geochem. 31, 745–749. https://doi.org/10.1016/S0146-6380(00)00081-4.
Flörke, O., Hollmann, R., von Rad, U., Rösch, H., 1976. Intergrowth and twinning in opal-CT lepispheres. Contrib. Mineral. Petrol. 58, 235–242. https://doi.org/10.1007/BF00402354.
Francis, W., 1961. Coal: Its Formation and Composition. Edward Arnold, London, p. 806.
Gallot-Lavallée, O., Teyssedre, G.C., Laurent, S.R., 2005. Identification of photoluminescence features of an epoxy resin based on components features and curing effects. Polymer 46, 2722–2731. https://doi.org/10.1016/j.polymer.2005.02.003.
Given, P.H., 1984. An essay on the organic geochemistry of coal. In: Gorbaty, M.L., Larsen, J.W., Wender, I. (Eds.), Coal Science, vol. 3. Academic Press, London, pp. 63–252.
Given, P.H., Spackman, W., Painter, P.C., Rhoads, C.A., Ryan, N.J., 1984. The fate of cellulose and lignin in peats: an exploratory study of the input to coalification. Org. Geochem. 6, 399–407. https://doi.org/10.1016/0146-6380(84)90062-7.
Gothan, W., 1906. Die fossilen Coniferenhölzer von Senftenberg. Abhandlungen der Königlich Preussischen Geologischen Landesanstalt. Berlin, Neue Folge 46, 155–171.
Gothan, W., 1922. Ein Fund natürlicher Zellulose im Miozän des Niederlausitzer Braunkohlenreviers. Z. Dtsch. Geol. Ges. Band 74, 159–161.
Gothan, W., 1926. Neuere Beobachtungen aus der Braunkohle. Z. Dtsch. Geol. Ges. Band 78, 115–116.
Gothan, W., Benade, W., 1930. Über "Faserlignite" ("Faserkohle") in der Braunkohle und "Faserkohle" überhaupt. Braunkohle 14, 274–280.
Gregorová, A., Cibulková, Z., Košiková, B., Šimon, P., 2005. Stabilization effect of lignin in polypropylene and recycled polypropylene. Polym. Degrad. Stab. 89 (3), 553–558. https://doi.org/10.1016/j.polymdegradstab.2005.02.007.
Grice, K., Lu, H., Atahan, P., Asif, M., Hallmann, C., Greenwood, P., Maslen, E., Tulipani, S., Williford, K., Dodson, J., 2009. New insights into the origin of perylene in geological samples. Geochim. Geochim. Cosmochim. Acta 73, 6531–6543. https://doi.org/10.1016/j.gca.2009.07.029.
Haage, R., 1966. Beitrag zur Petrographie und Genese des Tertiärquarzits von Böhlen -Espenhain bei Leipzig. Ber. Dtsch. Ges. Geol. Wiss. Reihe B Mineral. Lagerstättenforsch. 11 (2), 229–237.
Haas, M., Daxner-Höck, G., Decker, K., Kolcon, I., Kovar-Eder, J., Meller, B., Sachsenhofer, R.F., 1998. Palaeoenvironmental studies in the Early Miocene lignite opencast mine Oberdorf, N Voitsberg, Styria, Austria. In: Steininger, F.F. (Ed.), The Early Miocene Lignite Deposit of Oberdorf N Voitsberg, 140. Jahrbuch Geologische Bundesanstalt, Wien, Styria, Austria, pp. 413–424.
Haberer, M.R., Mangelsdorf, K., Wilkes, H., Horsfield, B., 2006. Occurrence and palaeoenvironmental significance of aromatic hydrocarbon biomarkers in Oligocene sediments from the Mallik 5L-38 Gas Hydrate Production Research well (Canada). Org. Geochem. 37, 519–538. https://doi.org/10.1016/j.orggeochem.2006.01.004.

Hackley, P., Kus, J., 2015. Thermal maturity of Tasmanites microfossils from confocal laser scanning fluorescence microscopy. Fuel 143, 343–350. https://doi.org/10.1016/j.fuel.2014.11.052.
Hackley, P.C., Zhang, T., Jubb, A.M., Valentine, B.J., Dulong, F.T., Hatcherian, J.J., 2020. Organic petrography of Leonardian (Wolfcamp A) mudrocks and carbonates, Midland Basin, Texas: The fate of oil-prone sedimentary organic matter in the oil window. Mar. Pet. Geol. 112, 104086 https://doi.org/10.1016/j.marpetgeo.2019.104086.
Hámor-Vidó, A., Hofmann, T., Levente, A., 2010. *In situ* preservation and paleoenvironmental assessment of *Taxodiacea* fossil trees in the Bükkalja Lignite Formation, Bükkábrány open cast mine, Hungary. Int. J. Coal Geol. 81, 203–210. https://doi.org/10.1016/j.coal.2009.06.006.
Hatcher, P.G., 1988. Dipolar-dephasing 13C NMR studies of decomposed wood and coalified xylem tissue: evidence for chemical structural changes associated with defunctionalization of lignin structural units during coalification. Energy Fuel 2, 48–58. https://doi.org/10.1021/ef00007a008.
Hatcher, P.G., Breger, I.A., 1982. Nuclear magnetic resonance studies of ancient buried wood: II. Observations on the origin of coal from lignite to bituminous coal. Org. Geochem. 4, 9–18. https://doi.org/10.1016/0146-6380(82)90003-1.
Hatcher, P.G., Clifford, D.G., 1997. The organic geochemistry of coal: from plant materials to coal. Org. Geochem. 27, 251–274. https://doi.org/10.1016/S0146-6380(97)00051-X.
Havelcová, M., Sýkorová, I., Bechtel, A., Mach, K., Trejtnarová, H., Žaloudková, M., Matysová, P., Blažek, J., Boudová, J., Sakala, J., 2013. "Stump Horizon" in the Bílina Mine (Most Basin, Czech Republic) - GC–MS, optical and electron microscopy in identification of wood biological origin. Int. J. Coal Geol. 107, 62–77. https://doi.org/10.1016/j.coal.2012.09.008.
Hayek, E.W.H., Jordis, U., Moche, W., Sauter, F., 1989. A bicentennial of betulin. Phytochemistry 28, 2229–2242. https://doi.org/10.1016/S0031-9422(00)97961-5.
Hedges, J.I., Cowie, G.L., Ertel, J.R., Barbour, R.J., Hatcher, P.G., 1985. Degradation of carbohydrates and lignin in buried woods. Geochim. Cosmochim. Acta 49, 701–711. https://doi.org/10.1016/0016-7037(85)90165-6.
Heinicke, F., 1905. Beschreibung der miozänen - oberen - Braunkohlenablagerung in den Gemarkungen Schmeckwitz, Wendischbaselitz, Piskowitz und Rosenthal in der sächsischen Oberlausitz, 8 km östlich der Stadt Kamenz gelegen. Braunkohle 4 (129–131), 145–149.
Henchiri, M., 2007. Sedimentation, depositional environment and diagenesis of Eocene biosiliceous deposits in Gafsa basin (southern Tunisia). J. Afr. Earth Sci. 49, 187–200. https://doi.org/10.1016/j.jafrearsci.2007.09.001.
Hohl, R., 1957. Die Entstehung unserer Tertiärquarzitlagerstätten. Silikattechnik 8, 368–372.
Hook, B.A., Halfar, J., Bollmann, J., Gedalof, Z., Rahman, M.A., Reyes, J., Schulze, D.J., 2015. Extraction of α-cellulose from mummified wood for stable isotopic analysis. Chem. Geol. 405, 19–27. https://doi.org/10.1016/j.chemgeo.2015.04.003.
Hower, J.C., Rich, F.J., Williams, D.A., Bland, A.E., Fiene, F.L., 1990. Cretaceous and Eocene lignite deposits, Jackson Purchase, Kentucky. Int. J. Coal Geol. 16, 239–254. https://doi.org/10.1016/0166-5162(90)90053-2.
Hower, J.C., O'Keefe, J.M.K., Volk, T.J., Watt, M.A., 2010. Funginite–resinite associations in coal. Int. J. Coal Geol. 83, 64–72. https://doi.org/10.1016/j.coal.2010.04.003.
Hower, J.C., O'Keefe, J.M.K., Eble, C.F., Raymond, A., Valentim, B., Volk, T.J., Richardson, A.R., Satterwhite, A.B., Hatch, R.S., Stucker, J.D., Watt, M.A., 2011. Notes on the origin of inertinite macerals in coal: evidence for fungal and arthropod transformations of degraded macerals. Int. J. Coal Geol. 86, 231–240. https://doi.org/10.1016/j.coal.2011.02.005.
Hower, J.C., O'Keefe, J.M.K., Wagner, N.J., Dai, S., Wang, X., Xue, W., 2013. An investigation of Wulantuga coal (cretaceous, Inner Mongolia) macerals: Paleopathology of faunal and fungal invasions into wood and the recognizable clues for their activity. Int. J. Coal Geol. 114, 44–53. https://doi.org/10.1016/j.coal.2013.04.005.
Hower, J.C., Eble, C.F., O'Keefe, J.M.K., 2021. Phyteral perspectives: Every maceral tells a story. Int. J. Coal Geol. 247, 103849 https://doi.org/10.1016/j.coal.2021.103849.
Iler, R.K., 1979. The Chemistry of Silica: Solubility, Polymerization, Colloid and Surface Properties, and Biochemistry. Wiley, New York, USA, p. 896.
Inglis, G.N., Naafs, B.D.A., Zeng, Y., McClymont, E.L., Evershed, R.P., Pancost, R.D., 2018. Distribution of geohopanoids in peat: Implications for the use of hopanoid-based proxies in natural archives. Geochim. Cosmochim. Acta 224, 249–261. https://doi.org/10.1016/j.gca.2017.12.029.
Inglis, G.N., Farnsworth, A., Collinson, M.E., Carmichael, M.J., Naafs, B.D.A., Lunt, D.J., Valdes, P.J., Pancost, R.D., 2019. Terrestrial environmental change across the onset of the PETM and the associated impact on biomarker proxies: A cautionary tale. Glob. Planet. Chang. 181, 102991 https://doi.org/10.1016/j.gloplacha.2019.102991.
International Commission on Stratigraphy, 2023. International Chronostratigraphic Chart, version 2023/09. https://stratigraphy.org/chart (Accessed 30 April 2022).
Ishikura, K., Darung, U., Inoue, T., Hatano, R., 2018. Variation in soil properties regulate greenhouse gas fluxes and global warming potential in three land use types on tropical peat. Atmosphere 9, 465. https://doi.org/10.3390/atmos9120465.
ISO 1171, 1997. Methods for Analysis and Testing of Coal and Coke. Determination of Ash Content. International Organization for Standardization, Switzerland, p. 10.
Itoh, N., Sakagami, N., Torimura, M., Watanabe, M., 2012. Perylene in Lake Biwa sediments originating from *Cenococcum geophilum* in its catchment area. Geochim. Cosmochim. Acta 95, 241–251. https://doi.org/10.1016/j.gca.2012.07.037.
Jacob, J., Disnar, J.-R., Boussafir, M., Albuquerque, A.L.S., Sifeddine, A., Turcq, B., 2007. Contrasted distributions of triterpene derivatives in the sediments of Lake Caçó reflect paleoenvironmental changes during the last 20,000 yrs in NE Brazil. Org. Geochem. 38, 180–197. https://doi.org/10.1016/j.orggeochem.2006.10.007.
Jähnichen, H., 1965. Beiträge zur Tertiärflora der Lausitz – inkohlte Blätter und Epidermis Strukturen. Monatsberichte der Königlichen Preußische Akademie der Wissenschaften zu Berlin 7 (9), 663–670.
Jahren, A.H., Sternberg, L.S.L., 2008. Annual patterns within tree rings of the Arctic Middle Eocene (~45 Ma): Isotopic signatures of precipitation, relative humidity, and deciduousness. Geology 36 (2), 99–102. https://doi.org/10.1130/G23876A.1.
Jones, J.B., Segnit, E.R., 1971. The nature of opal I. Nomenclature and constituent phases. J. Geol. Soc. Aust. 18, 57–68. https://doi.org/10.1080/00167617108728743.
Jurasky, K.A., 1938a. Wandlungen des Holzes auf dem Weg zur Kohle. Ein Kapitel genetischer Kohlenpetrographie. Geol. Rundsch. 29 (3–4), 441–461.
Jurasky, K.A., 1938b. Die alten Bergwerksteiche als Umwelt reichen Pflanzenlebens. Mitteilungen des Naturwissenschaftlichen Vereins zu Freiberg 3, 34–40.
Kasiński, J.R., Słodkowska, B., 2016. Factors controlling Cenozoic anthracogenesis in the Polish Lowlands. Geol. Quart. 60, 959–974. https://doi.org/10.7306/gq.1321.
Kasiński, J.R., Kozdrój, W., Koźma, J., Krentz, O., Opletal, M., Stachowiak, A., 2004. Geological Map Lausitz-Jizera-Karkonosze and Muskau Arch Geopark as examples of cross-border cooperation of the national geological surveys of Poland, the Czech Republic and Germany. Prz. Geol. 52 (8/2), 724–730.
Kirk, T.K., 1973. The chemistry and biochemistry of decay. In: Nicholas, D. (Ed.), Wood Deterioration and its Prevention by Preservative Treatment. Syracuse University Press, pp. 149–181.
Kitin, P., Voelker, S.L., Meinzer, F.C., Beeckman, H., Strauss, S.H., Lachenbruch, B., 2010. Tyloses and phenolic deposits in xylem vessels impede water transport in low-lignin transgenic poplars: a study by cryo-fluorescence microscopy. Plant Physiol. 154, 887–898.
Kitin, P., Nakaba, S., Hunt, C.H., Lim, S., Funada, R., 2020. Direct fluorescence imaging of lignocellulosic and suberized cell walls in roots and stems. AoB PLANTS 12 (4). https://doi.org/10.1093/aobpla/plaa032 plaa032.
Klavins, M., Sire, J., Purmalis, O., Melecis, V., 2008. Approaches to estimating humification indicators for peat. Mires Peat 3, 1–15. http://www.mires-and-peat.net/pages/volumes/map03/map0307.php.
Klomínský, J., Jarchovský, T., Rajpoot, G.S., 2010. Atlas of Plutonic Rocks and Orthogneisses in the Bohemian Massif. 4. LUGICUM. Czech Geological Survey, Prague, p. 78.
Kohzu, A., Miyajima, T., Tateishi, T., Watanabe, T., Takahashi, M., Wada, E., 2005. Dynamics of 13C natural abundance in wood decomposing fungi and their ecophysiological implications. Soil Biol. Biochem. 37, 1598–1607. https://doi.org/10.1016/j.soilbio.2005.01.021.
Kojić, I., Bechtel, A., Aleksić, N., Životić, D., Trifunović, S., Gajica, G., Stojanović, K., 2021. Study of the synergetic effect of co-pyrolysis of lignite and high-density polyethylene aiming to improve utilization of low-rank coal. Polymers 13, 759. https://doi.org/10.3390/polym13050759.
Kolcon, I., Sachsenhofer, R.F., 1999. Petrography, palynology and depositional environment of the early Miocene Oberdorf lignite seam (Styrian Basin, Austria). Int. J. Coal Geol. 41, 275–308. https://doi.org/10.1016/S0166-5162(99)00023-3.
Krokene, P., Nagy, N.E., Krekling, T., 2008. Traumatic Resin Ducts and Polyphenolic Parenchyma Cells in Conifers. In: Schaller, A. (Ed.), Induced Plant Resistance to Herbivory. Springer Science+Bussiness Media, Luxemburg, pp. 147–169.
Kroner, U., Romer, R.L., 2010. Baltica meets Gondwana - the isotope geochemical record. In: Linnemann, U., Romer, R.L. (Eds.), Pre-Mesozoic Geology of Saxo-Thuringia-From Cadomian Active Margin to the Variscan Orogen. Schweitzerbart, Stuttgart, pp. 363–394.
Kröner, A., Heagner, E., Hammer, J., Haase, G., Bielicki, K.-H., Krauss, M., Eidam, J., 1994. Geochronology and Nd-Sr systematics of Lusatian granitoids: significance for the evolution of the Variscan orogen in the east-central Europe. Geol. Rundsch. 83, 357–376. https://doi.org/10.1007/BF00210551.
Krutzsch, W., 1970. Atlas der mittel- und jungtertiären dispersen Sporen und Pollen- sowie der Mikroplanktonformen des nördlichen Mitteleuropas. Liferung VII: Monoporate, Monocolpate, Longicolpate, Dicolpate und Ephedrioide (Polyplicate) Pollenformen VEB Gustav Fischer Verlag, Jena, Germany, 175 pp.
Krutzsch, W., Blumenstengel, H., Kiesel, Y., Rüffle, L., 1992. Paläobotanische Klimagliederung des Alttertiärs (Mitteleozän bis Oberoligozän) in Mitteldeutschland und das.
Kühner, R., 2009. Neue Ergebnisse zum Nachweis neotektonischer Aktivitäten im Quartär des Tagebaus Welzow-Süd, Südbrandenburg. New results regarding proof of neotectonical activities in the Quaternary of the Welzow-Süd open-cast mine, South Brandenburg. Brandenburgische Geowissenschaftliche Beiträge 16 (1/2), 87–93.
Kunzmann, L., Schneider, W., Standke, G., Dolezych, M., Eberlein, M., 2009. Geologie und Phytostratigraphie im Paläogen und Neogen Mittel- und Ostdeutschlands. Exkursionsführer und Veröffentlichungen der Deutschen Gesellschaft für Geowissenschaften 24, 47–115.
Kunzmann, L., Li, S.-F., Huang, J., Utescher, T., Su, T., Zhou, Z.-K., 2022. Assessment of Phytogeographic Reference Regions for Cenozoic vegetation: a case study on the Miocene flora of Wiesa (Germany). Fossil Imprint 78 (1), 1–43. https://doi.org/10.37520/fi.2022.002.
Kürschner, K., Hoffer, A., 1929. Ein neues Verfahren zur Bestimmung der Cellulose in Hölzern und Zellstoffen. Technologie und Chemie der Papier- und Zellstoff-Fabrikation 26, 125–129.
Kus, J., Dolezych, M., Schneider, W., Hofmann, T., Visiné Rajczi, E., 2020. Coal petrological and xylotomical characterization of Miocene lignites and in-situ fossil tree stumps and trunks from Lusatia region, Germany: Palaeoenvironment and taphonomy assessment. Int. J. Coal Geol., 103283 https://doi.org/10.1016/j.coal.2019.103283.

Lafargue, E., Marquis, F., Pillot, D., 1998. Rock-Eval 6 applications in Hydrocarbon Exploration, production, and Soil Contamination Studies. Revue de l'Institut Francais du Petrole 53, 421–427. https://doi.org/10.2516/ogst:1998036.
Lane, C.S., 2017. Modern n-alkane abundances and isotopic composition of vegetation in a gymnosperm-dominated ecosystem of the southeastern U.S. coastal plain. Org. Geochem. 105, 33–36. https://doi.org/10.1016/j.orggeochem.2016.12.003.
Lang, R., 1920. Die Entstehung von Braunkohle und Kaolin im Tertiär Mitteldeutschlands. Ein geologisch-bodenkundliches Problem. Jahrbuch des Halleschen Verbandes für die Erforschung der Mitteldeutschen Bodenschätze und Ihrer Verwertung 2, 65–92.
Lechien, V., Rodriguez, Ch., Ongena, M., Hiligsmann, S., Rulmont, A., Thonart, P., 2006. Physicochemical and biochemical characterization of non-biodegradable cellulose in Miocene gymnosperm wood from the Entre-Sambre-et-Meuse, southern Belgium. Org. Geochem. 37, 1465–1476. https://doi.org/10.1016/j.orggeochem.2006.07.002.
Li, W., Yao, W., Wang, J., Qiu, Z., Tang, J., Yang, S., Zhu, M., Xu, Z., Hu, R., Qin, A., Tang, B.Z., 2017. Studying a novel AIE coating and its handling process via fluorescence spectrum. RSC Adv. 7, 41127–41135. https://doi.org/10.1039/C7RA06527B.
Liesegang, M., Mielke, R., Berthold, C., 2018. Amorphous silica maturation in chemically weathered clastic sediments. Sediment. Geol. 365, 54–61. https://doi.org/10.1016/j.sedgeo.2018.01.001.
Lorenz, V., Suhr, P., Goth, K., 2003. Maar-diatreme volcanism – causes and consequences. The Guttau Volcano Group in eastern Saxony as an example for the complex processes and relationships. Z. Geol. Wiss. 31 (4–6), 267–312.
Lucas, A.J., Given, P.H., Spackman, W., 1988. Studies of peat as the input to coalification, I. Rationale and preliminary examination of polysaccharides in peats. Int. J. Coal Geol. 9, 235–251. https://doi.org/10.1016/0166-5162(88)90015-8.
Lücke, A., Helle, G., Schleser, G.H., Figueiral, I., Mosbrugger, V., Jones, T.P., Rowe, N.P., 1999. Environmental history of the German Lower Rhine Embayment during the Middle Miocene as reflected by carbon isotopes in brown coal. Palaeogeogr. Palaeoclimatol. Palaeoecol. 154, 339–352. https://doi.org/10.1016/S0031-0182(99)00122-4.
Lukens, W.E., Eze, P., Schubert, B.A., 2019. The effect of diagenesis on carbon isotope values of fossil wood. Geology 47, 987–991. https://doi.org/10.1130/G46412.1.
Mackenzie, A.S., Patience, R.L., Maxwell, J.R., 1981. Molecular changes and the maturation of sedimentary organic matter. In: Atkinson, G., Zuckermann, J.J. (Eds.), Origin and Chemistry of Petroleum. Proc. 3rd Annual Karcher Symposium. Pergamon Press, Oxford, pp. 1–31.
Madelaine, B., Bruch, A.A., Selmeier, A., 2007. The reconstruction of Early and Middle Miocene climate and vegetation in Southern Germany as determined from the fossil wood flora. Palaeogeogr. Palaeoclimatol. Palaeoecol. 253, 91–114. https://doi.org/10.1016/j.palaeo.2007.03.035.
Mai, D.H., 2000. Die untermiozänen Floren der Spremberger Folge und dem 2. Flözhorizont in der Lausitz Teil IV: Fundstellen und Paläobiologie. Palaeontogr. Abt. B 25, 65–176. https://doi.org/10.1127/palb/254/2000/65.
Mai, D.H., 2001. Die mittelmiozänen und obermiozänen Floren aus der Meuroer und Raunoer Folge in der Lausitz. Teil III: Fundstellen und Paläobiologie. Palaeontographica B 258, 1–85.
Mann, U., Disko, U., Hofmann, D., van der Burgh, Vos, H., 2017. Chemotaxonomy of fossil woods from the Lower Rhine Embayment, Germany. Int. J. Coal Geol. 171, 37–48.
Marin-Carbonne, J., Robert, F., Chaussidon, M., 2014. The silicon and oxygen isotope compositions of Precambrian cherts: A record of oceanic paleo-temperatures? Precambrian Res. 247, 223–234. https://doi.org/10.1016/j.precamres.2014.03.016.
Marynowski, L., Zatoń, M., 2010. Organic matter from the Callovian (Middle Jurassic) deposits of Lithuania: Compositions, sources and depositional environments. Appl. Geochem. 25, 933–946. https://doi.org/10.1016/j.apgeochem.2010.04.002.
Marynowski, L., Smolarek, J., Bechtel, A., Philippe, M., Kurkiewicz, S., Simoneit, B.R.T., 2013. Perylene as an indicator of conifer fossil wood degradation by wood-degrading fungi. Org. Geochem. 59, 143–151. https://doi.org/10.1016/j.orggeochem.2013.04.006.
Marynowski, L., Bucha, M., Smolarek, J., Wendorff, M., Simoneit, B.R.T., 2018. Occurrence and significance of mono-, di- and anhydrosaccharide biomolecules in Mesozoic and Cenozoic lignites and fossil wood. Org. Geochem. 116, 13–22. https://doi.org/10.1016/j.orggeochem.2017.11.008.
Marynowski, L., Goryl, M., Bucha, M., Smolarek-Lach, J., Detman, A., Sikora, A., Chojnacka, A., Simoneit, B.R.T., 2019. Trehalose, mannitol and arabitol as indicators of fungal metabolism in Late Cretaceous and Miocene deposits. Int. J. Coal Geol. 201, 51–61. https://doi.org/10.1016/j.coal.2018.11.003.
Marynowski, L., Goryl, M., Lempart-Drozd, M., Bucha, M., Majewski, M., Stępień, M., Loręc, R., Brocks, J., Simoneit, B.R.T., 2023. Differences in hemicellulose composition and pectin detection in Eocene and Miocene xylites. Chem. Geol. 624, 121416 https://doi.org/10.1016/j.chemgeo.2023.121416.
Mastalerz, M., Bustin, R.M., 1994. Variation in reflectance and chemistry of vitrinite and vitrinite precursors in a series of Tertiary Coals, Arctic Canada. Org. Geochem. 22, 921–933. https://doi.org/10.1016/0146-6380(94)90029-9.
Meinel, G., 1986. Zur Bildung des Tertiärquarzites. Z. Angew. Geol. 32 (1), 22–23.
Meyers, P.A., 1994. Preservation of elemental and isotopic source identification of sedimentary organic matter. Chem. Geol. 114, 289–302. https://doi.org/10.1016/0009-2541(94)90059-0.
Meyers, P.A., Ishiwatari, R., 1993. Lacustrine organic geochemistry an overview of indicators of organic matter sources and diageneses in lake sediments. Org. Geochem. 20, 867–900. https://doi.org/10.1016/0146-6380(93)90100-P.
Mishra, M., Shukla, Y.N., Kumar, S., 2000. Euphane triterpenoid and lipid constituents from Butea monosperma. Phytochemistry 54, 835–838. https://doi.org/10.1016/S0031-9422(00)00136-9.
Mishra, G., Collings, D.A., Altaner, C.M., 2018. Cell organelles and fluorescence of parenchyma cells in Eucalyptus bosistoana sapwood and heartwood investigated by microscopy. N. Z. J. For. Sci. 48, 1–10. https://doi.org/10.1186/s40490-018-0118-6.
Misra, B.K., 1992. Spectral fluorescence analysis of some liptinite macerals from Panandhro lignite (Kutch), Gujarat, India. Int. J. Coal Geol. 20, 145–163. https://doi.org/10.1016/0166-5162(92)90008-K.
Mitrović, D., Đoković, N., Životić, D., Bechtel, A., Šajnović, A., Stojanović, K., 2016. Petrographical and organic geochemical study of the Kovin lignite deposit, Serbia. Int. J. Coal Geol. 168, 80–107. https://doi.org/10.1016/j.coal.2016.07.008.
Moers, M.E.C., de Leeuw, J.W., Baas, M., 1994. Origin and diagenesis of carbohydrates in ancient sediments. Org. Geochem. 21, 1093–1106. https://doi.org/10.1016/0146-6380(94)90072-8.
Morey, E.D., Jacks, T.J., Hebert, J.J., Morey, P.R., 1983. Cellulose in fossil woods. Palaeontogr. Abt. B Band 185 (4–6), 79–82.
Mosbrugger, V., Gee, C.T., Belz, G., Ashraf, A.R., 1994. Three-dimensional reconstruction of an *in-situ* Miocene peat forest from the Lower Rhine Embayment, northwestern Germany—new methods in palaeovegetation analysis. Palaeogeogr. Palaeoclimatol. Palaeoecol. 110, 295–317. https://doi.org/10.1016/0031-0182(94)90089-2.
Murayama, S., Bakar, Z.A., 1996. Decomposition of tropical peat soils. Jpn. Agricult. Res. Quart. 30, 145–151.
Mustoe, G.E., Viney, M., Mills, J., 2019. Mineralogy of Eocene Fossil Wood from the "Blue Forest" Locality, Southwestern Wyoming. United States. Geosciences 9, 35. https://doi.org/10.3390/geosciences9010035.
Nakamura, H., Sawada, K., Takahashi, M., 2010. Aliphatic and aromatic terpenoid biomarkers in Cretaceous and Paleogene angiosperm fossils from Japan. Org. Geochem. 41, 975–980. https://doi.org/10.1016/j.orggeochem.2010.03.007.
Neunlist, S., Rohmer, M., 1985. Novel hopanoids from the methylotrophic bacteria *Methylococcus capsulatus* and *Methylomonas methanica*. (22S)-35-aminobacteriohopane-30,31,32,33,34-pentol and (22S)-35-amino-3β-methylbacteriohopane-30,31,32,33,34-pentol. Biochem. J. 231, 635–639. https://doi.org/10.1042/bj2310635.
Nytoft, H.P., Kildahl-Andersen, G., Lindström, S., Rise, F., Bechtel, A., Mitrović, D., Đoković, N., Životić, D., Stojanović, K., 2019. Dehydroicetexanes in sediments and crude oils: Possible markers for Cupressoideae. Org. Geochem. 129, 14–23. https://doi.org/10.1016/j.orggeochem.2019.01.001.
Oikonomopoulos, I.K., Kaouras, G., Tougiannidis, N., Ricken, W., Gurk, M., Antoniadis, P., 2015. The depositional conditions and the palaeoenvironment of the Achlada xylite-dominated lignite in western Makedonia, Greece. Palaeogeogr. Palaeoclimatol. Palaeoecol. 440, 777–792. https://doi.org/10.1016/j.palaeo.2015.09.031.
O'Keefe, J.M.K., Bechtel, A., Christanis, K., Dai, S., DiMichele, W.A., Eble, C.F., Esterle, J.S., Mastalerz, M., Raymond, A.L., Valentim, B.V., Wagner, N.J., Ward, C.R., Hower, J.C., 2013. On the fundamental difference between coal rank and coal type. Int. J. Coal Geol. 118, 58–87. https://doi.org/10.1016/j.coal.2013.08.007.
O'Keefe, J.M.K., Matthew, J.P., Riding, J.B., Vane, C.H., 2020. Cellular preservation and maceral development in lignite and wood from the Brassington Formation (Miocene), Derbyshire, UK. Int. J. Coal Geol. 222, 103452 https://doi.org/10.1016/j.coal.2020.103452.
Økland, R.H., Økland, T., Rygdren, K., 2001. A Scandinavian perspective on ecological gradients in north-west European mires: reply to Wheeler and Proctor. J. Ecol. 89, 481–486. https://doi.org/10.1046/j.1365-2745.2001.00573.x.
Ottenjann, K., Wolf, M., Wolff-Fischer, E., 1982. Das Fluoreszenzverhalten der Vitrinite zur Kennzeichnung der Kokungseigenschaften von Steinkohlen. Glückauf Forschungshefte 43, 173–179.
Otto, A., Wilde, V., 2001. Sesqui-, di-, and triterpenoids as chemosystematic markers in extant conifers – a review. Bot. Rev. 67, 141–238. https://doi.org/10.1007/BF02858076.
Ourisson, G., Albrecht, P., Rohmer, M., 1979. The hopanoids: palaeo-chemistry and biochemistry of a group of natural products. Pure Appl. Chem. 51, 709–729. https://doi.org/10.1351/pac197951040709.
Page, S.E., Rieley, J.O., Wüst, R., 2006. Lowland tropical peatlands of Southeast Asia. In: Martini, I.P., Martinez Cotezas, M., Chesworth, W. (Eds.), Peatlands: Evolution and Records of Environmental and Climate Changes. Elsevier, Amsterdam, pp. 145–172. https://doi.org/10.1016/S0928-2025(06)09007-9.
Pancost, R.D., Steart, D.S., Handley, L., Collinson, M.E., Hooker, J.J., Scott, A.C., Grassineau, N.V., Glasspool, I.J., 2007. Increased terrestrial methane cycling at the Palaeocene–Eocene thermal maximum. Nature 449, 332–336. https://doi.org/10.1038/nature06012.
Pandey, K.K., 1999. A study of chemical structure of soft and hardwood and wood polymers by FTIR spectroscopy. J. Appl. Polym. Sci. 71 (12), 1097–4628. https://doi.org/10.1002/(SICI)1097-4628(19990321)71:12<1969::AID-APP6>3.0.CO;2-D.
Passer, M., 1957. Analytical procedure for the organic constituents of peat. In: Report no. 14, Chemical Products from Peat Project. University of Minnesota, p. 38.
Peters, K.E., Cassa, M.R., 1994. Applied source rock geochemistry. In: Magoon, L.B., Dow, W.G. (Eds.), The Petroleum System-from Source to Trap. AAPG Memoir 60, Tulsa, pp. 93–120. https://doi.org/10.1306/M60585C5.
Pettersen, R.C., 1984. The Chemistry of Solid Wood. Advances in Chemistry Series 20, Chapter 2. ACS, Washington DC, pp. 57–126. https://doi.org/10.1021/ba-1984-0207.ch002.
Pfeiffer, L., Suhr, P., 2008. Tertiärer Vulkanismus. In: Pälchen, W., Walter, H. (Eds.), Geologie von Sachsen. E. Schweizerbart'sche Verlagsbuchhandlung (Nägele u. Obermiller), Stuttgart, pp. 486–494.

Pfeiffer, L., Kaiser, G., Pilot, J., 1984. K-Ar-Datierung von jungen Vulkaniten im Süden der DDR. Freiberger Forschungshefte Reihe C 389, 93–97.
Pickel, W., Kus, J., Flores, D., Kalaitzidis, S., Christanis, C., Cardott, B.J., Misz-Kennan, M., Rodrigues, S., Hentschel, A., Hámor-Vidó, M., Crosdale, P.J., Wagner, N., 2017. Classification of liptinite - ICCP System 1994. Int. J. Coal Geol. 169, 40–61. https://doi.org/10.1016/j.coal.2016.11.004.
Piotrowski, J.A., Geletneky, J., Vater, R., 1999. Soft-bedded subglacial meltwater channel from the Welzow-Süd open-cast lignite mine, Lower Lusatia, eastern Germany. Boreas 28, 363–374. https://doi.org/10.1111/j.1502-3885.1999.tb00226.x.
Poole, I., Dolezych, M., Kool, J., Van der Burgh, J., Van Bergen, P.F., 2006. Do stable carbon isotopes of brown coal woods record changes in lower Miocene palaeoecology? Palaeogeogr. Palaeoclimatol. Palaeoecol. 236, 345–354. https://doi.org/10.1016/j.palaeo.2005.11.013.
Potonié, H., 1895. Über Autochthonie von Carbonkohlen-Flötzen und des Senftenberger Braunkohlen-Flötzes. Jahrbuch der Königlich Preussischen geologischen Landesanstalt zu Berlin 16, 1–35.
Poynter, J.G., Farrimond, P., Robinson, N., Eglinton, G., 1989. Aeolian-derived higher plant lipids in the marine sedimentary record: Links with paleoclimate. In: Leinen, M., Sarnthein, M. (Eds.), Paleoclimatology and Paleometeorology: Modern and Past Patterns of Global Atmospheric Transport. Hingham, Mass, Kluwer Academic, Dordrecht, pp. 435–462.
Radke, M., Willsch, H., Welte, D.H., 1980. Preparative hydrocarbon group type determination by automated medium pressure liquid chromatography. Anal. Chem. 52, 406–411. https://doi.org/10.1021/ac50053a009.
Radtke, H., 1966. Die Tertiärquarzite im Abraum der Braunkohle des Weißelsterbeckens. Z. Angew. Geol. 12, 74–77.
Rascher, J., Escher, D., Fischer, J., Dutschmann, U., Kästner, S., 2005. Geologischer Atlas Tertiär Nordwestsachsen 1:250.000. GEOmontan GmbH Freiberg. Sächsisches Landesamt für Umwelt und Geologie, pp. 22–Dresden.
Rascher, J., Escher, D., Fischer, J., Dutschmann, U., Schneider, G., Volkmann, N., Stiewe, J., Hoth, N., Dilbat, M., 2006. Abschlussbericht zum FuE-Vorhaben: Lithofazielle Modellierung tertiärer Fazieseinheiten in Bergbaufolgelandschaften. GEOmontan GmbH Freiberg und TU Bergakademie Freiberg, Dresden/Freiberg, p. 102.
Regnery, J., Püttmann, W., Koutsodendris, A., Mulch, A., Pross, J., 2013. Comparison of the paleoclimatic significance of higher land plant biomarker concentrations and pollen data: a case study of lake sediments from the Holsteinian interglacial. Org. Geochem. 61, 73–84. https://doi.org/10.1016/j.orggeochem.2013.06.006.
Rieley, G., Collier, R.J., Jones, D.M., Eglinton, G., Eakin, P.A., Fallick, A.E., 1991. Sources of sedimentary lipids deduced from stable carbon-isotope analyses of individual compounds. Nature 352, 425–427. https://doi.org/10.1038/352425a0.
Rochdi, A., Landais, P., 1991. Transmission micro-infrared spectroscopy: an efficient tool for microsample characterization of coal. Fuel 70, 367–371. https://doi.org/10.1016/0016-2361(91)90124-S.
Roselt, G., 1978. Methode und Anleitung zur weitgehend objektiven Ermittlung der Varietäten humifizierter Xylite unserer Weichbraunkohlen. Freiberger Forschungshefte C 335, 113–145.
Rowell, R.M., Pettersen, R., Tshabalala, M.A., 2012. Handbook of Wood Chemistry and Wood Composites. CRC Press, Boca Raton, p. 704.
Russell, N.J., Barron, P.F., 1984. Gelification of Victorian Tertiary soft brown coal wood. II. Changes in chemical structure associated with variation in the degree of gelification. Int. J. Coal Geol. 4, 119–142. https://doi.org/10.1016/0166-5162(84)90011-9.
Sakala, J., 2002. First record of fossil angiosperm wood (*Ulmoxylon*, Ulmaceae) from the famous locality of Bílina (Czech Republic, early Miocene). Comptes Rendus Palevol 1, 161–166. https://doi.org/10.1016/S1631-0683(02)00025-8.
Schellenberg, F., Kleeberg, K., 1997. Kaolinlagerstätten der Lausitz - ihre Entstehung, Nutzung und industrielle Bedeutung. Aufschluss 48, 267–279.
Schellenberger, H., 2011. Lithofazielle Dokumentation und Korrelation ausgewählter Profile der Meuro-Formation in der Lausitz (Tagebaue Nochten, Welzow-Süd und Jänschwalde). Unveröff. Diplomarbeit, 93. TU Bergakademie Freiberg.
Schleser, G.H., Frielingsdorf, J., Blair, A., 1999. Carbon isotope behaviour in wood and cellulose during artificial aging. Chem. Geol. 158, 121–130. https://doi.org/10.1016/S0009-2541(99)00024-8.
Schneider, W., 1966. Beziehungen zwischen Pflanzeninhalt und petrographischer Beschaffenheit von Weichbraunkohlen am Beispiel der miozänen Braunkohlen der Oberlausitz. Berichte der Deutschen Gesellschaft für Geologische Wissenschaften Reihe A, Geologie und Paläontologie 11 (5), 615–633.
Schneider, W., 1967. Tertiäre Cuticulae dispersae. In: Taxonomie, fazielle Aussage und praktische Bedeutung disperser Kutikulen aus Braunkohlen der DDR unter besonderer Berücksichtigung des 2. Dissertation, Bergakademie Freiberg, Lausitzer Flözes, p. 219.
Schneider, W., 1969a. Cuticulae dispersae aus dem 2. Lausitzer Flöz (Miozän) und ihre fazielle Aussage. Freiberger Forschungshefte, Reihe C 222, 1–75.
Schneider, W., 1969b. Zur kutikularanalytischen Kennzeichnung technologisch bedeutsamer Braunkohlen-Lithotypen im 2. Lausitzer Flöz. Freiberger Forschungshefte, Reihe C 242, 29–34.
Schneider, W., 1984. Angewandte Paläobotanik und Braunkohlenpetrologie - pflanzlicher Gewebe als Gefügebildner in der Braunkohle. Freiberger Forschungshefte, Reihe C 381, 14–19.
Schneider, W., 1992. Flora successions in Miocene swamps and bogs of Central Europe. Z. Geol. Wiss. 20 (5–6), 555–570.
Schneider, W., 1995. Palaeohistological studies on Miocene brown coals of Central Europe. Int. J. Coal Geol. 28, 229–249. https://doi.org/10.1016/0166-5162(95)00019-4.
Schneider, W., 1998. Kohlenpetrographie und Faziesentwicklung der Flöze des Berzdorfer Beckens. Arbeitsbericht BG 2–53 (LAUBAG), 22.
Schneider, W., 2004. Eine blätterführende Taphocoenose im 2. Miozänen Flöz von Nochten (Lausitz): Taxonomie, Taphonomie und Phytostratigraphie. Palaeontogr. Abt. B 268 (1–3), 1–74.
Schneider, W., 2009. Zur Paläobotanik des Tertiärs von Piskowitz bei Kamenz. Teil 1: Koniferen. Veröffentlichungen des Museums der Westlausitz Kamenz 29, 15–50.
Schneider, W., 2010. Zur Paläobotanik des Tertiärs von Piskowitz bei Kamenz. Teil 2: Das Kieselblatt *Silicophyllum heerlenense* Weyland, Kilpper et Berendt. Veröffentlichungen des Museums der Westlausitz Kamenz 30, 35–62.
Schwanninger, M., Rodrigues, J.C., Pereira, H., Hinterstoisser, B., 2004. Effects of short-time vibratory ball milling on the shape of FT-IR spectra of wood and cellulose. Vib. Spectrosc. 36, 23–40. https://doi.org/10.1016/j.vibspec.2004.02.003.
Schwark, L., Zink, K., Lechterbeck, J., 2002. Reconstruction of postglacial to early Holocene vegetation history in terrestrial Central Europe via cuticular lipid biomarkers and pollen records from lake sediments. Geology 30, 463–466. https://doi.org/10.1130/0091-7613(2002)030<0463:ROPTEH>2.0.CO;2.
Sen, J., 1956. Fine structure in degraded, ancient and buried wood, and other fossilized plant derivates. Bot. Rev. 22 (4), 343–374. https://doi.org/10.1007/BF02872482.
Senftle, J., Larter, S., Bromley, B., Brown, J., 1986. Quantitative chemical characterization of vitrinite concentrates using pyrolysis–gas chromatography. Org. Geochem. 9, 345–350. https://doi.org/10.1016/0146-6380(86)90115-4.
Seyfullah, L.J., Beimforde, C., Dal Corso, J., Perrichot, V., Rikkinen, J., Schmidt, A.R., 2018. Production and preservation of resins – past and present. Biol. Rev. 93, 1684–1714. https://doi.org/10.1111/brv.12414.
Siever, R., Scott, R.A., 1963. Organic geochemistry of silica. In: Breger, I.A. (Ed.), Organic Geochemistry. International Series of Monographs on Earth Sciences. Pergamon, New York, pp. 579–595.
Singh, K., Risse, M., Das, K.C., Worley, J., 2009. Determination of Composition of Cellulose and Lignin Mixtures using Thermogravimetric Analysis. J. Energy Resour. Technol. 131, 022201 https://doi.org/10.1115/1.3120349.
Sohn, A.W., Reiff, F., 1942. Natriumchlorit als Aufschlußmittel. Der Papierfabrikant 40, 1–7.
Spackman, W., Cohen, A.D., Given, P.H., Casagrande, D.J., 1976. The Comparative Study of the Okefenokee Swamp and the Everglades-Mangrove Swamp-Marsh Complex of Southern Florida. A short course presentation of the Pennsylvania State, p. 396.
Spackman, W., Ryan, N.J., Rhoads, C.A., Given, P.H., 1988. Studies of peat as the input to coalification, II. Sampling sites and preliminary fractionation. Int. J. Coal Geol. 9, 253–265. https://doi.org/10.1016/0166-5162(88)90016-X.
Standke, G., 2006. Paläogeographisch-fazielle Modellierung des Unter−/Mittelmiozän-Grenzbereichs in der Lausitz (Brieske Folge/Formation). Schriftenreihe für Geowissenschaften 14, 130.
Standke, G., 2008. Tertiär. In: Pälchen, W., Walter, H. (Eds.), Geologie von Sachsen. E. Schweizerbart'sche Verlagsbuchhandlung Nägele u. Obermiller, Stuttgart, pp. 358–419.
Standke, G., 2010. Tertiär: Regionalgeologischer Überblick, Kenntnisstandsentwicklung, Stratigraphie und Schichtenfolge. In: Bahrt, W., Bönisch, R., Krentz, O., Kühner, R., Lapp, M., Petzold, H., Schneider, W., Schulze, H., Seibel, B., Standke, G. (Eds.), Die geologische Entwicklung der Lausitz. Vattenfall Europe Mining AG, Cottbus, pp. 41–75.
Standke, G., Strauss, C., 1991. Neue Ergebnisse zur Stratigraphie der Oberlausitzer Braunkohlenlagerstätten. Mitteilungen aus der Geologischen Landesuntersuchung 758, 84–89.
Standke, G., Rascher, J., Strauss, C., 1993. Relative Sea Level fluctuations and brown coal formation around the Early-Middle Miocene Boundary in the Lusation Brown Coal District. Geol. Rundsch. 82 (2951714), 305. https://doi.org/10.1007/BF00191835.
Stankiewicz, B.A., Poinar, H.N., Briggs, D.E.G., Evershed, R.P., Poinar Jr., G.O., 1998. Chemical preservation of plants and insects in natural resins. Proc. R. Soc. Lond. B 265, 641–647. https://doi.org/10.1098/rspb.1998.0342.
Stefanova, M., Markova, K., Marinov, S., Simoneit, B.R.T., 2005a. Molecular indicators for coal-forming vegetation of the Miocene Chukurovo lignite, Bulgaria. Fuel 84, 1830–1838. https://doi.org/10.1016/j.fuel.2005.04.009.
Stefanova, M., Markova, K., Marinov, S., Simoneit, B.R.T., 2005b. Biomarkers in the fossils from the Miocene-aged Chukurovo lignite, Bulgaria: sesqui- and diterpenoids. Bull. Geosci. 80, 93–97.
Stefanova, M., Kortenski, J., Zdravkov, A., Marinov, S., 2013. Paleoenvironmental settings of the Sofia lignite basin: Insights from coal petrography and molecular indicators. Int. J. Coal Geol. 107, 45–61. https://doi.org/10.1016/j.coal.2012.09.014.
Stein, C.L., 1982. Silica recrystallization in petrified wood. J. Sediment. Petrol. 52, 1277–1282. https://doi.org/10.1306/212F8116-2B24-11D7-8648000102C1865D.
Stojanović, K., Životić, D., 2013. Comparative study of Serbian Miocene coals – insights from biomarker composition. Int. J. Coal Geol. 107, 3–23. https://doi.org/10.1016/j.coal.2012.09.009.
Stout, S., 1992. Aliphatic and aromatic triterpenoid hydrocarbons in a Tertiary angiospermous lignite. Org. Geochem. 18, 51–66. https://doi.org/10.1016/0146-6380(92)90143-L.
Stout, S.A., Bensley, D.F., 1987. Fluorescing macerals from wood precursors. Int. J. Coal Geol. 7, 119–133. https://doi.org/10.1016/0166-5162(87)90016-4.
Stout, S.A., Spackman, W., 1987. A microscopic investigation of woody tissues in peats. Some processes active in the peatification of ligno-cellulosic cell walls. Int. J. Coal Geol. 8, 55–58. https://doi.org/10.1016/0166-5162(87)90022-X.
Stout, S.A., Boon, J.J., Spackman, W., 1988. Molecular aspects of the peatification and early coalification of angiosperm and gymnosperm woods. Geochim. Cosmochim. Acta 52 (2), 405–415. https://doi.org/10.1016/0016-7037(88)90096-8.

Suhr, P., Goth, K., Lorenz, V., Suhr, S., 2006. Long lasting subsidence and deformation in and above maar-diatreme volcanoes – a never ending story. Z. Dtsch. Ges. Geowiss. 157 (3), 491–511.
Süß, M., 1959. Petrologische Untersuchungen des Braunkohlenvorkommens von Piskowitz bei Kamenz. Freiberger Forschungshefte C 50, 63–98.
Süss, M., Rammler, E., 1965. The Nochten brown coal deposit of the Schwarze Pumpe undertaking – problems of coal quality. Neue Bergbautechnik 15, 68–78.
Sykes, R., Snowdon, L.R., 2002. Guidelines for assessing the petroleum potential of coaly source rocks using Rock-Eval pyrolysis. Org. Geochem. 33, 1441–1455. https://doi.org/10.1016/S0146-6380(02)00183-3.
Sýkorová, I., Pickel, W., Christanis, K., Wolf, M., Taylor, G.H., Flores, D., 2005. Classification of huminite – ICCP System 1994. Int. J. Coal Geol. 62, 85–106. https://doi.org/10.1016/j.coal.2004.06.006.
Taylor, G.H., Teichmüller, M., Davis, A.C.F.K., Diessel, C.F.K., Littke, R., Robert, P., 1998. Organic Petrology. Gebrüder Borntraeger, p. 704.
Teichmüller, M., Durand, B., 1983. Fluorescence microscopical rank studies on liptinites and vitrinites in peat and coals, and comparison with results of the Rock-Eval pyrolysis. Int. J. Coal Geol. 2, 197–230. https://doi.org/10.1016/0166-5162(83)90001-0.
Teichmüller, M., Teichmüller, R., 1968. Geological aspects of coal metamorphism. In: Murchison, D.G., Westoll, T.S. (Eds.), Coal and Coal Bearing Strata. Oliver and Boyd, Edinburgh, pp. 233–267.
Thiergart, F., 1937. Die Pollenflora der Niederlausitzer Braunkohle, besonders im Profil der Grube Marga bei Senftenberg. Jahrbuch der Königlich Preussischen Geologischen Landesanstalt und Bergakademie zu Berlin 58, 282–351.
Tietz, O., Büchner, J., Suhr, P., Goth, K., 2013. Field trip 3: Volcanology of the Lusatian Volcanic Field – new insights in old well-known. In: Büchner, J., Rapprich, V., Tietz, O. (Eds.), Abstracts & excursion guides to the scientific conference "Ba-salt 2013. Cenozoic magmatism in Central Europe", Görlitz, 24.–28.4.2013. Czech Geological Survey, Prague, pp. 275–297.
Tietz, O., Büchner, J., Lapp, M., Scholle, T., 2018. The Stolpen Volcano in the Lausitz Volcanic Field (East Germany) – volcanological, petrographic and geochemical investigations at the type locality of basalt. J. Geosci. 63, 299–315. https://doi.org/10.3190/jgeosci.275.
Ting, F.T.C., 1977. Quantitative fluorescence microscopy and fluorescence characteristics of thermally altered liptinites. Palynology 1, 27–32.
Trendel, J.M., Lohmann, F., Kintzinger, J.P., Albrecht, P., Chiaroni, A., Riche, C., Cesario, M., Guilhem, J., Pascard, C., 1989. Identification of des-A-triterpenoid hydrocarbons occurring in surface sediments. Tetrahedron 45, 4457–4470. https://doi.org/10.1016/S0040-4020(01)89081-5.
Uçar, G., Meier, D., Faix, O., Wegener, G., 2005. Analytical pyrolysis and FTIR spectroscopy of fossil *Sequoiadendron giganteum* (Lindl.) wood and MWLs isolated hereof. Holz Roh Werkst. 63, 57–63. https://doi.org/10.1007/s00107-004-0530-x.
van Bergen, P.F., Poole, I., 2002. Stable carbon isotopes of wood: a clue to palaeoclimate? Palaeogeogr. Palaeoclimatol. Palaeoecol. 182 (1–2), 31–45. https://doi.org/10.1016/S0031-0182(01)00451-5.
van Bergen, P.F., Goni, M., Collinson, M.E., Barrie, P.J., Sinninghe, Damste, J.S., de Leeuw, J.W., 1994. Chemical and microscopical characterisation of inner seed coats of fossil water plants. Geochim. Cosmochim. Acta 58, 231–239. https://doi.org/10.1016/0016-7037(94)90460-X.
van der Heijden, E., Boon, J.J., 1994. A combined pyrolysis spectrometric and light microscopic study of peatified Calluna wood isolated from raised bog peat deposits. Org. Geochem. 22, 903–919. https://doi.org/10.1016/0146-6380(94)90028-0.
van Winden, J.F., Talbot, H.M., Kip, N., Reichart, G.-J., Pol, A., McNamara, N.P., Jetten, M.S.M., Op den Camp, H.J.M., Sinninghe Damsté, J.S., 2012. Bacteriohopanepolyol signatures as markers for methanotrophic bacteria in peat moss. Geochim. Cosmochim. Acta 77, 52–61. https://doi.org/10.1016/j.gca.2011.10.026.
Venkatesan, M.I., Ohta, K., Stout, S.A., Steinberg, S., Oudin, J.L., 1993. Diagenetic trends of lignin phenols in Mahakam Delta coals: correlation between laboratory simulation and natural samples. Org. Geochem. 20, 463–473. https://doi.org/10.1016/0146-6380(93)90093-Q.
Volkman, J.K., 1986. A review sterol markers for marine and terrigenous organic matter. Org. Geochem. 9, 83–99. https://doi.org/10.1016/0146-6380(86)90089-6.
Vu, T.T.A., Zink, K.-G., Mangelsdorf, K., Sykes, R., Wilkes, H., Horsfield, B., 2009. Changes in bulk properties and molecular compositions within New Zealand Coal Band solvent extracts from early diagenetic to catagenetic maturity levels. Org. Geochem. 40, 963–977. https://doi.org/10.1016/j.orggeochem.2009.06.002.
Wakeham, S.G., 1990. Algal and bacterial hydrocarbons in particulate material and interfacial sediment of the Cariaco Trench. Geochim. Cosmochim. Acta 54, 1325–1336. https://doi.org/10.1016/0016-7037(90)90157-G.
Wang, S.H., Griffiths, P.R., 1985. Resolution enhancement of diffuse reflectance i.r. spectra of coals by Fourier self-deconvolution. 1. C-H stretching and bending modes. Fuel 64, 229–236. https://doi.org/10.1016/0016-2361(85)90223-6.
Wang, L.-Y., Wang, N.-L., Yao, X.-S., Miyata, S., Kitanaka, S., 2003. Euphane and tirucallane triterpenes from the roots of Euphorbia kansui and their in vitro effects on the cell division of Xenopus. J. Nat. Prod. 66, 630–633. https://doi.org/10.1021/np0205396.
Weyland, H., 1957. Kritische Untersuchungen zur Kutikularanalyse tertiärer Blätter III. Monokotylen der Rheinischen Braunkohle. Palaeontogr. Abt. B 103 (1–3), 34–74.
Widera, M., Ćwikliński, W., Karman, R., 2008. Cenozoic tectonic evolution of the Poznań-Oleśnica Fault Zone, central-western Poland. Acta Geol. Pol. 58, 455–471.
Widera, M., Bechtel, A., Chomiak, L., Maciaszek, P., Słodkowska, B., Wachocki, R., Worobiec, E., Worobiec, G., Zieliński, T., 2021. Palaeoenvironmental reconstruction of the Konin Basin (central Poland) during lignite accumulation linked to the mid-Miocene climate optimum. Palaeogeogr. Palaeoclimatol. Palaeoecol. 568, 110307 https://doi.org/10.1016/j.palaeo.2021.110307.
Wiesberg, L., 1974. Die C-13 Abnahme in Holz von Baumjahresringen, eine Untersuchung zur anthropogenen Beeinflussung des CO_2 Haushalts der Atmosphäre. Rheinisch Westfälische Technische Hochschule, Aachen. PhD thesis (unpubl.).
Wolfe, A.P., Csank, A.Z., Reyes, A.V., McKellar, R.C., Tappert, R., Muehlenbachs, K., 2012. Pristine Early Eocene Wood buried deeply in Kimberlite from Northern Canada. PLoS One 7 (9), e45537. https://doi.org/10.1371/journal.pone.0045537.
Wolff, G.A., Ruskin, N., Marshal, J.D., 1992. Biogeochemistry of an early diagenetic concretion from the Birchi Bed (L. Lias, W. Dorset, UK). Org. Geochem. 19, 431–444. https://doi.org/10.1016/0146-6380(92)90010-U.
Worobiec, E., Widera, M., Worobiec, G., Kurdziel, B., 2021. Middle Miocene palynoflora from the Adamów lignite deposit, Central Poland. Palynology 45, 59–71. https://doi.org/10.1080/01916122.2019.1697388.
Yang, H., Huang, Y., Leng, Q., LePage, B.A., Williams, C.J., 2005. Biomolecular preservation of Tertiary Metasequoia Fossil Lagerstätten revealed by comparative pyrolysis analysis. Rev. Palaeobot. Palynol. 134, 237–256. https://doi.org/10.1016/j.revpalbo.2004.12.008.
You, Y., Huber, M., Müller, R.D., Poulsen, C.J., Ribbe, J., 2009. Simulation of the Middle Miocene climate Optimum. Geophys. Res. Lett. 36, l04702 https://doi.org/10.1029/2008GL036571.
Zdravkov, A., Bechtel, A., Sachsenhofer, R.F., Kortenski, J., Gratzer, R., 2011. Vegetation differences and diagenetic changes between two Bulgarian lignite deposits – Insights from coal petrology and biomarker composition. Org. Geochem. 42, 237–254. https://doi.org/10.1016/j.orggeochem.2010.12.006.
Zeikus, J.G., Wellstein, A.L., Kirk, T.K., 1982. Molecular basis for the biodegradative recalciterance of lignin in anaerobic environments. Federation Eur. Microbiol. Soc. Microbiol. Lett. 1, 193–197. https://doi.org/10.1111/J.1574-6968.1982.TB00066.X.
Zhang, X., Xu, Y., Ruan, J., Ding, S., Huang, X., 2014. Origin, distribution and environmental significance of perylene in Okinawa Trough since last glaciation maximum. Org. Geochem. 76, 288–294. https://doi.org/10.1016/j.orggeochem.2014.09.008.
Ziegler, P.A., Cloetingh, S., van Wees, J.-D., 1995. Dynamics of intra-plate compressional deformation: the Alpine foreland and other examples. Tectonophysics 252, 7–59. https://doi.org/10.1016/0040-1951(95)00102-6.
Životić, D., Stojanović, K., Gržetić, I., Jovančićević, B., Cvetković, O., Šajnović, A., Simić, V., Stojaković, R., Scheeder, G., 2013. Petrological and geochemical composition of lignite from the D field, Kolubara basin (Serbia). Int. J. Coal Geol. 111, 5–22. https://doi.org/10.1016/j.coal.2012.10.014.